Nonlinear Optical Beam Processing in 3D Nonlinear Photonic Crystals

Shan Liu

November 2023

A THESIS SUBMITTED FOR THE DEGREE OF DOCTOR OF PHILOSOPHY

OF THE AUSTRALIAN NATIONAL UNIVERSITY

Department of Electronic Materials Engineering

Research School of Physics

College of Sciences

The Australian National University

Declaration

This thesis reports the research I conducted during 2019 to 2023, at the Research School of Physics, the Australian National University, Canberra, Australia.

To the best of my knowledge, the material reported here is original except where acknowledged and reference in appropriate manner. It has not been previously published by others, or submitted in whole or in part for any university degrees.

Shan Liu

November 2023

Acknowledgements

I wish to express my gratitude to those who have directly or indirectly contributed to my PhD study.

First and foremost, I want to thank my supervisors, Dr. Yan Sheng, Professor Wieslaw Krolikowski, and Professor Lan Fu. Dr. Yan has provided me with immense freedom in my research life, enabling me to explore ideas that intrigued me. Her encouragement was particularly crucial when I felt pessimistic about the prospects of my research. This support was vital. Without it, I could not have achieved what I have today. I am grateful to Professor Wieslaw Krolikowski for help and guidance. He always manages to hit the nail on the head during discussions, offering precise and constructive insights. His rich experience and extensive knowledge frequently guide and enlighten me. Professor Lan Fu has given me numerous significant pieces of advice beyond the realm of academic research. Her guidance has been decisive in helping me make critical decisions at key points.

I would also like to extend my gratitude to the staff and colleagues at the Research School of Physics and Engineering (RSPE) with whom I have had the privilege of working. Special thanks to Mr. Xin Chen for teaching me how to use laboratory equipment and for sharing experiences in laser experiments, which introduced me to the world of scientific research. I'm thankful to Mr. Tianxiang Xu for imparting skills in polishing crystals and knowledge in materials science.

Gratitude is also due to Mr. Boqing Liu and Mr. Dawei Liu. The times we spent together having interesting conversations were truly enjoyable. Also, my thanks go to Dr. Leszek Mateusz Mazur, whose conversations greatly broadened my horizons.

I am also immensely grateful to my family, my parents, and my wife Mrs. Sijing Zou. Despite my engagement in such a strange job that they may not fully understand, their unwavering support has always been there for me.

Abstract

For decades, scientists have focused on how to efficiently facilitate various nonlinear optical processes in the field of nonlinear optics, particularly second harmonic generation. Limited by the dispersion properties of natural nonlinear materials and the resulting phase mismatch between light waves, only a portion of these nonlinear processes can be efficiently conducted. However, artificial manipulation of nonlinear materials can achieve Quasi-phase matching (QPM), significantly expanding the application range of nonlinear material. Such artificially processed materials are known as nonlinear photonic crystals (NPCs).

The traditional method of fabricating NPCs is the electric field poling technique, which involves preparing microelectrodes of specific shapes on the surface of the nonlinear material wafer and applying high voltage on both sides of the wafer to locally alter the material's properties. This method processes the material from underneath the electrodes right through to the other side, thus making it unsuitable for fabricating complex three-dimensional structure NPCs. The latest technique, however, utilizes femtosecond laser direct writing. This technique focuses femtosecond laser pulses inside the nonlinear material, where multi-photon absorption and the material's interaction at the focal point allow for artificial manipulation. This technique is highly innovative, and both the technology itself and its applications are worthy of further research.

This thesis focuses on the aforementioned issues, exploring the design, fabrication, and characterization of various types of 3D NPCs fabricated by the femtosecond laser direct writing technique. Specifically, this thesis is organized as follows. In Chapter 1, we review the development history and significant research breakthroughs in the field of nonlinear photonic crystals. Some important concepts are also discussed. The purpose of this chapter is to provide readers who are unfamiliar with this field with a general understanding. Those already familiar with the subject may choose to skip this chapter. Chapter 2 delves into more specific physical concepts and models required in the field of nonlinear optics. It also introduces essential mathematical tools like Fourier transformation, which will be utilized in subsequent chapters.

From Chapter 3 onwards, we present specific research projects. Chapter 3 describes our use of femtosecond laser direct writing to fabricate 3D NPCs capable of nonlinear wavefront shaping. This work experimentally demonstrates the superiority of 3D NPCs over 2D NPCs. Chapter 4, building upon the foundation laid in Chapter 3, improves the structure of the 3D NPCs. Using the theory of nonlinear volume holography, we designed and fabricated 3D NPCs with high nonlinear conversion efficiency capable of nonlinear wavefront shaping. Chapter 5 systematically studies the mechanism of laser poling and optimizes this technique, enabling us to fabricate larger and more efficient 3D NPCs. Chapter 6 showcases large-volume 3D NPCs achieved through the improved technique and mature 3D NPC structural design theory. These samples have a nonlinear conversion efficiency of up to 4.6%.

List of publications

Publication in peer-reviewed journals:

[1] Y. Wang, Y. Sheng, **S. Liu**, R. Zhao, T. Xu, T. Xu, F. Chen, W. Krolikowski. "Wavelength-dependent nonlinear wavefront shaping in 3D nonlinear photonic crystal." *Chin. Opt. Lett.*, vol. 22, no. 7, p. 071901, Jul. 2024

[2] Y. Sheng, X. Chen, T. Xu, **S. Liu**, R. Zhao, and W. Krolikowski, "Research Progress on Femtosecond Laser Poling of Ferroelectrics," *Photonics*, vol. 11, no. 5, 2024

[3] Y. Sheng, **S. Liu**, X. Hu, X. Chen, T. Xu, R. Zhao, W. Krolikowski, "Second-harmonic generation in periodic fork-shaped χ(2) gratings at oblique incidence," *Chin. Opt. Lett.*, vol. 22, no. 4, p. 041902, Apr. 2024

[4] X. Hu, Y. Sheng, R. Zhao, **S. Liu**, T. Xu, and F. Chen, "Bottle-shaped second harmonic generation with adjustable locations," *Laser Physics*, vol. 34, no. 5, p. 055403, Mar. 2024

[5] N. Wang, **S. Liu**, T. Xu, R. Zhao, T. Xu, W. Krolikowski, Y Sheng, "Structuring light beams via nonlinear diffraction in 3D nonlinear photonic crystal," *Optics & Laser Technology*, vol. 168, p. 109994, 2024

[6] X. Hu, **S. Liu**, T. Xu, Y. Sheng, R. Zhao, and W. Krolikowski, "Nonlinear generation of an optical bottle beam in domain-engineered ferroelectric crystals," *Opt. Lett.*, vol. 48, no. 21, pp. 5527–5530, Nov. 2023

[7] **S. Liu**, Y. Sheng, and W. Krolikowski, "Polarization-dependent optical engineering of ferroelectric domains," *ChemPhysMater*, 2023

[8] X. Chen, C. Xu, **S. Liu**, D. Liu, B. Tan, Y. Zhang, H. Chen, Y. Sheng, J. Wang, "Influences of focusing conditions on optical poling in lithium niobate using a 1035 nm femtosecond fiber laser," *Appl. Opt.*, vol. 62, no. 23, pp. 6212–6217, Aug. 2023

[9] **S. Liu**, L. Wang, L. M. Mazur, K. Switkowski, B. Wang, F. Chen, A. Arie, W. Krolikowski, Y. Sheng, "Highly Efficient 3D Nonlinear Photonic Crystals in Ferroelectrics," *Advanced Optical Materials*, vol. 11, no. 14, p. 2300021, 2023

[10] S. Wang, **S. Liu**, D. Liu, N. Wang, R. Zhao, Y. Liu, Z. Li, G. Mao, F. Chen, Y. Sheng, T. Xu, W. Krolikowski, "Ferroelectric domain engineering with femtosecond pulses of different wavelengths," *Opt. Express*, vol. 31, no. 4, pp. 5843–5852, Feb. 2023

[11] N. Wang, **S. Liu**, R. Zhao, T. Xu, F. Chen, A. Arie, W. Krolikowski, Y. Sheng, "Effect of spatial variation of the duty cycle in transverse second-harmonic generation," *Opt. Lett.*, vol. 47, no. 15, pp. 3656–3659, Aug. 2022

[12] X. Chen, L. M. Mazur, D. Liu, **S. Liu**, X. Liu, Z. Xu, X. Wei, J. Wang, Y. Sheng, Z. Wei, W. Krolikowski, "Quasi-phase matched second harmonic generation in a PMN-38PT crystal," *Opt. Lett.*, vol. 47, no. 8, pp. 2056–2059, Apr. 2022

[13] Y. Chen, C. Yang, **S. Liu**, S. Wang, N. Wang, Y. Liu, Y. Sheng, R. Zhao, T. Xu, W. Krolikowski, "Optically Induced Nonlinear Cubic Crystal System for 3D Quasi-Phase Matching," *Advanced Photonics Research*, vol. 3, no. 4, p. 2100268, 2022

[14] K. Zhou, B. Wang, S. Tang, Y. Gao, **S. Liu**, Y. Sheng, J. Chen, S. Dai, X. Shen, "Mid-infrared biomimetic moth-eye-shaped polarization-maintaining and angle-insensitive metalens," *Opt. Express*, vol. 30, no. 7, pp. 12048–12060, Mar. 2022

[15] X. Chen, D. Liu, **S. Liu**, L. M. Mazur, X. Liu, X. Wei, Z. Xu, J. Wang, Y. Sheng, Z. Wei, W. Krolikowski, "Optical Induction and Erasure of Ferroelectric Domains in Tetragonal PMN-38PT Crystals," *Advanced Optical Materials*, vol. 10, no. 4, p. 2102115, 2022

[16] L. M. Mazur, **S. Liu**, X. Chen, W. Krolikowski, and Y. Sheng, "Localized Ferroelectric Domains via Laser Poling in Monodomain Calcium Barium Niobate Crystal," *Laser & Photonics Reviews*, vol. 15, no. 9, p. 2100088, 2021

[17] B. Wang, **S. Liu**, T. Xu, R. Zhao, P. Lu, W. Krolikowski, Y. Sheng, "Nonlinear Talbot self-healing in periodically poled LiNbO3 crystal," *Chin. Opt. Lett.*, vol. 19, no. 6, p. 060011, Jun. 2021

[18] B. Wang, X. Hong, K. Wang, X. Chen, **S. Liu**, W. Krolikowski, P. Lu, Y. Sheng, "Nonlinear detour phase holography," *Nanoscale*, vol. 13, no. 4, pp. 2693–2702, 2021

[19] **S. Liu**, L. M. Mazur, W. Krolikowski, and Y. Sheng, "Nonlinear Volume Holography in 3D Nonlinear Photonic Crystals," *Laser & Photonics Reviews*, vol. 14, no. 11, p. 2000224, Nov. 2020

[20] D. Liu, **S. Liu**, L. M. Mazur, B. Wang, P. Lu, W. Krolikowski, Y. Sheng, "Smart optically induced nonlinear photonic crystals for frequency conversion and control," *Applied Physics Letters*, vol. 116, no. 5, p. 051104, Feb. 2020

[21] **S. Liu**, K. Switkowski, C. Xu, J. Tian, B. Wang, P. Lu, W. Krolikowski, Y. Sheng, "Nonlinear wavefront shaping with optically induced three-dimensional nonlinear photonic crystals," *Nature Communications*, vol. 10, no. 1, p. 3208, Jul. 2019

Conference:

[1] L. M. Mazur, **S. Liu**, X. Chen, W. Krolikowski, and Y. Sheng, "Femtosecond Laser Ferroelectric Domains Reversal in Monodomain Calcium Barium Niobate Crystal," in Frontiers in Optics + Laser Science 2021, Optica Publishing Group, 2021, p. JTu1A.15.

[2] **S. Liu**, L. M. Mazur, W. Krolikowski, and Y. Sheng, "Beam Shaping In

Optically Induced Nonlinear Volume Holograms," in OSA Advanced Photonics Congress (AP) 2020 (IPR, NP, NOMA, Networks, PVLED, PSC, SPPCom, SOF), Optica Publishing Group, 2020, p. NpTh3D.2.

[3] L. M. Mazur, **S. Liu**, W. Krolikowski, and Y. Sheng, "Perfect Vortices via Second Harmonic Generation In Optically Induced Nonlinear Hologram," in OSA Advanced Photonics Congress (AP) 2020 (IPR, NP, NOMA, Networks, PVLED, PSC, SPPCom, SOF), Optica Publishing Group, 2020, p. NpW2D.7.

[4] **S. Liu**, L. M. Mazur, W. Krolikowski, and Y. Sheng, "Beam shaping in nonlinear volume holograms via optically engineered ferroelectric domain patterns," in AOS Australian Conference on Optical Fibre Technology (ACOFT) and Australian Conference on Optics, Lasers, and Spectroscopy (ACOLS) 2019, A. Mitchell and H. Rubinsztein-Dunlop, Eds., SPIE, 2019, p. 112000A.

Table of Contents

Chapter 1 Background and motivation

1.1 Introduction

This chapter aims to review the developmental history of the relevant research field, presenting key theoretical and technological milestones in chronological order. The purpose is to provide readers with a general understanding of the research area addressed in this thesis. A more detailed and in-depth technical introduction, along with the theories that will be employed in this thesis, will be thoroughly discussed in Chapter 2.

1.2 Laser and nonlinear optics

Light Amplification by Stimulated Emission of Radiation, or LASER, has a history dating back to the early 20th century when scientists began exploring the interaction between light and matter. Albert Einstein laid the theoretical foundation for stimulated emission in 1917 [1]. He proposed that atoms could not only produce spontaneous radiation but also stimulated radiation, which forms the theoretical basis for lasers. However, due to technological limitations at the time, lasers only existed in theory, and it took more than 40 years for research on lasers to become a reality.

In 1958, Charles H. Townes and Arthur L. Schawlow proposed a technological theory for generating lasers [2]. Just two years later, in 1960, Theodore H. Maiman created the world's first laser using a ruby rod as the active medium [3]. Following this breakthrough, research on lasers experienced explosive growth, leading to the invention of various types of lasers, including but not limited to gas lasers, semiconductor lasers, and fibre lasers [4].

The birth of the laser also gave rise to a new research field: nonlinear optics. This field studies the interactions between light and matter that involve non-linear responses, the material's dielectric polarization *P* responds nonlinearly to the applied light electric field *E*. In 1961, Franken successfully generated a beam of light with a new wavelength (half the original wavelength) by illuminating a quartz crystal with a laser, marking the first observation of a nonlinear optical process known as second-harmonic generation (SHG) [5]. This breakthrough not only represented the first-time researchers observed nonlinear optical phenomena in the laboratory but also makes the birth of experimental nonlinear optics. Since then, a wide range of nonlinear phenomena have been observed and studied, including sum frequency generation [6], [7], difference frequency generation [8], parametric amplification and oscillation [9], [10], multi-photon absorption [11], self-focusing [12], and stimulated scattering [13], etc.

Another milestone in this field was work by J. A. Armstrong et al. who theoretically investigated essential issues and presenting explicit analytical solutions to three and four coupled wave nonlinear equations. They proposed, for the first time, that the phase matching condition could be fulfilled by periodically changing the sign of nonlinear susceptibility of the media [14]. This technique, now known as quasi-phase matching (QPM), has become a widely used solution to the problem of phase mismatch.

Additionally, the work of Kleinman, who published a paper discussing the physical mechanisms of nonlinear dielectric polarization in optical media, greatly facilitated the study of nonlinear optics [15]. He systematically studied the notation used to describe nonlinear properties of crystals and greatly simplifying calculations. Midwinter and Warner also made significant contributions by investigating the effect of symmetry properties on the strength of the phase-matched output signal for non-centrosymmetric uniaxial crystals and tabulating the second-order susceptibility tensor for each of the uniaxial crystals [16].

Since then, the field of nonlinear optics has progressed rapidly and expanded into new areas with the help of tunable lasers and ultra-short pulsed lasers. Include a wide range of sophisticated applications, such as nonlinear optical microscopy[17], high-energy laser sources, laser material processing[18], and laser pointers. Additionally, it plays a crucial role in optical signal processing[19], quantum communication, quantum sensing, and quantum computing[20]. The exploration of nonlinear optical materials has become increasingly diverse, with many types of materials, including ferroelectric crystals[21], 2D material [22], and semiconductors[23], [24], demonstrating nonlinearities. Even materials that do not inherently possess nonlinearity can be manipulated to exhibit nonlinear properties by applying electric field or other methods to disrupt their internal structural symmetry[25].

The goal of this chapter is to provide a review of the background of nonlinear optics in quadratic media. We will begin by giving a brief introduction to the Quasi-Phase Matching (QPM) technique and explaining how it can be achieved through nonlinear photonics crystal fabricated by electric poling methods. Following this, we will introduce the concept of nonlinear photonic crystals (NPCs) and provide examples of past 1D NPC research. Next, we will discuss more complex 2D NPCs and their applications in nonlinear wavefront shaping, including transverse nonlinear wavefront shaping and in-plane nonlinear wavefront shaping. We will then explore how the latest laser poling techniques have successfully expanded the fabrication of NPC structures into 3D and review the most recent research findings in 3D NPCs. Finally, we will present the motivation for this thesis and outline the content structure of the subsequent chapters.

1.3 Quasi-phase matching

Quasi-phase-matching (QPM) is an important technique for frequency conversion in nonlinear optics, first proposed by J. Armstrong and others in 1962[14]. In 1998, V. Berger extended it to two-dimensional structures and introduced the concept of nonlinear photonic crystals[26]. Efficient nonlinear processes require a stable phase difference between the interacting light waves, but the dispersion characteristics of nonlinear crystals make it difficult to achieve this requirement. The phase velocity difference caused by dispersion must be compensated in some way to achieve phase matching. The reciprocal lattice vectors, which representing periodicity of nonlinearity modulation, provided by nonlinear periodic structures can help to achieve phase matching. By constructing periodically modulated $\chi^{(2)}$ structure in nonlinear media (nonlinear photonic crystals), they can effectively implement efficient nonlinear processes. Compared with conventional perfect phase matching (temperature matching, angle matching), this method, called quasi-phase matching, allows one to utilize larger effective nonlinear coefficients and avoid the spatial walk-off effect[27]. As a result, this technique has now been widely applied in the field of nonlinear optics and has achieved some phenomena that are difficult to achieve in conventional crystals.

Although the theory of quasi-phase matching was proposed early on, the implementation of phase matching in the first 25 years of nonlinear optics was primarily achieved through birefringent matching. This limitation was mainly due to the immature crystal growth and polarization technology at the time, which made it challenging to prepare nonlinear photonic crystals with micron-scale periodic structures. It was not until the 1990s that the development of lithography and other micro-nano fabrication technologies paved the way for the fabrication of nonlinear photonic crystals. In 1993, Yamada and colleagues first employed the method of electric poling to create an optical superlattice[28]. In 1995, M. Fejer and others fabricated bulk periodically poled lithium niobate (PPLN) crystals [29]. In 1997, N.B. Ming and colleagues developed a quasi-periodic polarization optical superlattice and, for the first time, used a single beam of light and a single crystal to generate green light at the third harmonic [30]. In 1999, N. Broderick and colleagues created the first two-dimensional nonlinear photonic crystal and verified nonlinear Bragg diffraction [31]. In 2018, T. Xu and D. Wei independently fabricated three-dimensional nonlinear photonic crystals, enabling 3D QPM[32], [33].

Currently, quasi-phase matching technology in nonlinear photonic crystals is widely employed in the generation of second, third, and higher harmonics, as well as in parametric conversion processes.

1.3.1 Electric poling

Ferroelectric crystals are the most commonly used nonlinear materials, and by periodically reversing their polarization or performing domain reversal, the sign of the nonlinear coefficient can be periodically changed, thereby achieving QPM. External electric field poling (EEP) is an important technology for achieving controllable domain reversal of ferroelectric crystals. This technique was first proposed by Matsumoto et al. in 1991, who deposited periodic aluminum electrodes on the +z surface of LiTaO3 crystals, raised the crystal temperature close to the Curie temperature to reduce the coercive field, applied a small electric field to polarize the crystal beneath the electrodes, and then lowered the temperature to lock the polarization status [34]. This polarization method relies on high temperatures near the Curie temperature, which can cause a series of issues, such as crystal aging. In 1993, Yamada et al. successfully prepared periodically poled lithium niobate (PPLN) at room temperature using external electric field poling and achieved a second harmonic generation (SHG) normalized conversion efficiency of up to 6 W^{-1} [28]. Myers et al. further improved the electric field poling technology based on this work [29]. They used lithography techniques to create high-precision periodic electrodes on the crystal surface and used electrolytes as electrodes. This technology remains the most mainstream electric field poling technology to this day. Following is a sketch of such electric poling technique.

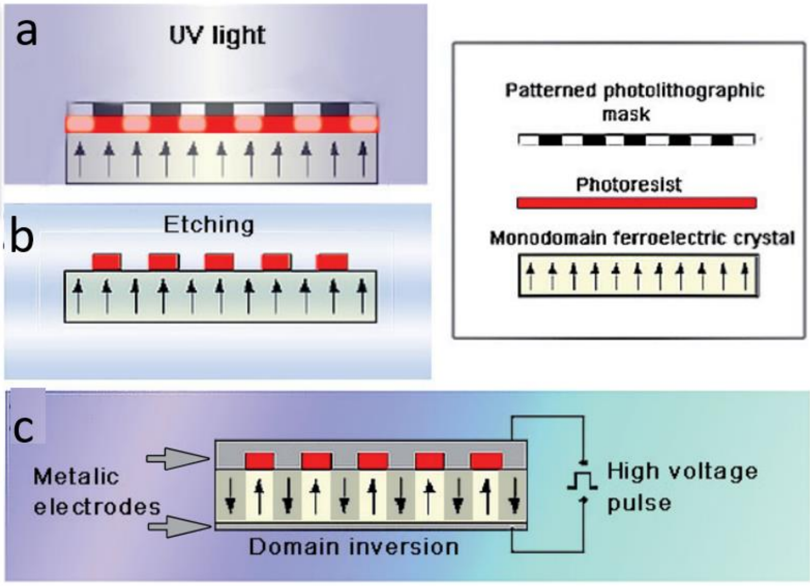

Figure 1.3.1 The concept of electrical poling. a) Photolithography of a photoresist-coated ferroelectric crystal. b) Etching of exposed areas in the photoresist. The top and bottom surfaces of the crystal are then coated with electrodes. c) A high voltage pulse reverses the sign of the electrical dipoles in areas in which the top metal is in contact with the crystal [35].

With the advancement of electric field poling technology and the successful fabrication of periodically poled nonlinear materials, researchers began to explore more complex structures for nonlinear optical processes. In the following section, we will delve into the development and applications of 1D NPCs.

1.3.2 1D NPCs

One-dimensional nonlinear photonic crystals (1D NPCs) with periodic polarization along a single direction represent the simplest and most widely used nonlinear photonic crystal structures. A single period Λ can provide the maximum reciprocal lattice vector $G = 2\pi/\Lambda$, to satisfy phase matching in nonlinear optical processes, thus achieving high-efficiency frequency conversion. However, the working wavelength and reciprocal lattice vector often correspond one-to-one, meaning that single-period nonlinear photonic crystals cannot simultaneously satisfy nonlinear processes at different wavelengths. To address this issue, in 1996, Myers et al. fabricated a periodically poled lithium niobate (PPLN) nonlinear photonic crystal with multiple gratings with different periods [36]. As shown in Figure 1.3.2 (a), 25 gratings are arranged side by side, each with periods ranging from 26 μm to 32 μm. The multi-grating QPM optical parametric oscillator (OPO) built with this crystal can efficiently generate output light with wavelengths ranging from 1.36 μm to 4.83 μm when pumped with a 1.064 μm laser. A schematic representation of this configuration is shown in Figure 1.3.2 (b).

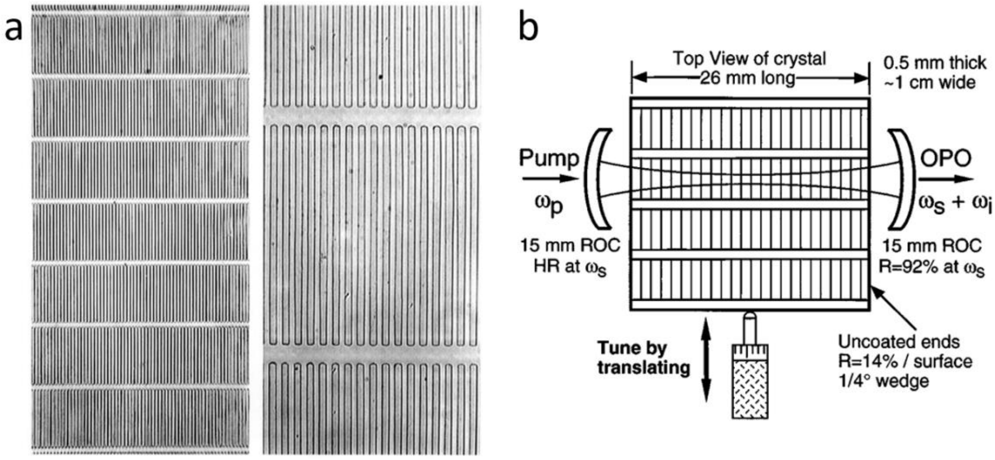

Figure 1.3.2 a) Portion of the +z surface of multi-QPM PPLN after HF etching to visualize the domain structures. The periods of gratings are from 26 to 32 um with a step of 0.25 um. Left column shows gratings with period from 29 to 30.5 um and right column show a magnified image of the grating with 29 um period. b) Sketch of the multi-grating QPM OPO setup. Translate the NPC in cavity to make the pump interact with different gratings. ROC, radius of curvature. HR, highly reflective [36].

The working principle of multi-grating structures is quite intuitive and easy to fabricate. However, due to the presence of period gaps between adjacent gratings, these NPCs cannot provide all the required reciprocal lattice vectors within a wavelength range, necessitating the use of temperature adjustments to assist in achieving truly broadband phase matching. To overcome this limitation, Powers et al. fabricated an optical parametric oscillator (OPO) based on a fan-out PPLN crystal in 1998 [37]. As illustrated in Figure 1.3.3, this nonlinear photonics crystal features continuously varying periods from small to large to provide a continuous range of reciprocal lattice vectors without the requirement for temperature adjustments. Fan-out NPC structures are still widely used in OPOs to this day.

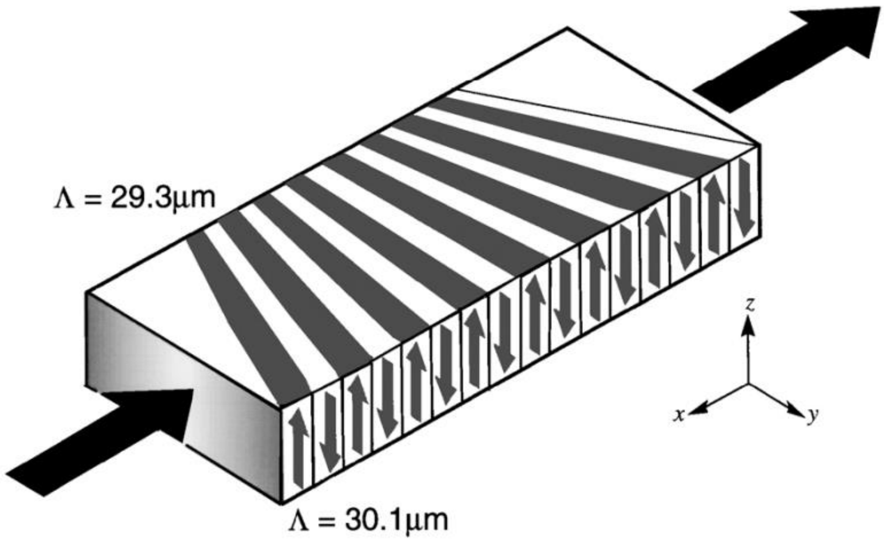

Figure 1.3.3 Sketch of the fan-out pattern on the PPLN crystal, the period differences are enlarged for better illustration. The arrows on the side of the crystal indicate the poling direction. By shifting the position of this crystal in the cavity, the laser only propagates through a single suitable period [37].

Although both multi-grating and fan-out PPLN possess two-dimensional (2D) structures physically, they are essentially still the simplest single-period nonlinear photonic crystals. This is because, under working conditions, the laser interacts only with the single-period crystal structure, keeping their nature fundamentally one-dimensional.

During the same period, researchers also conducted studies on longitudinal multi-period 1D NPCs. A landmark work by Kintaka et al. demonstrated third harmonic generation (THG) using two abutting PPLN crystals with different periods, producing 335 nm wavelength ultraviolet light [38]. The first section of PPLN crystal doubled the frequency of the pump light, and the second section of PPLN crystal performed sum frequency generation (SFG) with the newly generated second harmonic and the pump light. Additionally, Arbore et al. fabricated periodically chirped gratings to accommodate broadband wavelength conversion[39]. Another versatile achievement was the summed Fourier component gratings proposed by Norton and Sterke[40]. Their design method superimposed structures with different periods, theoretically enabling the generation of any set of reciprocal lattice vectors on a single 1D NPC. This result not only has significant implications for the design of 1D NPCs, but can also be extended to 2D and 3D NPCs.

With the development of 1D NPCs and the growing understanding of their capabilities and limitations, researchers have sought to extend the concept of periodic structures into higher dimensions. This has led to the exploration of two-dimensional (2D) nonlinear photonic crystals, which offer increased flexibility and versatility for unprecedented functions, especially the nonlinear wavefront shaping. In the following section, we will delve into the topic of nonlinear wavefront shaping in 2D NPCs and discuss the advantages and applications of more complex structures.

1.4 Nonlinear wavefront shaping in 2D NPCs

In 1998, Berger theoretically investigated the possibility of extending photonic crystals to 2D and expanded some concepts from linear photonic crystals to the field of nonlinear optics. The concepts he proposed, such as the nonlinear Bragg law and the nonlinear Ewald shell, provided a theoretical framework for the subsequent design of more complex 2D and 3D NPCs [26]. In 2000, Broderick et al. first reported the fabrication of 2D NPCs, with the structure of their NPCs shown in Figure 1.3.1. The hexagonal lattice provides multiple directions with different lengths of reciprocal lattice vectors, supporting a wider variety of nonlinear processes [31]. Their technique for fabricating 2D NPCs has excellent versatility and has been used in subsequent follow-up studies to create complex 2D NPC structures including quasicrystals. A wide range of 2D NPCs has been studied since then, realizing applications such as third and fourth harmonics, simultaneous wavelength interchange, all-optical deflection, and splitting, etc [41], [42], [43], [44].

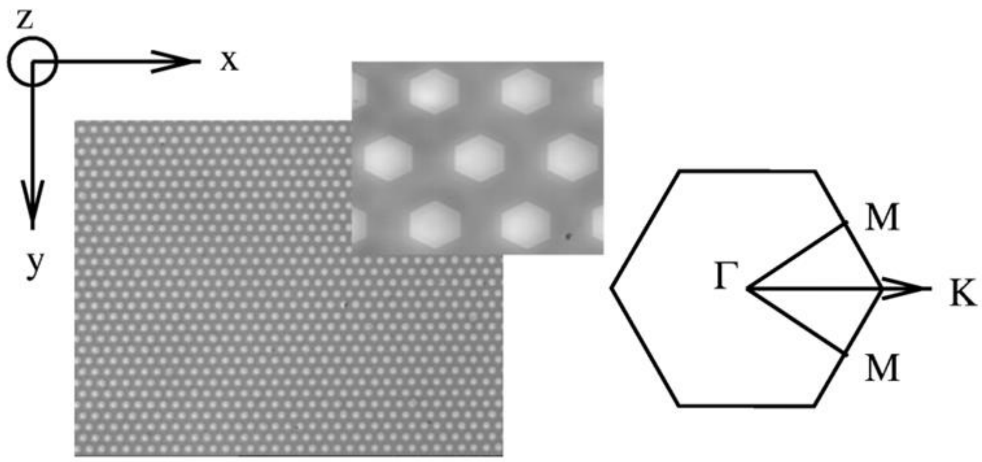

Figure 1.4.1 Left: image of the hexagonal periodically poled nonlinear crystal with a period of 18.05um. Right: the first Brillouin zone of the nonlinear photonics crystal [31].

An unprecedented function of 2D NPCs is nonlinear wavefront shaping, which cannot be achieved by 1D NPCs. In the earlier-discussed nonlinear processes, laser beams have simple Gaussian profiles, and additional optical elements are needed for shaping to fit the application environment. However, this shaping work can be directly accomplished by NPCs. Nonlinear wavefront shaping not only reduces costs but also simplifies the system by reducing optical elements. It can achieve functions that are difficult to realize in linear optics, such as all-optical control of beam parameters [45]. NPCs are not only limited to shaping the spatial distribution of the laser beam but can also shape the laser pulse in the time domain [46], [47]. These unique properties make nonlinear wavefront shaping of great research value in the fields of optical trapping, optical communication, super-resolution microscopy, and quantum optics. In the subsequent sections of this chapter, several landmark nonlinear wavefront shaping works will be introduced.

1.4.1 In-plane nonlinear wavefront shaping

The initial work on nonlinear wavefront shaping was carried out by Imeshev and his colleagues in 1998. In this study, they achieved non-uniform second harmonic generation (SHG) by varying the length of the QPM grating laterally. Under the premise of Gaussian pump light, they produced a flat-top profile SH in the near field[48]. The schematic of the structure is shown in Figure 1.4.2. Subsequently, Ellenbogen et al. designed an all-optical deflector based on nonlinear photonic crystals using a similar approach. This deflector can generate multiple Gaussian beams in different directions by changing the experimental conditions [49].

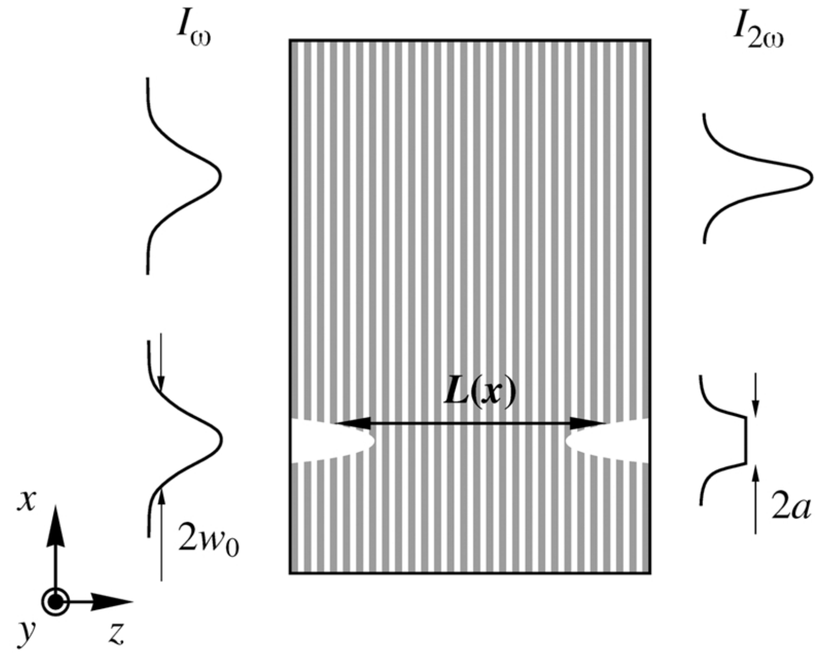

Figure 1.4.2 A QPM grating containing a region of unmodulated material (white region on sketch) whose length decreases with distance from the beam axis results in the effective interaction length's being shorter in the center and longer in the wings of the beam, resulting in a flat top Gaussian output.

Not only can the intensity of nonlinear light be directly modulated by NPCs, but the phase can also be controlled. The first realization of phase control for nonlinear light was accomplished by Kurz et al., who created a nonlinear lens [50]. As shown in Figure 1.4.3, they achieved cylindrical lens focusing of the second harmonic by transverse patterning of periodic gratings for quasi-phase-matching (QPM). Later, Ellenbogen et al. used a similar technique to generate a nonlinear Airy beam, a unique type of light beam that accelerates during propagation [51]. In this study, the authors actually employed a rather versatile NPC design theory to achieve arbitrary nonlinear wavefront shaping. A more systematic summary of research was later accomplished by Shapira and his colleagues in a series of studies, where they introduced nonlinear computer-generated holograms, which have since become one of the most practical design method for nonlinear wavefront shaping [52], [53], [54].

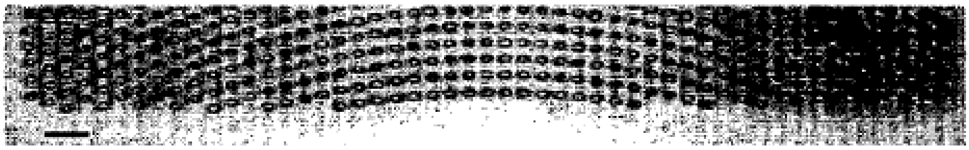

Figure 1.4.3 Transverse patterning of periodic gratings with a parabolic phase for quasi-phase-matching. Scale bar indicate a length of 50μm [50].

1.4.2 Transverse nonlinear wavefront shaping

All research works on nonlinear wavefront shaping mentioned above share a common characteristic: lights propagation occurs within the same plane, and beam shaping is limited to one dimension. In 2007, Bahabad and Arie proposed a 3D NPC structure with spiral shape supporting two-dimensional nonlinear wavefront shaping, but at that time, the external electric field poling technique is a planar process, unable to support the fabrication of complex 3D NPCs [55]. In fact, 2D NPC structures can support two-dimensional nonlinear wavefront shaping. However, due to significant differences in design approaches, researchers overlooked this possibility for some time. It was not until 2012 that Bloch et al. fabricated a fork-like 2D NPC on stoichiometric lithium tantalate crystals using electric field poling, generating a nonlinear vortex beam in a transverse configuration, as shown in Fig 1.4.4 [56]. The theory of this transverse nonlinear wavefront shaping was soon summarized by Shapira from the same research group, who developed a computer-generated nonlinear holography method applicable to 1D, 2D, and even 3D NPC structures [52], [53].

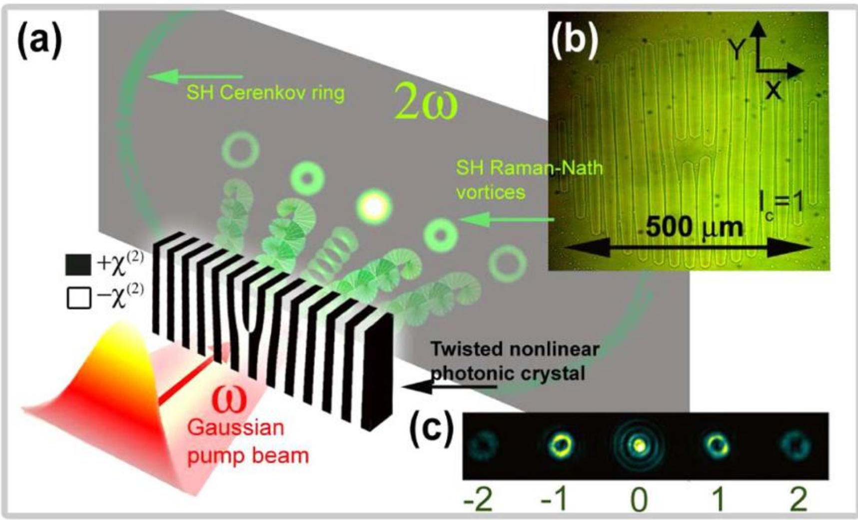

Figure 1.4.4 (a) A Gaussian pump beam transversely enters a fork shaped 2D nonlinear photonics crystal, several nonlinear vortex beams are generated. (b) Image of the 2D NPC, fork shaped domain pattern is revealed after etching. (c) Experimental image of the generated nonlinear vortex beams[56].

Although transverse nonlinear wavefront shaping based on 2D NPCs can generate complex 2D nonlinear structured light, the nonlinear conversion efficiency is extremely low due to the inability to satisfy phase-matching conditions, significantly limiting its development and application. A solution to this problem was proposed by Bahabad and Arie, which is to extend the NPC structure to 3D, achieving phase matching while realizing 2D nonlinear wavefront shaping [55]. However, the limitations of the poling process kept this solution theoretical until 2018 when Xu and Wei independently fabricated 3D NPCs using infrared femtosecond laser direct writing technique [32], [33]. Since then, research on 3D NPCs has once again gained momentum, and we will introduce key research findings in the next section.

1.5 3D NPC

When Berger proposed the concept of NPCs in 1998, there were no available technologies for fabricating 3D NPCs. Therefore, experimental research on

NPCs focused on 1D and 2D structures for an extended period. However, valuable theoretical research on 3D NPCs was conducted by researchers, such as Bahabad and Arie, who proposed a 3D NPC structure capable of generating nonlinear optical vortices[55]. Chen and his team carried out a series of studies exploring QPM in 3D NPCs and generating conical and spherical second harmonics through 3D NPCs[57], [58]. Hong et al. designed and fabricated 2D NPCs using nonlinear volume holography theory, which can also be extended to 3D[59].

Compared to 2D NPCs, the additional dimension of nonlinearity modulation provided by 3D NPCs offers unprecedented possibilities for controlling nonlinear processes, A comprehensive example is nonlinear photonic chips, where varying the input light signal parameters can yield different nonlinear light outputs at the output end[60]. In terms of nonlinear wavefront shaping, 3D NPCs can theoretically not only perform complex nonlinear light modulation but also significantly improve nonlinear conversion efficiency. Due to the advantages and potential applications of 3D NPCs mentioned above, researchers have been seeking a viable 3D NPC fabrication technique for over 20 years. It was not until 2018 that Xu and Wei independently fabricated 3D NPCs using two different fabrication techniques based on infrared femtosecond laser direct writing[32], [33]. These two techniques will be discussed in detail in this chapter.

1.5.1 Laser poling technique

The initial research on laser poling of ferroelectric crystals was not focused on exploring fabrication techniques for 3D NPCs but rather on overcoming some technical drawbacks of external electric field poling. For instance, sideway growth limits the precision of electric field poling, making it unsuitable for fabricating devices with high spatial frequencies [61], [62], [63]. Additionally, electric field poling is difficult to apply to x-cut or y-cut ferroelectric crystals, while some nonlinear optical devices need to be fabricated on x-cut crystals, such as electro-optic modulators and whispering gallery mode (WGM) harmonic resonators [64]. Moreover, traditional external electric field poling techniques rely on photolithography, which makes the entire poling process complex and expensive, particularly for large-area poling. Due to these reasons, researchers have turned their attention to light-assisted poling or even all-optical poling techniques. These approaches promise improved precision, compatibility with various crystal cuts, and the potential for more cost-effective and simpler fabrication processes, especially when working with large-area or complex devices.

Researchers initially used ultraviolet (UV) light for studies on optical poling because common nonlinear ferroelectric crystals exhibit strong absorption of UV light, allowing UV to strongly interact with the material and alter its properties. One widely studied UV light poling technique is poling inhibition, in which focused UV light is used to pre-treat the crystal surface before traditional electric field poling. The pre-irradiated crystal is less susceptible to polarization during electric field poling, allowing controlled crystal polarization [65], [66]. Another optical poling technique is all-optical poling, also known as direct laser poling, in which a laser is used to directly perform domain inversion on ferroelectric crystals without the need for further processing. This technique was first proposed by Muir et al., who used focused UV light with a wavelength of 244 nm to scan the z surface of a lithium niobate crystal, successfully achieving direct laser poling [67]. As shown in Figure 1.5.1, they found that the laser power and scanning speed strongly influenced the quality of domain inversion. As the conditions changed from low laser power and high scanning speed to high laser power and low scanning speed, the inverted domains in the crystal gradually transitioned from discrete scattered points to large-area, uniform domains.

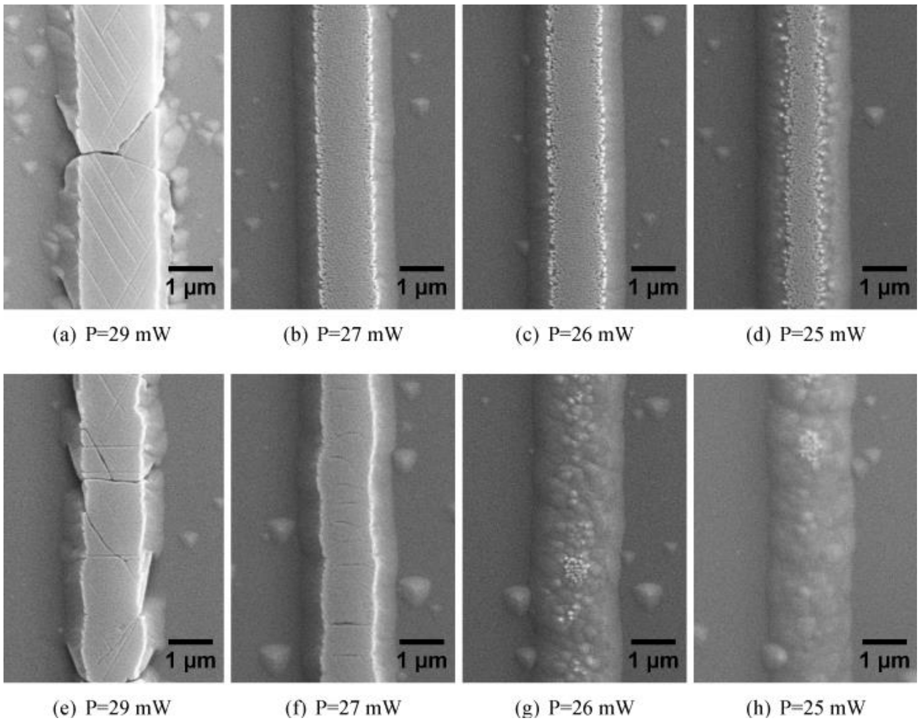

Figure 1.5.1 Domain structures under different scanning speeds and laser powers. The laser irradiates the -z face of the lithium niobate crystal, and the scanning direction is in the y-direction. The images are SEM images taken after HF etching. The first row has a scan speed of 50 μm/s. The second row has a scanning speed of 200 μm/s [67].

Steigerwald et al. later successfully performed direct laser poling on x and y surfaces of lithium niobate crystals using UV light [68]. Their work convincingly described the mechanism of direct laser poling: the crystal absorbs light energy, causing localized heating and a temperature gradient, which in turn induces a thermoelectric field that causes domain inversion within the crystal, sketch shown in Fig 1.5.2. This theory has had a guiding significance for the development of direct laser poling techniques in subsequent research. However, UV light poling has some inherent drawbacks that are difficult to overcome. Due to the high power of UV light, the poling process often involves unavoidable high-temperature damage to crystals. Moreover, because of the high absorption rate of UV light by the crystal, the poling laser has difficulty penetrating deep into the crystal to achieve deep poling or 3D poling [69].

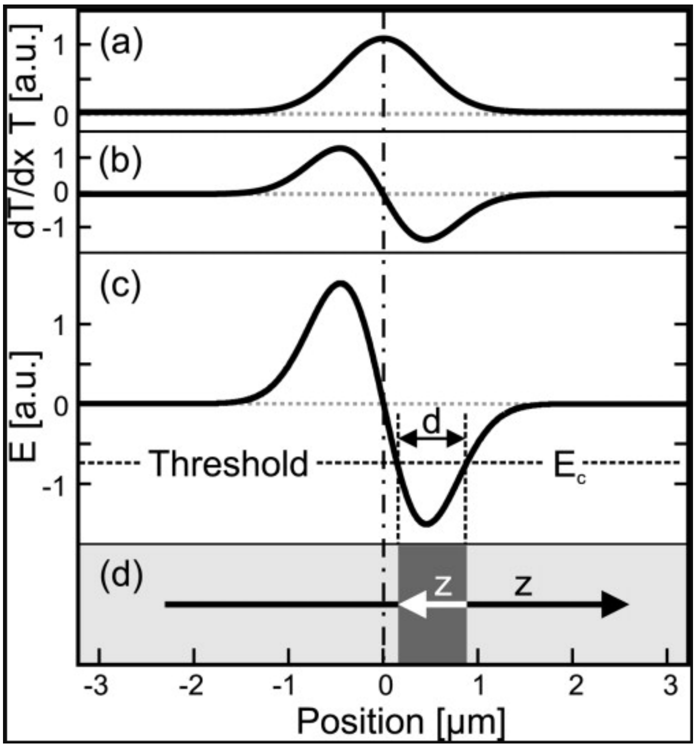

Figure 1.5.2 Schematic diagram of the mechanism of laser direct poling on x and y-cut crystals. (a) The crystal absorbs UV light, causing a local temperature increase, (b) the uneven temperature causes a temperature gradient, (c) the temperature gradient further induces a thermoelectric field, and the intensity of this electric field within a region with a width of d exceeds the coercive field of the crystal, (d) subsequently causing domain inversion within this region [68].

In order to overcome the limitations of UV light poling techniques mentioned earlier, researchers turned their attention to near-infrared (NIR) femtosecond laser direct poling. Since most nonlinear crystals have good transparency to near-infrared light, NIR light can easily penetrate into the crystal, giving the potential for 3D poling using infrared light. However, the transparency of the crystal to infrared light also raises a problem, which is the weak interaction between the light wave and the crystal. To allow infrared light to strongly interact with the crystal and achieve poling, researchers utilized the nonlinear absorption of the crystal to achieve this goal. Different from UV light exerting influence on the crystal through linear absorption, the interaction between femtosecond infrared light and the crystal is based on nonlinear absorption. This process strongly depends on the intensity of light, and only an extremely strong light field can cause significant nonlinear absorption. The high-energy pulses of femtosecond lasers perfectly meet this requirement.

Xin et al. were the first to achieve controllable domain inversion on the z-face of lithium niobate crystals using near-infrared femtosecond lasers with 800nm wavelength, and they used this technique to fabricate NPCs that could be used for QPM [70], [71]. Although in their results, the near-infrared femtosecond laser direct poling technique did not overcome the main limitations of traditional poling techniques to achieve 3D poling, the advantages of this technique were already beginning to show. Unlike the external electric field techniques that require complex and expensive lithography techniques, also, this technique does not cause permanent crystal damage like UV poling techniques. Subsequently, Xu et al. and Wei et al. independently fabricated 3D NPCs using two different infrared femtosecond direct writing techniques [32], [33].

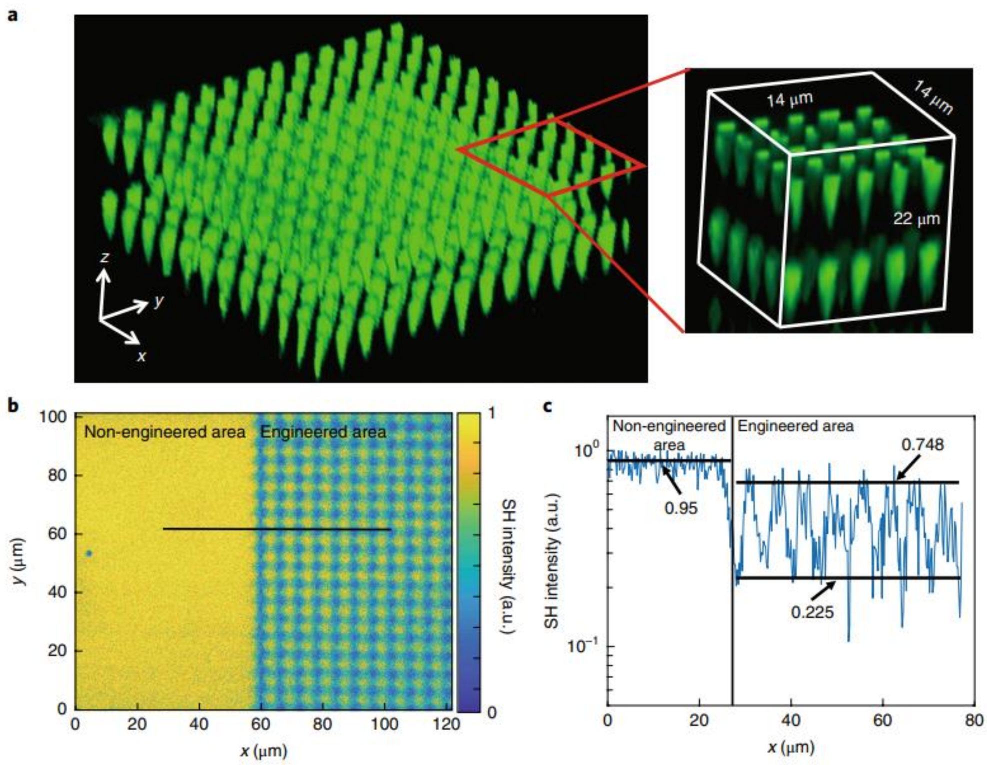

Figure 1.5.3 (a) χ^2 erasing type 3D NPC nonlinear confocal microscopy image. Two layers of periodical structures are clearly shown. (b) SH intensity map of laser engineered crystal on x-y plane, captured by a nonlinear confocal microscope. (c) SH intensity distribution corresponding to the line in (b). [32]

In Wei et al.'s work, they used a special technique of laser χ^2 erasing to achieve the fabrication of 3D NPCs in lithium niobate crystals, the nonlinear confocal image of such 3D NPC is shown in Figure 1.5.3 (a). This laser engineering technique was first proposed by Thomas et al., but they only used it to manufacture 1D and 2D NPCs without extending it to 3D [72]. Instead of modulating χ^2 through ferroelectric domain inversion, they used stronger pulsed lasers to locally decrystallize the crystal, thereby reducing the nonlinear coefficient of the nonlinear crystal (Figure 1.5.3 (b) and (c)). As shown in Figure 1.5.4 (blue line), the 3D NPCs fabricated in this way have lower conversion efficiency during QPM process compared to traditional periodically poled NPCs, but the second harmonic conversion efficiency is still much better than that of the original crystal without any phase matching. One major advantage of this laser processing technique is that it does not require overly stringent requirements for materials and lasers. In theory, as long as micrometer-level damage is caused inside the nonlinear crystal, the modulation of the nonlinear coefficient can be achieved. A good example is Lithium Niobite, as the most common nonlinear crystal material, has a high Curie temperature and coercive field, making it extremely difficult to perform 3D poling. This technique bypasses this technical challenge. Moreover, since the modulation of the nonlinear coefficient in this technique is not based on ferroelectric domain inversion, it can be used to process non-ferroelectric nonlinear materials, such as quartz and semiconductor. However, modulating the nonlinear coefficient in the form of amorphous crystal also has its inherent drawbacks. In addition to the lower QPM efficiency mentioned earlier, this technique also introduces additional changes in the refractive index. The changes in structure of the material causes strong light scattering, leading to power loss, and making the design of the polarization period difficult to predict. The disturbance of the refractive index not only interferes with the QPM process but also introduces noise during wave shaping in 3D NPCs. Due to the continuous accumulation of noise during light propagation, the adverse effects of refractive index changes on large-volume 3D NPCs can render them completely unable to function normally[73].

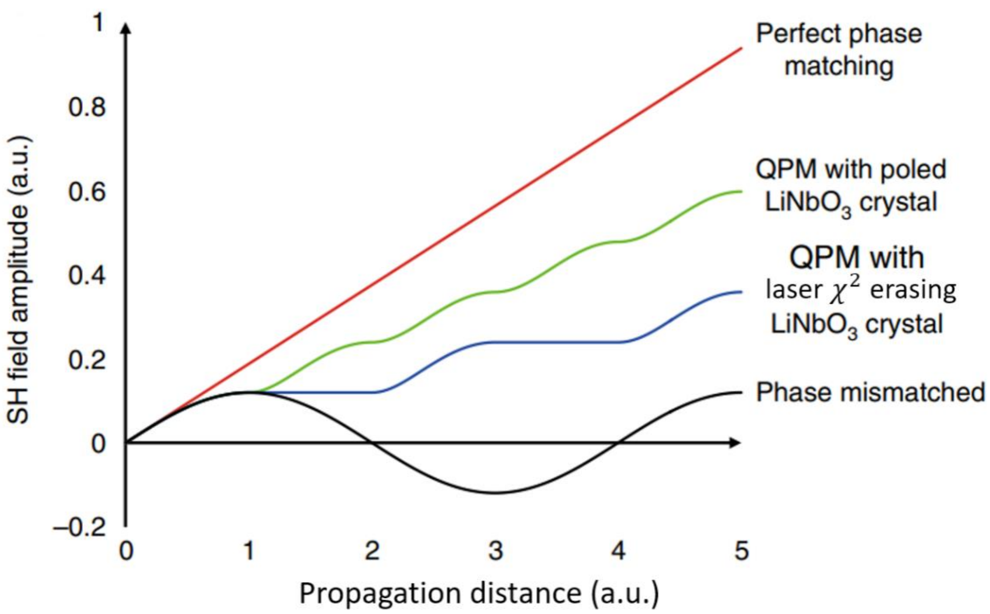

Figure 1.5.4 Amplitude of second harmonic field generated in parametric wave interaction as a function of propagation (interaction) distance. In the case of phase mismatch between fundamental and SH, the amplitude of the SH will vary periodically and cannot accumulate (black line). In the case of perfect phase matching, the SH field amplitude will increase linearly with propagation distance (red line). QPM based on periodically poled NPC allows the SH field amplitude to oscillate and increase as it propagates (green line). QPM based on laser χ^2 erassure can also cause the SH field amplitude to oscillate and increase with propagation, but the rate of increase is weaker than that of QPM based on ferroelectric domain inversion (blue line). [32]

Xu's 3D NPC was created by using femtosecond infrared lasers to perform periodic domain inversion on ferroelectric crystals barium calcium titanate (BCT, $Ba_{0.77}Ca_{0.23}TiO_3$). The principle of this technique is almost identical to that of UV laser poling, in which the focused laser spot locally heats the crystal to form a thermal gradient. This then induces a thermoelectric field to polarize the crystal [68]. Unlike UV poling, which can only be implemented on the surface of nonlinear crystals due to strong absorption of UV light, the femtosecond infrared laser used by Xu can penetrate the crystal and interact with it through nonlinear absorption. Since this technique is based on ferroelectric domain inversion, it can achieve perfect QPM under ideal conditions (green line in Figure 1.5.3) and avoid the side effects of refractive index changes. In fact, the side effect of refractive index changes caused by laser direct writing on crystals is always difficult to avoid, but as long as the crystal atoms still maintain their lattice structure, fluctuations in the refractive index can be eliminated through annealing [70]. However, this technique has its limitations. Although it employs laser beam, it essentially relies on an electric field to reverse ferroelectric domains, making it challenging to work with ferroelectric crystals with large coercive fields and high Curie temperatures. Unfortunately, the most commercially valuable nonlinear crystals, such as lithium niobate, often have these characteristics. Furthermore, the mechanism of this technique needs further exploration, as the UV poling mechanism cannot explain all experimental phenomena. Numerous factors play a role in the laser writing process, including but not limited to stress caused by temperature, charge distribution, and the influence of higher harmonics on poling.

In summary, the two different infrared femtosecond laser writing techniques for 3D NPC fabrication are breakthrough works in this research field. However, both techniques have their drawbacks and large room for improvement, warranting further exploration by researchers. In this thesis, the mechanism and optimization of laser-induced ferroelectric domain inversion technology will be discussed in subsequent chapters.

1.5.2 Advantages and potential of 3D NPCs in nonlinear wavefront shaping

The importance of nonlinear photonic crystals in the field of nonlinear optics is unquestionable, as they serve as the underlying basis for many significant phenomena and applications. The transition from 2D to 3D in such fundamental structures leads to substantial and comprehensive changes, benefiting numerous research areas related to nonlinear optics, such as quantum optics, quantum communications, and optical signal processing. Considering that this thesis focuses on NWS, this section will discuss content relevant to NWS.

For NWS, the most apparent benefit brought by 3D NPCs is the improvement in efficiency. Section 1.3.2 mentioned the use of 2D NPCs for NWS, but the nonlinear conversion efficiency in these works is extremely low. This is limited by the inability of 2D NPCs to provide reciprocal lattice vectors in the light propagation direction to satisfy QPM conditions. In contrast, 3D NPCs can easily solve this problem by simply repeating specific 2D structures in the light propagation direction to meet the QPM conditions and achieve high-efficiency

NWS. The advancements brought by 3D NPCs in NWS are not limited to this aspect. Direct IR laser writing technology can construct arbitrary complex $\chi(2)$ structures in space, making multifunctional NWS possible. Unlike previous NWS based on 2D NPCs that could only have a single shaping function, multiple different NWS functions can be superimposed within a single NPC through the additional dimension provided by 3D NPCs. This technology has important applications in optical signal processing and encryption [74]. On the other hand, some previously theoretical studies can now be experimentally verified, such as realizing true nonlinear volume holography and generating optical vortex beams through 3D spiral structures. The processing of signals by 3D NPCs is also a research direction worth exploring. Unlike linear optics or 2D NPCs, 3D NPCs can integrate multiple functions on a single crystal to affect different input lights differently. This technology can be used for high-dimensional multiplexing of optical signals, including wavelength multiplexing, directional multiplexing, and optical vortex charge multiplexing. Furthermore, 3D NPCs made based on domain inversion are theoretically erasable and reusable, making programmable nonlinear photonic chips a possibility.

1.6 Motivation and thesis arrangement

Although the fundamental theory of nonlinear photonic crystals (NPCs) has matured and numerous real-world applications have been developed, research on NPCs has historically focused on 1D and 2D NPCs due to the limitations of traditional fabrication techniques. Research on 3D NPCs has been largely limited to speculative theoretical work without the possibility of practical experimentation. However, the recent emergence of femtosecond laser direct writing techniques for NPC fabrication has made the fabrication of 3D NPCs feasible. This breakthrough technology has significantly expanded the potential applications of NPCs, making previously theoretical applications possible.

Furthermore, since the fabrication of 3D NPCs was previously confined to theoretical discussions, few researchers have devoted significant effort to studying 3D NPCs, leaving ample room for exploration in this field. On the other hand, laser direct writing, as a relatively new technology, has not yet reached maturity. The fundamental physical principles underlying this technology require further investigation, and there is significant room for improvement in its practical application.

This thesis aims to address the opportunities and challenges associated with 3D NPC design theory and fabrication processes. The content is organized as follows:

Chapter 2: Introduction of fundamental in NPCs

In this chapter, we will introduce the fundamental knowledge of nonlinear optics, along with some commonly used mathematical tools and analysis methods. This includes a more detailed description of the physical process of phase matching, the mathematical representation of reciprocal lattice vectors for periodic structures, and the powerful tool of Fourier transform.

Chapter 3: Nonlinear wave front shaping in 3D NPC

In this chapter, we will introduce 3D NPCs in CBN crystals fabricated by femtosecond laser direct-write poling techniques. Unlike traditional 1D or 2D NPCs, the 3D NPCs we prepared can incorporate multiple nonlinear wave front shaping functionalities within a single crystal and can dynamically adjust these functions by changing the incident laser. These unprecedented capabilities can only be achieved by 3D NPCs. The relevant work has already been published [75].

Chapter 4: Nonlinear volume holography

In this chapter, we continue our previous research and refine the design of the 3D NPC structure to satisfy phase matching conditions in the collinear direction, thereby significantly improving the nonlinear conversion efficiency. In this study, we used the nonlinear volume holography theory to design a nonlinear volume hologram that can produce a nonlinear vortex beam, and completed the processing in a nonlinear crystal using femtosecond laser writing techniques. This design theory and fabrication method have a high degree of universality, allowing us to design 3D NPCs to produce any desired nonlinear beams. The relevant work has already been published [76].

Chapter 5: Optimization of laser poling

In Chapter 4, we successfully fabricated nonlinear volume holograms and achieved a higher nonlinear conversion efficiency than before. However, the limitations of the laser poling process prevented us from achieving industrially valuable high efficiency in nonlinear conversion. This is primarily due to the difficulty of processing deep within the crystal using existing laser poling techniques, and the impact of the poling process on the refractive index of the nonlinear crystal. In this chapter, we explored the intrinsic mechanisms of the interaction between lasers and nonlinear crystals during the laser poling process. Based on this understanding, we optimized the parameters of the laser poling technique. This optimization allowed the laser to fabricate large volumes of 3D NPCs deep inside the crystal, while minimizing the impact of the laser on the crystal’s refractive index to the greatest extent possible. The relevant work has already been published [77].

Chapter 6: Highly efficient large volume 3D NPC

To achieve the most efficient nonlinear generation of special beams, we utilized the largest effective nonlinear coefficient of the nonlinear crystal during the design process of the nonlinear volume holography. Furthermore, we simplified the NPC structure as much as possible without compromising the final nonlinear beam output to facilitate fabrication. Ultimately, using the optimized laser poling technique, we produced a 1mm-long nonlinear volume hologram for the generation of a nonlinear vortex beam. The measured raw conversion efficiency reached as high as 4.6%, and normalize conversion efficiency reached $1.2 \times 10^{-5} W^{-1}$ when pumped with a CW laser. Such conversion efficiency is ~10^5 times higher than previous reported results. The relevant work has already been published [78].

Chapter 7: Conclusions and outlook

Chapter 2 Introduction of fundamental in NPCs

2.1 Introduction

In the first chapter, we introduced the history of NPC development and some important research results on nonlinear wavefront shaping based on NPCs. However, the relevant theoretical and technical details were not presented in detail. The purpose of this chapter is to provide a theoretical framework for readers to better understand the subsequent chapters. We will begin with the discussion of optical harmonic generation, followed by an explanation of how phase mismatch occurs and its impact on the efficiency of nonlinear optical frequency conversion. After that, we will introduce how to overcome the negative effects of phase mismatch, namely two phase-matching techniques: Birefringent phase matching and Quasi-phase matching. Based on the understanding of QPM technology, we will introduce the concepts of reciprocal lattice vectors and Fourier transformation. These two concepts play important roles in analyzing complex nonlinear processes and nonlinear wavefront shaping. Subsequently, we will introduce two commonly used NPC design methods for realizing nonlinear wavefront shaping, which are nonlinear volume holography and inverse Fourier transform. Finally, we will introduce the nonlinear materials we use for fabricating 3D NPCs.

2.2 Nonlinear optical interactions

In the field of optics, a fundamental problem is to describe the propagation of light in a medium and how light interacts with the medium. The propagation of light waves in a medium can be described using Maxwell's equations. When light waves propagate in a non-magnetic transparent medium, Maxwell's equations take the following form:

$$\nabla \times \boldsymbol{E} = -\frac{\partial \boldsymbol{B}}{\partial t} \tag{2.2.1}$$

$$\nabla \times \boldsymbol{H} = \boldsymbol{J} + \frac{\partial \boldsymbol{D}}{\partial t} \tag{2.2.2}$$

$$\nabla \cdot \boldsymbol{D} = \rho \tag{2.2.3}$$

$$\nabla \cdot \boldsymbol{B} = 0 \tag{2.2.4}$$

where $\boldsymbol{E}$ and $\boldsymbol{H}$ are electric and magnetic field vectors respectively, $\boldsymbol{D}$ is a dielectric displacement, $\boldsymbol{B}$ is magnetic induction, $\boldsymbol{J}$ is electric current density and ρ is electric charge density.

The material equations are:

$$\boldsymbol{B} = \mu_0 \boldsymbol{H} + \boldsymbol{M} \tag{2.2.5}$$

$$\boldsymbol{D} = \varepsilon_0 \boldsymbol{E} + \boldsymbol{P} \tag{2.2.6}$$

where ε_0 and μ_0 are the permittivity and permeability of the vacuum, $\boldsymbol{M}$ is magnetization and $\boldsymbol{P}$ represents polarization of the medium. In this thesis we consider charge and current free nonmagnetic medium, so $\rho = 0$, $\boldsymbol{J} = 0$ and $\boldsymbol{M} = 0$. By substituting material equations back to Maxwell's equations and eliminating H, we obtain the most general wave equation:

$$\nabla(\nabla \cdot \boldsymbol{E}) - \nabla^2 \boldsymbol{E} + \frac{1}{c}\frac{\partial^2 \boldsymbol{E}}{\partial t^2} = -\frac{1}{\varepsilon_0 c^2}\frac{\partial^2 \boldsymbol{P}}{\partial t^2} \tag{2.2.7}$$

Equation stated above describe the propagation of light waves in a non-magnetic transparent medium and can be used to explain numerous optical phenomena, such as reflection, refraction, birefringence, polarization, interference, and diffraction of light. In the following we will concentrate on quasi-plane wave solution to the equation 2.2.7. Hence the first term will be neglected as it is identically zero for plane wave.

When light propagates through a medium, the electrons in the medium resonate synchronously with the frequency of the light wave. This causes a relative displacement of the positive and negative charge centers of atoms or molecules in the medium, thus giving rise to the phenomenon of polarization. In isotropic media, the polarization ***P*** is directly proportional to the electric field ***E*** of the light. However, in anisotropic media the relationship between the polarization ***P*** and the electric field ***E*** is no longer a simple direct proportionality. Instead, it is expressed as:

$$P_i = \sum_j X_{ij} \boldsymbol{E}_j \tag{2.2.8}$$

In this equation, X_{ij} is the polarizability of the crystal. It is a second-order symmetric tensor, where i,j = 1,2,3, and it consists of nine components. However, this formula only applies in the case of low light intensity. When the light intensity is extremely high, the higher-order terms in equation play an important role in the polarization ***P*** of the media. The relationship between the polarization ***P*** and the light electric field ***E*** is:

$$P_{\boldsymbol{i}} = \sum_j \chi_{ij}^{(1)} E_j(\omega_1) + \sum_{jk} \chi_{ijk}^{(2)} E_j(\omega_1) E_k(\omega_2) + \sum_{jkl} \chi_{ijkl}^{(3)} E_j(\omega_1) E_k(\omega_2) E_l(\omega_3) \tag{2.2.9}$$

In this equation, $\chi_{ij}^{(1)}$ is the linear susceptibility of the media; $\chi_{ijk}^{(2)}$, $\chi_{ijkl}^{(3)}$... are the second and third order susceptibilities, etc. ω_1, ω_2, ω_3... are the angular frequencies of different optical electric field. The sum is over all nonlinear susceptibilities. Because the numerical values of each coefficient decrease by several orders of magnitude successively, only when the light intensity is sufficiently high, can the higher-order terms have a significant effect, thereby revealing nonlinear optical phenomena.

It's worth noting that in practice, nonlinear media exhibit losses, and the $\chi^{(n)}$ exhibits dispersion for light of different frequencies. This makes the associated calculations extremely complex, and often unnecessary, as losses and dispersion can be neglected in most cases. Under this assumption, one is able to reduce the number of matrix elements as all n+1 subscripts of the tensor matrix elements are interchangeable, what is known as the Kleinman's symmetry condition. Using $\chi^{(2)}$ as an example, we have $\chi_{ijk}^{(2)} = \chi_{ikj}^{(2)} = \chi_{il}^{(2)}$, j and k can be permuted by l:

$$[jk] = \begin{bmatrix} 11 & 12 & 13 \\ 21 & 22 & 23 \\ 31 & 32 & 33 \end{bmatrix} = [l] = \begin{bmatrix} 1 & 6 & 5 \\ 6 & 2 & 4 \\ 5 & 4 & 3 \end{bmatrix} \quad (2.2.10)$$

Then we have:

$$\underline{\underline{\underline{\chi^{(2)}}}} = \begin{pmatrix} \chi_{11}^{(2)} & \chi_{12}^{(2)} & \chi_{13}^{(2)} & \chi_{14}^{(2)} & \chi_{15}^{(2)} & \chi_{16}^{(2)} \\ \chi_{21}^{(2)} & \chi_{22}^{(2)} & \chi_{23}^{(2)} & \chi_{24}^{(2)} & \chi_{25}^{(2)} & \chi_{26}^{(2)} \\ \chi_{31}^{(2)} & \chi_{32}^{(2)} & \chi_{33}^{(2)} & \chi_{34}^{(2)} & \chi_{35}^{(2)} & \chi_{36}^{(2)} \end{pmatrix} \quad (2.2.11)$$

For SHG intensity calculation, we use second order nonlinear coefficient:

$$d_{il} = \frac{1}{2}\chi_{il}^{(2)} \quad (2.2.12)$$

The SH polarization:

$$\begin{bmatrix} P_x(2\omega) \\ P_y(2\omega) \\ P_z(2\omega) \end{bmatrix} = \varepsilon_o \begin{bmatrix} d_{11}^{(2)} & d_{12}^{(2)} & d_{13}^{(2)} & d_{14}^{(2)} & d_{15}^{(2)} & d_{16}^{(2)} \\ d_{21}^{(2)} & d_{22}^{(2)} & d_{23}^{(2)} & d_{24}^{(2)} & d_{25}^{(2)} & d_{26}^{(2)} \\ d_{31}^{(2)} & d_{32}^{(2)} & d_{33}^{(2)} & d_{34}^{(2)} & d_{35}^{(2)} & d_{36}^{(2)} \end{bmatrix} \cdot \begin{bmatrix} E_x(\omega)^2 \\ E_y(\omega)^2 \\ E_z(\omega)^2 \\ 2E_y(\omega)E_z(\omega) \\ 2E_x(\omega)E_z(\omega) \\ 2E_x(\omega)E_y(\omega) \end{bmatrix} \quad (2.2.13)$$

Furthermore, the 18 elements d_{ij} in the above matrix are not completely independent of each other. This is because the first two subscripts of the element are also exchangeable, i.e., $\chi_{ijk}^{(2)} = \chi_{jik}^{(2)}$, which means $d_{12} = d_{26}$. In addition, nonlinear mediums are often crystals with symmetric structures, further reducing the number of tensor matrix elements, as many elements will have a value of 0. For instance, the second-order nonlinear coefficient matrix for CBN crystal has form of [79]:

$$d_{il} = \begin{pmatrix} 0 & 0 & 0 & 0 & d_{15} & 0 \\ 0 & 0 & 0 & d_{15} & 0 & 0 \\ d_{31} & d_{31} & d_{33} & 0 & 0 & 0 \end{pmatrix} \quad (2.2.14)$$

The subscript l represents the polarization of the light wave. Thus, when the light wave has a specific polarization, we only need to consider the related nonlinear processes, further simplifying the calculation. For instance, when the light is linearly polarized along the x direction, only d_{i1} needs to be used in the calculation.

2.2.1 Harmonic generation

Light is an electromagnetic wave, and when it propagates in a nonlinear crystal, the periodically changing electric field drives the charges in the medium to move periodically. Although the electric wave of light has a sinusoidal function, due to the complex potential structure in nonlinear crystals, such periodic motion of charges may not be simple harmonic motion. For any periodical movement, it could be considered as the sum of a series of harmonic motions with different frequencies, as shown in Fig 2.2.1. A periodical movement (a) could be seen as a sum of harmonic motions (b), (c), and (d). A periodically moving charge will emit an electromagnetic wave that has the same frequencies as its motion. Since the motion of the charge is not sinusoidal and includes many frequencies as stated above, the emitted wave will also include many harmonic frequencies, and those frequencies different from the incident light are the sources of harmonic light.

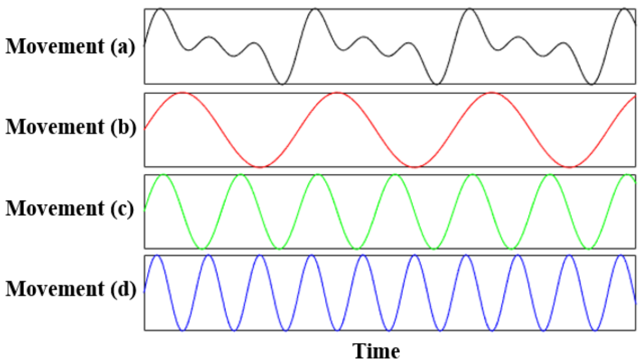

Figure 2.2.1 A periodic motion (a) can be viewed as the superposition of multiple harmonic motions (b)-(d).

Therefore, the lattice potential energy structure within the material determines its nonlinear optical properties, and engineering the material's lattice potential energy structure can change its nonlinear optical properties. Ferroelectric materials have a significant advantage in this regard, as the invertible ferroelectric domains can provide completely opposite lattice potential energy structures at different positions within the material, thus controlling harmonic generation.

In the previous section, we discussed the polarization of a nonlinear medium when excited by light waves. By combining the linear terms in the equation (2.2.7), we arrive at the following nonlinear wave equation:

$$\nabla^2\boldsymbol{E}-\frac{\varepsilon}{c^2}\frac{\partial^2\boldsymbol{E}}{\partial t^2}=\frac{1}{\varepsilon_0 c^2}\frac{\partial^2\boldsymbol{P}_{NL}}{\partial t^2} \tag{2.2.15}$$

Where $\boldsymbol{P}_{NL}=\boldsymbol{P}-\varepsilon_0\chi^{(1)}\boldsymbol{E}$ represents the nonlinear polarization, $\varepsilon=1+\chi^{(1)}$ is the relative permittivity of the media, with $\varepsilon=n^2$, where n is the refractive index.

Based on symmetry considerations, the nonlinear optical effects caused by the second order term $\chi^{(2)}$ require material to be non-centrosymmetric. Since the subsequent discussions in this thesis are based on second-order nonlinear effects, for clarity, we will focus solely on harmonic generation driven by $\chi^{(2)}$. Essentially, this process involves the interaction between three different waves. Consider a light field is a superposition of three sinusoidal waves with angular frequency of ω_1, ω_2 and ω_3:

$$\boldsymbol{E}(\boldsymbol{r},t)=\sum_{n=1,2,3}\boldsymbol{E}_n(\boldsymbol{r})e^{-i\omega_n t}+cc. \tag{2.2.16}$$

Substituting equation (2.2.16) into equation (2.2.9) gives $\boldsymbol{P}$, then substituting $\boldsymbol{P}$ into the nonlinear wave equation (2.2.15) and differentiate twice with respect to time, we get the time independent nonlinear wave equation:

$$\nabla^2\boldsymbol{E}_n(\boldsymbol{r})+k_n^2\boldsymbol{E}_n(\boldsymbol{r})=-\frac{\omega_n^2}{\varepsilon_0 c^2}\boldsymbol{P}_n(\boldsymbol{r}) \tag{2.2.17}$$

Where $k_n = \sqrt{\mu\varepsilon}\omega_n$ is the wave number.

Let us consider here the simplified case of 1-dimensional SHG. The x-polarized fundamental plane wave E_1 (of frequency ω_1 , and wavelength λ_1) traveling in z direction, will generate the x-polarized second harmonic wave E_2 (with frequency $\omega_2 = 2\omega_1$ and wavelength $\lambda_2 = \lambda_1/2$). The optical fields can then be written as:

,
$$E_1 = A_1(z)e^{-ik_1 z} \qquad (2.2.18a)$$

$$E_2 = A_2(z)e^{-ik_2 z} \qquad (2.2.18b)$$

Substituting equations (2.2.18) into (2.2.17), the specific crystal orientation here simplifies the vectorial equations to following scalar equations:

$$\frac{d^2E_1(z)}{dz^2} + k_1^2E_1(z) = -\frac{\omega_1^2}{\varepsilon_0 c^2}P_1(z) \qquad (2.2.19a)$$

$$\frac{d^2E_2(z)}{dz^2} + k_2^2E_2(z) = -\frac{\omega_2^2}{\varepsilon_0 c^2}P_2(z) \qquad (2.2.19b)$$

According to equation (2.2.13) the nonlinear polarization terms are:

$$P_1(z) = 4\varepsilon_0 d_{ij}E_2(z)E_1^*(z) \qquad (2.2.20a)$$

$$P_2(z) = 2\varepsilon_0 d_{ij}E_1^2(z) \qquad (2.2.20b)$$

We apply now the so called slowly varying envelope approximation which assumes that wave amplitudes change slowly in propagation in comparison to wavelength. Formally this condition is expressed as $\frac{dE}{dz}k \gg \frac{d^2E}{dz^2}$. Also apply equations (2.2.20), then the equations (2.2.19) become:

$$\frac{dA_1(z)}{dz} = -\frac{2id_{ij}\omega_1^2}{c^2k_1}A_2(z)A_1^*(z)e^{-i\Delta kz} \qquad (2.2.21a)$$

$$\frac{dA_2(z)}{dz} = -\frac{id_{ij}\omega_2^2}{c^2k_2}A_1^2(z)e^{i\Delta kz} \qquad (2.2.21b)$$

Where $\Delta k = k_2 - 2k_1$ is the phase mismatch parameter.

By assuming undepleted pump approximation ($\frac{dE_1}{dz} \approx 0$) in equation (2.2.21), we get the following formula for amplitude of the second harmonic wave generated along propagation in nonlinear medium:

$$A_2(z) = -\frac{iA_1^2 d_{ij}\omega_2^2}{c^2 k_2} z\, sinc\left(\frac{\Delta kz}{2}\right) e^{\frac{i\Delta kz}{2}} \tag{2.2.22}$$

From this expression we find intensity of SH beam:

$$I_2(z) = \frac{2d_{ij}^2 I_1^2 \omega_1^2}{c^3 n_1^2 n_2 \varepsilon_0} z^2 sinc^2\left(\frac{\Delta kz}{2}\right) \tag{2.2.23}$$

and conversion efficiency:

$$\eta(z) = \frac{I_2(z)}{I_1} = 8\left(\frac{\mu_0}{\varepsilon_0}\right)^{\frac{3}{2}} \frac{\omega_1^2 d_{ij}^2 I_1 z^2}{n^3}\ sinc^2\left(\frac{\Delta kz}{2}\right) \tag{2.2.24}$$

$n \approx \sqrt{\frac{\varepsilon_1}{\varepsilon_0}}$ is the refractive index of medium.

Clearly, the conversion efficiency strongly depends on the phase mismatch Δk, and reaches its maximum when $\Delta k = 0$, which represents the perfect phase matching. Usually, the phase matching cannot be fulfilled in a nonlinear medium due to the material dispersion, thus an efficient SHG does not generally occur in nature. However, several techniques have been proposed to solve this problem. In the next section we will discuss the physical significance of phase mismatch and introduce two methods to achieve phase matching.

2.3 Phase mismatch and phase matching techniques

The conversion efficiency of nonlinear optical processes is a crucial factor to consider, especially given that the intensity of harmonic light is typically much weaker compared to the incident light. Compounding this issue, phase mismatching conditions inherently limit the accumulation of harmonic light intensity. To explain the concept of phase mismatching, we use the example of collinear second harmonic generation (SHG).

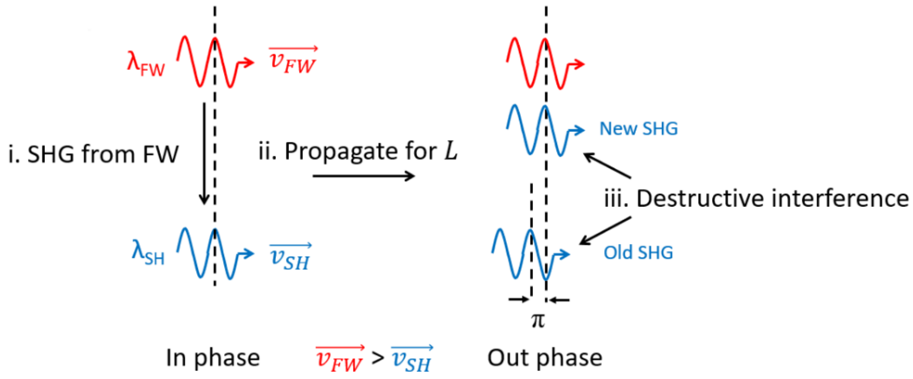

Fig 2.3.1 Phase mismatch in SHG. (i) Fundamental frequency light interacts with the medium's nonlinear polarization to generate harmonic light. (ii) The harmonic light and fundamental frequency light propagate together in the forward direction. Due to the material's dispersion, their respective propagation speeds are v_{FW} and v_{SH}. (iii) After propagating a distance $L = \lambda_{SH} \cdot \frac{v_{FW}}{2(v_{FW}-v_{SH})}$, the newly generated harmonic light and the original harmonic light acquire a phase difference of π. Consequently, the two lights contributions interfere distractively,

As depicted in Fig 2.3.1, a fundamental wave (FW) enters a nonlinear medium and generates a second harmonic (SH). Both the FW and SH propagate forward in the medium in parallel. Due to dispersion, the FW and SH exhibit different phase velocities within the medium, resulting in a distance $\Delta L = t(v_{FW} - v_{SH})$ between the FW and the initially generated SH after time t. Concurrently, the FW continues to generate SH waves with the same phase as the FW.

When ΔL reaches $\frac{\lambda_{SH}}{2}$, or the propagation distance $L = \lambda_{SH} \cdot \frac{v_{FW}}{2(v_{FW}-v_{SH})}$, the newly generated SH possesses an opposite phase relative to the initially generated SH, leading to destructive interference between the two. Consequently, the SH waves cancel each other out, preventing the accumulation of SH intensity in the nonlinear medium, as shown in Fig 2.3.2

(ii). From a mathematical perspective, if $L = \lambda_{SH} \cdot \frac{v_{FW}}{2(v_{FW}-v_{SH})} = \infty$, the aforementioned destructive interference will never occur. This implies that $v_{FW} - v_{SH}$, or the phase mismatch factor Δk, should be zero. We will introduce a method to achieve $\Delta k = 0$ in the next section.

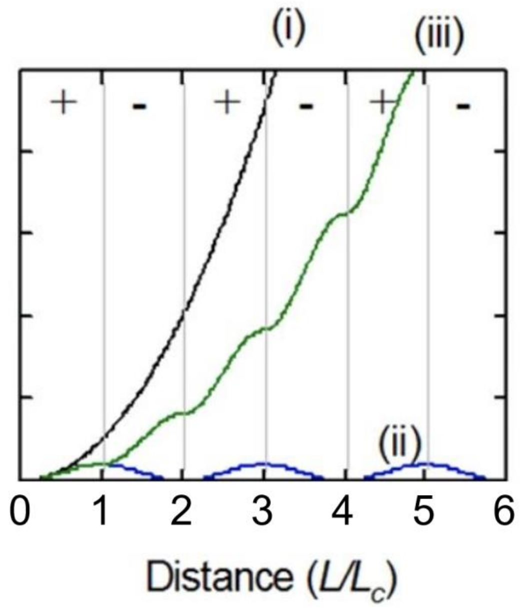

Figure 2.3.2 Dependence of SH intensity as a function of propagation distance with (i) phase matching, (ii) non-phase matching and (iii) quasi-phase matching.

2.3.1 Birefringent phase matching

Phase velocity difference of FW and harmonic waves in nonlinear medium causes phase mismatching and low conversion efficiency from FW to harmonic waves. A straightforward method to increase the low conversion efficiency is eliminate the phase velocity difference between FW and harmonic waves, which could be achieved by birefringent phase matching (BPM) technique.

BPM is a technique that allows one to eliminate the phase velocity difference between the FW and SH in birefringent crystals. This is achieved by carefully selecting the polarization and propagation direction of the waves in a birefringent nonlinear medium. Such technique was firstly reported by Giordmaine and Maker, et al. independently [10], [80]. According to their research, the intensity of SH generated from a KDP crystal was enhanced by 300 times with BPM. Later, Midwinter, et al. expanded BPM to a more general case of three-wave mixing [14].

To fully understand the BPM technique, it is important to first understand the concept of birefringence. Birefringence is a property of certain transparent optical materials, where the refractive index changes based on the polarization direction. Crystals with non-cubic structures are typically birefringent, and one or two specific directions, known as the optic axis, govern their optical anisotropy. The material's optical behaviour does not change when rotated around this axis. Light with polarization perpendicular to the optic axis ($\theta=90°$) is governed by the ordinary refractive index n_o, such polarized light is the so-called o-light. While light with polarization in the direction of the optic axis ($\theta=0°$) experiences an extraordinary refractive index n_e, such polarized light is the so-called e-light. If the angle is between 0° and 90°, the refractive index $n_e(\theta)$ could be calculated with following equation:

$$n_e(\theta) = \frac{1}{\sqrt{\frac{cos^2\theta}{n_o^2}} + \sqrt{\frac{sin^2\theta}{n_e^2}}}$$

As states at the beginning of this section, the aim of BPM is to enhance the SHG efficiency by eliminate the phase velocity differences between FW and SH. Since the refractive indices are depend on both wavelength λ and polarization angle against optic axis θ, it is possible to synchronize the refractive index of FW and SH by change the angle θ of FW or SH, i.e. $n(\lambda_{FW}, 0) = n(\lambda_{SH}, \theta)$ or $n(\lambda_{FW}, \theta) = n(\lambda_{SH}, 0)$. Consequently, the propagation velocities of FW and SH become identical in the nonlinear media, hence phase matching is achieved, as shown in figure 2.3.3. Thus, the intensity of SH is able to accumulate in propagation as shown in figure 2.3.2 (i).

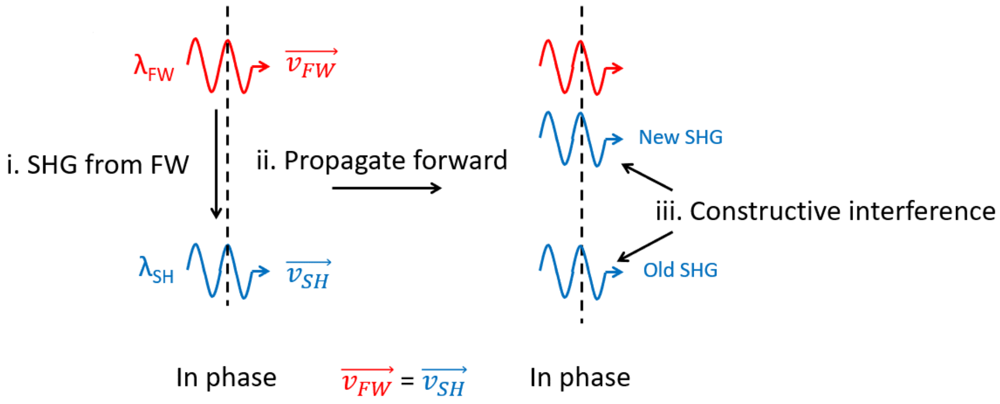

Fig 2.3.3 Birefringent phase matching SHG.

Figure 2.3.4, for instance, demonstrates how the refractive indices of o-light and e-light change with the direction of propagation. The figure also illustrates the refractive indices corresponding to FW and SH. It is evident that when the propagation direction of FW is in the direction indicated by blue arrow A, $n(\lambda_{FW}, 0) = n(\lambda_{SH}, \theta)$, meaning FW and SH have the same refractive index, and the phase matching condition is satisfied.

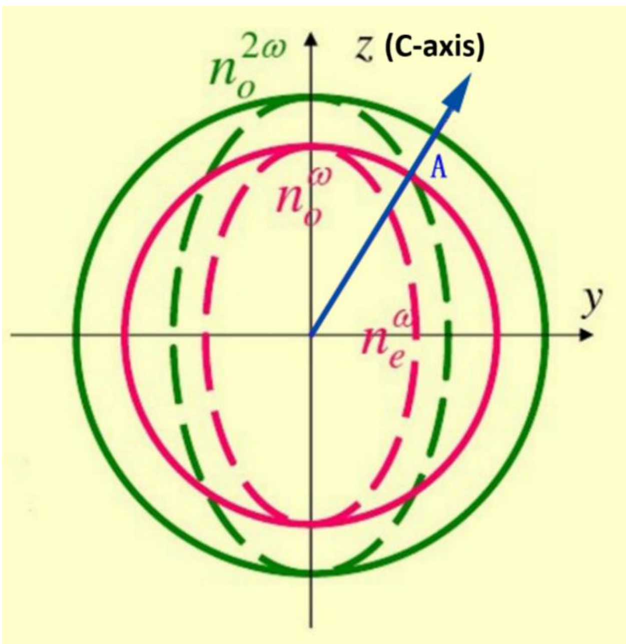

Figure 2.3.4 The indices ellipsoid projection of a negative uniaxial crystal. Propagation along the A arrow direction allows the nonlinear process fulfill phase matching condition.

We can also use the concept of momentum conservation to understand the BPM technique. The momentum of a photon is given by:

$$p = \frac{nh}{\lambda}$$

where n is the refractive index of the medium, h is Planck's constant and λ is the photon wavelength.

In case of SHG, the momentum of FW photons and SH photons are:

$$p_{FW} = \frac{n_{FW}h}{\lambda_{FW}}$$

$$p_{SH} = \frac{n_{SH}h}{\lambda_{SH}}$$

As the wavelength of SH is half of FW, $\mathrm{n_{FW}} = n_{SH}$ is required for momentum conservation $2p_{FW} = p_{SH}$

The technique of birefringent phase matching (BPM) has been widely applied in nonlinear optics, but it also has several drawbacks. One major issue is that the optical frequencies do not propagate in a collinear manner due to the fact that the extraordinary wave in a birefringent crystal has a Poynting vector that is not parallel to the propagation vector. This leads to a "walk-off" effect, which reduces the effective interaction length between the waves and lowers the efficiency of the nonlinear mixing process. Although this problem can be moderated by temperature tuning, there are two other inherent disadvantages of BPM that make it necessary to explore alternative phase matching techniques. Firstly, due to the restrictive angular, temperature, and wavelength acceptances, it is difficult to achieve phase matching in arbitrary crystals and for arbitrary wavelengths. Some materials, such as gallium arsenide (GaAs), may have no birefringence or insufficient birefringence to compensate for the dispersion over the desired wavelength range. Secondly, BPM is limited to off-diagonal nonlinear tensor elements, which in many crystals like $LiNbO_3$, $LiTaO_3$, and $KTiOPO_4$ have low effective nonlinear coefficient.

2.3.2 Quasi-phase matching

To overcome the BPM limitations states above, Quasi-phase matching (QPM) technique was proposed in 1962 by Armstrong and Bloembergen [14]. Several approaches were stated in their work include the QPM based on periodically engineered nonlinear photonics crystal which become the most popular QPM technique nowadays.

In this section, we use second-harmonic generation (SHG) as an example to elucidate the mechanism of Quasi-Phase Matching (QPM) in nonlinear photonic crystals. As discussed in the previous section of this chapter, the accumulation of overall second-harmonic (SH) intensity is impeded by periodically destructive interference between SHs with opposing phases. The core principle of QPM involves reversing the phase of one of these out-of-phase SHs, ensuring that all SH contributions are either in phase or exhibit a phase difference of less than 90°. As a result, constructive interference takes place, and the SH intensity accumulates throughout the nonlinear medium.

As depicted in Figure 2.3.45, SH is generated by the FW and propagates forward together. Due to the nonlinear medium's dispersion, the phase velocity of the FW in the nonlinear medium is in this case, greater than that of the SH ($v_{FW} > v_{SH}$). After the FW and SH have propagated together for a distance of $L = \lambda_{SH} \cdot \frac{v_{FW}}{2(v_{FW}-v_{SH})}$, they exhibit a phase delay of $\frac{\lambda_2}{2}$. Simultaneously, the FW continues to generate new SH light.

The newly generated SH light should have a phase difference of π compared to the initially generated SH light, leading to destructive interference between the two. However, at this point, the FW has propagated into the reversed nonlinear crystal, which generates SH with a reversed phase. Consequently, the newly generated SH and the initially generated SH have the same phase, resulting in coherent interference between the two. This process allows the SH wave energy to grow monotonically. In this process, the phase between consecutive SH contributions are not always perfectly in sync, but it is always less than π, which is why this technique is called quasi-phase-matching.

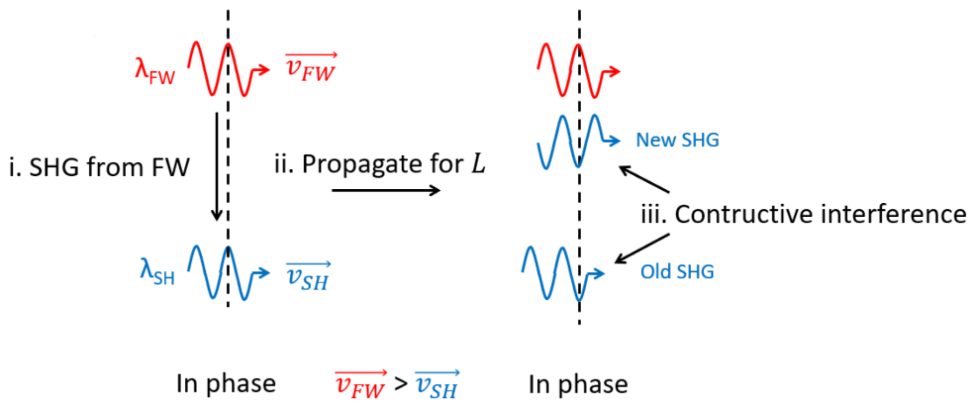

Fig 2.3.5 Quasi-phase matching SHG.

It should be mentioned that QPM does not have to include domain reversal. It can also work albeit weaker by modulating the strength of the nonlinearity. This method has been demonstrated in Lithium Niobate. In this case one can use strong laser beam to periodically destroy the crystal structure of the quadratic material, In the most extreme case this laser processing leads to local amorphization of the medium. Such created nonlinearity grating in which strength of the nonlinearity varies between its maximum and zero can support monotonous growth of the second harmonic, however with lower rate than in case of domain reversal[72].

Interestingly, phase matching in frequency conversion can be also achieved by periodic modulation of refractive index of the nonlinear material. However, this technique requires linear index grating to have high contrast in order to achieve efficient frequency conversion [81]

In the remainder of this Thesis I will concentrate on the QPM techniques which involves spatial modulation of the material's nonlinearity only. The size of the period depends on the material's dispersion properties, wavelength, and the designed nonlinear process. It can be said that the periodicity of the structure plays a core role in QPM techniques; therefore, concise and efficient description of the periodic properties of complex nonlinear structures is crucial. We employ the concept of reciprocal vectors to describe periodicity of nonlinearity. This aspect will be explored in greater detail in later chapters.

In conclusion, the concept of quasi-phase matching (QPM) addresses the challenge of destructive interference in nonlinear optical processes, such as second-harmonic generation (SHG). By manipulating the sign or magnitude of the nonlinearity, constructive interference is promoted, allowing for the accumulation of harmonic light intensity. Overall, QPM techniques offer essential solutions for enhancing the efficiency of nonlinear optical processes and provide additional flexibility in design and optimization of nonlinear structures.

2.4 Reciprocal lattice vector and Fourier transform

In the previous section, we used a one-dimensional (1D) co-linear periodically modulated nonlinear material as an example to explain the concept of QPM and how it enhances the efficiency of nonlinear processes. The 1D co-linear structure is the simplest configuration, allowing us to describe and analyze the physical mechanisms directly. However, when dealing with higher-dimensional or non-periodical cases, such descriptions and analyses can become exceedingly complex. Consequently, it is essential to introduce mathematical tools that facilitate a deeper understanding of these situations. Two such tools are the reciprocal lattice vector (RLV) and the Fourier transform (FT).

2.4.1 Reciprocal lattice vector

The RLV (reciprocal lattice vector) is a powerful concept in solid-state physics and crystallography, which simplifies the analysis of wave propagation and scattering in periodic structures. It provides a mathematical framework for describing the periodicity of a lattice in reciprocal space, making it a valuable tool for studying the interaction of light with periodic nonlinear photonic crystals. The use of RLV enables a systematic investigation of phase-matching conditions in complex structures, shedding light on the behaviour of nonlinear processes in higher-dimensional or non-periodical configurations.

To elucidate the concept of the RLV and its utility in the analysis of nonlinear photonic crystals (NPCs), we will begin with the simplest case: a one-dimensional (1D) periodical pattern. As depicted in Fig 2.4.1 (a), a 1D periodical pattern exhibits a periodicity of Λ_1 and repeats itself horizontally. For such a periodical pattern, two crucial properties are the periodicity and direction, which can be easily represented by a vector. The corresponding vector is shown on the right side of the pattern; it is a horizontal bi-arrow vector with a length of $\frac{2\pi}{\Lambda_1}$. If the size of the period increases, for example, from Λ_1 to Λ_2, the length of its corresponding RLV will decrease to $\frac{2\pi}{\Lambda_2}$, as shown in Fig 2.4.1 (b). If the direction of the period changes, for example, from horizontal to a 30° angle with the horizontal direction, the direction of its corresponding RLV will also be at a 30° angle with the horizontal direction, as shown in Fig 2.4.1 (c).

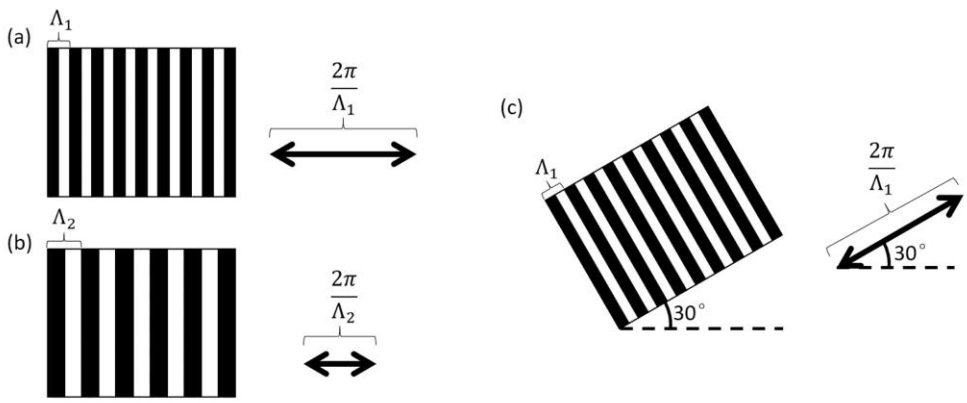

Figure 2.4.1 1D periodical pattern and their RLVs.

With the aid of the powerful concept of RLV, we can abstract the SHG process under QPM conditions into a set of simple vector diagrams. As shown in Fig 2.4.2 (a), on the left is an SHG schematic based on periodically poled 1D NPC. A FW with a wavelength of λ_1 incident into a 1D NPC with a periodicity of Λ_1, producing a SHG with a wavelength of λ_2. However, the intensity of the SHG is very weak because the 1D NPC cannot satisfy the phase matching condition for SHG. On the right side of the figure, the vector diagram clearly depicts this phase mismatching. The diagram is plotted in reciprocal space. Here, $k_2 = \frac{2\pi n_2}{\lambda_2}$ represents the wavevector of the SH, $k_1 = \frac{2\pi n_1}{\lambda_1}$ represents the wavevector of the FW, and $G = \frac{2\pi}{\Lambda_1}$ is the RLV provided by the 1D NPC on the left. It can be observed that k_2, $2k_1$, and G cannot form a closed figure, leaving a gap of size $\Delta k \neq 0$. If such a gap exists in the vector diagram in reciprocal space, the corresponding nonlinear process does not satisfy the phase matching condition, and thus cannot proceed efficiently.

To achieve efficient collinear SHG of a FW with a wavelength of λ_1, the Δk in the vector diagram needs to be zero. The most straightforward way to achieve this goal is to reduce the length of G. Translated into real space, this means increasing the period of the 1D NPC. This result is shown in figure (b). The period in this figure has been increased to Λ_2, reducing its corresponding RLV to $G = \frac{2\pi}{\Lambda_2}$. This now perfectly complements the vectors $2k_1$ and $k_2$to form a closed figure, making $\Delta k = 0$. With the QPM condition satisfied, SHG is efficiently generated as shown on the left side of this figure.

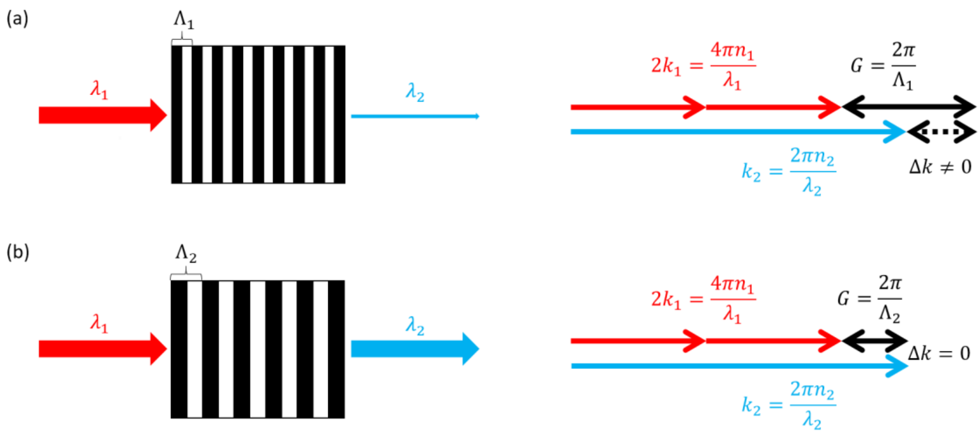

Figure2.4.2 Collinear SHG in a 1D periodically poled NPC, (a) phase mismatched and (b) QPM.

The analysis of SHG under noncollinear conditions is even more dependent on the vector diagram in reciprocal space. In Figure 2.4.3, the wavelengths and parameters of the 1D NPC are the same as in Fig. 2.4.2 (a), meaning efficient nonlinear conversion cannot be achieved under collinear conditions. However, by rotating the 1D NPC, efficient non-collinear SHG can be achieved. As seen in the vector diagram in reciprocal space on the right side of the figure, a closed triangle is formed by k_2, $2k_1$, and G. Here, the angle between the reciprocal lattice vector G and the horizontal direction is 75°, and the angle between the second harmonic wavevector k_2 and the horizontal is 23°. This means that by rotating the 1D NPC in real space to make an angle of 75° with the horizontal direction, SH will be efficiently generated in the direction of 23°, as demonstrated in the left of the figure.

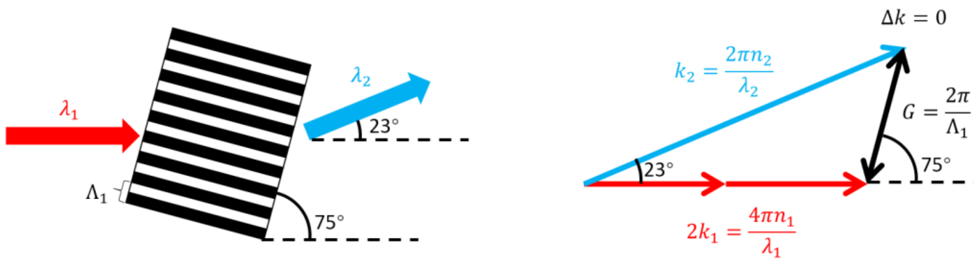

Figure 2.4.3 Noncollinear SHG in a 1D periodically poled NPC.

Essentially, the RLV encapsulates the periodic properties of the structure in a simple and concise manner, making it an invaluable tool for analyzing periodic structures and understanding their behaviour in nonlinear optical processes. Particularly in practical situations, an NPC may have a very complex structure, possessing numerous spatial frequencies of varying directions and magnitudes. This makes the role of the RLV even more indispensable. We will discuss such complex scenario further in the next section.

2.4.2 Fourier transform

The Fourier transform is a widely used mathematical tool that allows us to analyze functions or signals in terms of their frequency components. By transforming a signal from its original domain (e.g., time or space) into its frequency domain representation, the Fourier transform reveals the underlying frequencies that constitute the signal. In the context of nonlinear optics, the Fourier transform helps to analyze the spatial frequencies present in complex nonlinear photonic crystals, quickly calculating all the RLV and their intensities for any given structure. The value of the Fourier transform is not only manifested in the analysis of existing structures, but more importantly, it can also provide guidance for the design of complex functional nonlinear crystals. By revealing the relationship between the spatial frequencies and the performance of nonlinear optical processes, the Fourier transform offers valuable insights that can help optimize the design of nonlinear photonic crystals for specific applications.

Mathematically Fourier transform could be defined as:

$$\hat{f}(\xi) = \int_{-\infty}^{\infty} f(x) e^{-i2\pi\xi x} dx$$

Where $f(x)$ is the original function; $\hat{f}(\xi)$ is the Fourier transform of the original function; ξ is the frequency.

For simplification, denoting the Fourier transform operator by $\mathcal{F}$ and reverse Fourier transform operator by $\mathcal{F}^{-1}$:

$$\hat{f}(\xi) = \mathcal{F}\{f(x)\}(\xi)$$

$$f(\mathrm{x}) = \mathcal{F}^{-1}\{\hat{f}(\xi)\}(x)$$

In this thesis, we will use the Fourier Transform as a tool only, so we do not need to delve deeply into its mathematical form and related derivations. However, it is essential to understand some critical functional relationships and Fourier Transforms of common functions, as this knowledge is crucial for the analysis of certain $\chi^{(2)}$structures. In fact, we will primarily use the Fast Fourier Transform (FFT) algorithm implemented in software to apply the Fourier Transform. The FFT is a class of optimized numerical algorithms for the Fourier Transform, which significantly accelerates computation without substantially sacrificing accuracy. This feature is particularly crucial when analyzing and designing large-volume 3D nonlinear photonic crystals (NPCs), as it enables the efficient exploration of their complex structures and properties while maintaining acceptable computational time. In the following sections, I will provide some examples of nonlinear photonic crystal analyses using FFT to introduce important functional relationships and Fourier Transforms of common functions.

2.4.3 Convolution Theorem

The convolution theorem of the Fourier Transform takes the following mathematical form. Consider two functions $a(x)$ and $b(x)$ with Fourier transforms $A(\xi)$ and $B(\xi)$. The notation $a * b$ denotes the convolution of a and b and the convolution theorem states that the Fourier transform of it is equal to the product of their individual Fourier Transforms:

$$\mathcal{F}\{a(x) * b(x)\} = A(\xi)B(\xi)$$

The dual:

$$\mathcal{F}\{a(x)b(x)\} = A(\xi) * B(\xi)$$

This rule is especially useful when a function can be decomposed into a product or convolution of two simpler functions. The function of χ^2 distribution in nonlinear photonic crystals often exhibits these two scenarios.

A practical example is the 3D NPC fabricated in BCT crystals using infrared femtosecond laser poling technology[33]. Due to the fabrication method and the characteristics of the crystal, the laser-induced inverted domains in the crystal have a shape resembling the Greek letter theta (θ). As shown in Figure 2.4.4, in the work by Xu et al., they fabricated an NPC with a square lattice arrangement inside BCT crystals using femtosecond laser poling technique. Each unit has a θ shape. The overall structure can be considered as the convolution of a square lattice and a θ shaped unit ($a(x) * b(x) = c(x)$). By performing a Fourier transform on the square lattice and theta unit separately and then multiplying them, we can obtain the Fourier transform result of the entire structure ($A(\xi) \times B(\xi) = C(\xi)$). This feature of the Fourier transform can help us deduce the structure of the NPC from the shape of its SHG pattern.

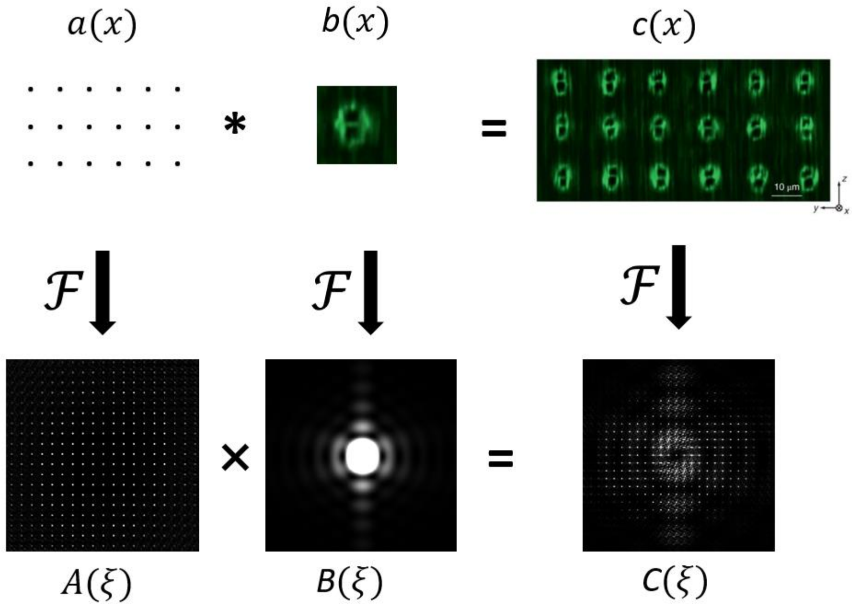

Figure 2.4.4 The convolution theorem of the Fourier Transform in NPC. An NPC structure in BCT crystal induced by laser poling technique $c(x)$ could be considered as the convolution of $a(x)$ and $b(x)$ (upper row). The Fourier transform of $a(x)$, $b(x)$ and $c(x)$ are $A(\xi)$, $B(\xi)$ and $C(\xi)$ respectively. They have a relation of $A(\xi) * B(\xi) = C(\xi)$ (bottom row).[33]

Continuing with the example of the structure mentioned above, the far-field diffraction pattern of the light wave is approximately the Fourier transform of the near-field wavefront, i.e. $C(\xi)$ should approximate the SHG pattern. As shown in Figure 2.4.3, the SHG far-field diffraction produced by the structure has a ring-like multi-peak pattern with significant intensity differences in two orthogonal directions. Based on the convolution theorem, we can conclude that the spacing and distribution of peaks are determined by the lattice structure of the NPC ($a(x)$), while the uneven distribution is determined by the shape of the unit ($b(x)$). From this, we can make targeted adjustments to the NPC structure based on the appearance of the SHG pattern.

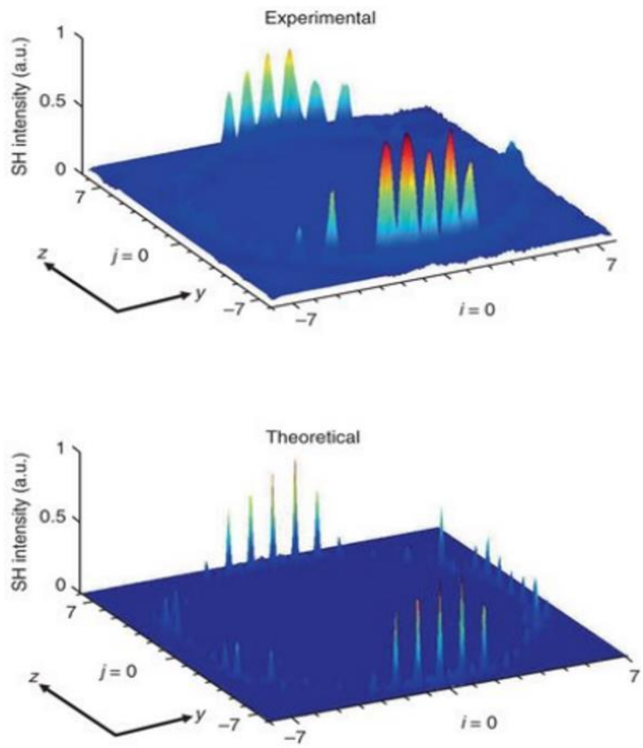

Figure 2.4.5 Far-field SHG pattern from a 3D NPC with square lattice structure in BCT crystal, experimental (up) and theoretical (bottom). The peaks intensity are unevenly distributed along z and y axis. Here i and j are nonlinear diffraction orders.[33]

The dual of the convolution theorem has a more common application in NPC-related research, which is the spectral broadening analysis of finite volume NPCs. Let's use the simplest example of a one-dimensional single-period QPM structure. As shown in Figure 2.4.4, a finite-length one-dimensional single-period QPM structure can be regarded as an infinitely long one-dimensional single-period structure multiplied by a finite-width square wave function, i.e., $a(x) \times b(x) = c(x)$. Their respective Fourier transforms are $A(\xi)$, $B(\xi)$ and $C(\xi)$, and satisfy $A(\xi) * B(\xi) = C(\xi)$. From this, we can know that for a finite-length NPC structure, its Fourier transform result will be convoluted by a Sinc function $B(\xi)$, causing the peaks to broaden. In other words, a shorter NPC structure can provide more different lengths of RLVs to satisfy the relatively wide-band QPM, but at the cost of lower conversion efficiency.

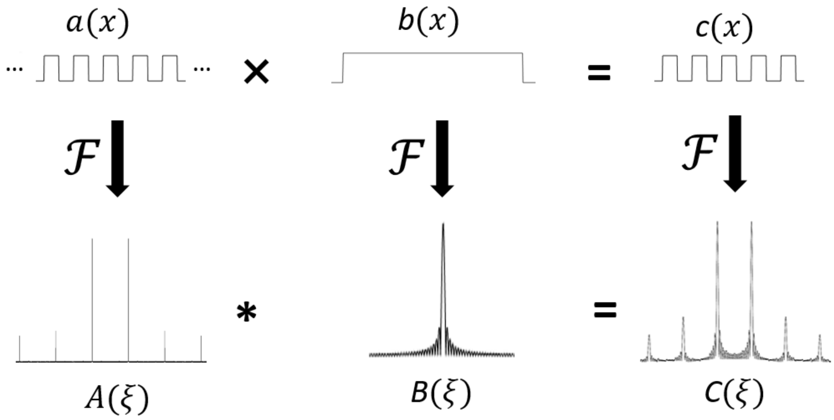

Figure 2.4.6 The dual of convolution theorem of the Fourier Transform. A finite length NPC structure $c(x)$ could be considered as the production of $a(x)$ and $b(x)$ (upper row). The Fourier transform of $a(x)$, $b(x)$ and $c(x)$ are $A(\xi)$, $B(\xi)$ and $C(\xi)$ respectively. They have a relation of $A(\xi) \times B(\xi) = C(\xi)$ (bottom row)

In summary, the RLV and the Fourier transform are essential mathematical tools for studying phase matching and nonlinear processes in higher-dimensional or non-periodical structures. By leveraging these tools, researchers can gain a deeper understanding of the underlying mechanisms and optimize the efficiency of nonlinear optical processes in complex systems.

2.5 Design and simulation of nonlinear wavefront shaping in 3D NPCs

In the research of this thesis, the simulation of 3D NPCs can be roughly divided into two parts. The first part is to analyze a known structure of 3D NPCs, simulate the nonlinear processes it supports, and then deduce how it can perform nonlinear wavefront shaping. Another part is to design the structure of 3D NPCs under the premise of a predetermined target nonlinear structured beam. In the following sections of this chapter, we will use nonlinear process of SHG as an example, to explain how to achieve the above simulation goals through 3D FFT.

2.5.1 Far-field SHG pattern simulation in 3D NPCs

One of the most common simulation tasks is to simulate the far-field distribution of the emitted SH under given FW conditions and a 3D NPC structure. To achieve this goal, our approach is to first perform a 3D FFT on the 3D NPC structure to find out all the RLVs that the structure can provide. On this basis, we determine which RLVs can assist QPM according to the parameters of the FW and the dispersion properties of the crystal, and which nonlinear optical processes can occur efficiently. Finally, we introduce the nonlinear coefficient tensor matrix of the crystal and adjust the intensity of the emitted SH accordingly. In this way, we obtain the far-field distribution of the SH.

In the following, we use a multi-layer fork structure in calcium barium niobate (CBN) crystal to generate SH as an example to explain the simulation process. A single-layer fork structure is often used to produce nonlinear vortex beams [56], but due to the inability to satisfy phase-matching conditions, its efficiency is extremely low. Wei et al. arranged the structure periodically in space in their work to satisfy QPM conditions and efficiently generate nonlinear vortex beams [82], as shown in Fig 2.5.1 (a). As described above, we first need to perform a 3D FFT on the 3D NPC χ^2 structure to find all the RLVs that the structure provided. Using Matlab's fftn() function to directly perform FFT on the 3D structure, we obtain the distribution of RLVs in reciprocal space, and the 3D FFT result is shown in Fig 2.5.1 (b). It can be seen that distribution of RLVs in the reciprocal space of the structure shows many donut-like shapes, and they are continuously repeated in the z-axis direction. In reciprocal space, each voxel corresponds to a RLV. The line connecting the voxel to the center point (zero point) in reciprocal space represents the vector of that RLV, and the brightness of such voxel in the image indicates the intensity of the Fourier coefficient F of that RLV. This Fourier coefficient will be utilized in our subsequent calculations.

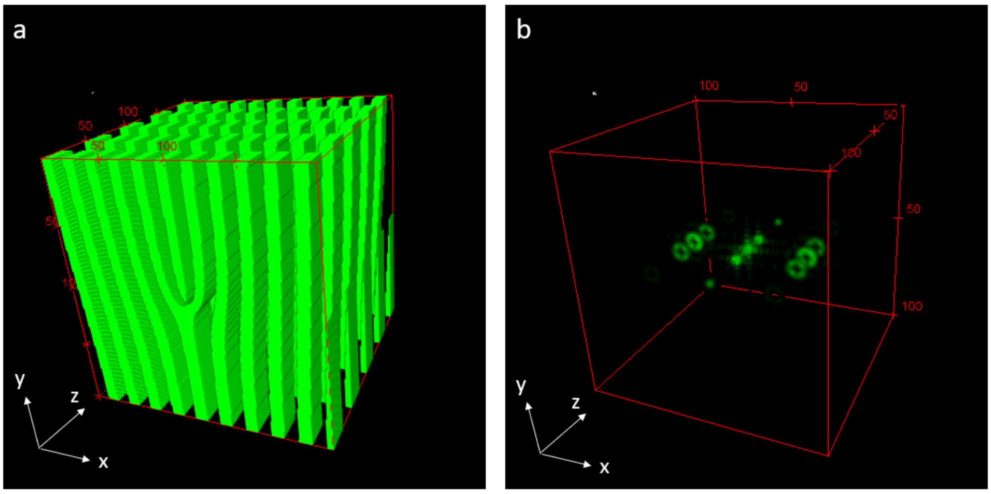

Figure 2.5.1 (a) Multi-layer forks 3D NPC structure and (b) its 3D FFT result which reveal the RLVs it can provide for QPM.

After obtaining the distribution of RLVs in reciprocal space, we need to determine which RLVs can assist in achieving QPM. Here, we draw an analogy to the concept of Ewald's shell in linear optics and construct a nonlinear Ewald's shell to determine which RLVs can assist in achieving QPM. The construction of the nonlinear Ewald's shell is shown in Fig 2.5.2 (a). First, draw the FW wave vector $k_1 = \frac{2\pi n_1}{\lambda}$, with its arrowhead at the center of reciprocal space. Then, draw a spherical shell with the tail end of $2k_1$ as the center and the radius of the SH wave vector length $k_2 = \frac{4\pi n_2}{\lambda}$. This spherical shell is the nonlinear Ewald's shell, and all RLVs that intersect with this shell in reciprocal space may support QPM and generate SH efficiently, with the emission direction of SH being the direction of the wave vector k_2. In other words, every point on Ewald's shell corresponds to a possible k_2, but only those points that intersect with the RLVs correspond to a k_2 that satisfies the QPM condition. Fig 2.5.2 (b) shows the nonlinear Ewald's shell in reciprocal space corresponding to the FW incident along the z-axis in a CBN crystal as well as the FFT result from the multi-layer fork structure. Fig 2.5.2 (c) is a zoom-in of (b), we can see many “donuts” in the space but only two “donuts” intersect with the Ewald’s shell which could support QPM. As the figure is from a numerical simulation, the space is pixelized and show some aliasing distortion, it is possible to obtain a more accurate simulation by decreasing the voxel size and the trade-off is longer simulation time. It is worth noting that nonlinear crystals are often birefringent crystals, so refractive index n is not only a function of wavelength, but also a function of light polarization and propagation direction, $n\left(\lambda, \theta, \frac{\vec{k}}{|k|}\right)$. This makes the nonlinear Ewald's shell often not a truly perfect spherical shell, but an ellipsoidal shell.

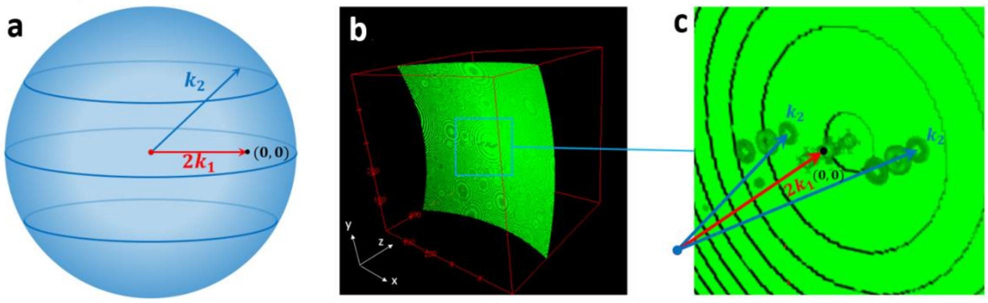

Figure 2.5.2 Ewald’s shell in SHG simulation. (a) How to construct an Ewald’s shell in reciprocal space. (b) A simulation result with Ewald’s shell and reciprocal vectors from a multi-layer forks 3D NPC. (c) Zoom-in of (b), although the multi-layer forks 3D NPC provide many RLV in reciprocal space and distribute in form of many “donuts”, only two “donuts” intersect with the Ewald’s shell. It is these two "donuts" that correspond to the RLV which satisfy the QPM conditions, thereby enhancing SHG.

Up to this point, we have identified all possible k_2 that can efficiently generate SH by using 3D Fourier transformation and constructing a nonlinear Ewald’s shell in reciprocal space. However, the specific intensity of the generated SH still requires further calculation, which involves considering the effective nonlinear coefficients of the material and the Fourier coefficients mentioned earlier. The intensity of SH is directly proportional to the square of the Fourier coefficient F ($I \propto F^2$). The influence of the nonlinear material on SH intensity has been detailed in the previous section 2.2, and the relative intensity of SH polarization can be calculated using formula (2.2.13), and the SH intensity is directly proportional to the square of the SH polarization ($I \propto P^2$).

Through the above steps, with the assistance of simulation software, we can rapidly calculate the far-field pattern of the SHG produced by a known NPC structure. Moreover, understanding this simulation technology allows us to deeply comprehend the process of SHG via 3D NPCs, laying a solid foundation for better design of complex functional 3D NPCs.

2.5.2 Nonlinear volume holography

This section will introduce nonlinear volume holography, a 3D NPC structure design method. The 3D NPC designed and manufactured through this method is also called a nonlinear volume hologram (NVH) [51], [59]. In fact, the multi-layer fork 3D NPC mentioned in the last section is essentially a type of NVH. However, its design is not through nonlinear volume holography, but follows a very intuitive structural design approach. That is, a 2D NPC cannot provide reciprocal lattice vectors in the direction of light propagation, therefore its efficiency is extremely low. By periodically repeating this 2D structure in that direction, reciprocal lattice vectors can be provided to satisfy phase matching and thus improve the SHG efficiency. Although NVH can be designed and fabricated through this method, this approach is far from perfect. An obvious problem is that the SHG distribution generated is in both left and right directions (in Figure 2.5.2 (c), there are two groups of donut-shaped RLVs that can satisfy QPM), and the energy cannot be concentrated on one side, which inherently limits the SHG efficiency. Even disregarding efficiency concerns, this design method, which relies on existing 2D structures, lacks flexibility. In contrast, 3D NPCs designed through nonlinear volume holography theory are, in principle, highly efficient in terms of energy conversion and offer great flexibility. Essentially, 3D NPC with any function can be designed using this method.

The theory of nonlinear volume holography is inspired by its counterpart in linear optics, namely optical holography. This is a technique that can record and reproduce the wavefront of incident light. Typically, an additional reference beam is used to overlap with the object beam in space to produce interference fringes. These interference fringes are recorded using some photosensitive material. This process is called recording, and the material that records the interference fringes is the hologram. Later, when the hologram is illuminated again by the reference beam in the same incident direction as before, the previously recorded object beam can be generated again. This process is called reconstruction.

Nonlinear volume holography is very similar to optical holography, except that the reference beam and objective beam have different wavelengths. In the reconstruction process, the reference beam serves as the pump beam and excites the nonlinear beam of a different frequency. Because the conversion of wavelength is involved, the material of the nonlinear volume hologram needs to be a nonlinear material. However, nonlinear materials often cannot simply imprint fringes through exposure and require more intense processing methods. Therefore, the preparation process of the nonlinear volume hologram involves the use of computers to simulate the appearance of the interference fringes in 3D space, which is the computer-generated hologram (CGH). Then, this structure is imprinted in the nonlinear material in some way.

In the subsequent Chapter 4, the design, preparation, and testing of the nonlinear volume hologram will be introduced in detail.

2.6 Nonlinear optical materials

Nonlinear optical materials hold significant value in the field of nonlinear photonics, as they enable interactions between lights and the wavelength conversion. The nonlinear optical properties of these materials are attributed to the unique features of their electronic and crystal structures, which give rise to new optical processes under the influence of light fields.

There is a wide variety of nonlinear optical materials, such as niobates, phosphates, borates, and silicates. These materials exhibit different degrees of nonlinear optical responses, which are typically described by nonlinear polarization coefficients $\chi^{(n)}$. Among them, second-order nonlinear optical materials (with non-zero $\chi^{(2)}$ coefficients) are particularly important in the field of photonics because they can realize various nonlinear optical processes, such as frequency doubling, difference frequency generation, and parametric oscillation.

Some typical second-order nonlinear optical materials include lithium niobate (LiNbO3), strontium barium niobate (SBN), potassium niobate (KNbO3), and potassium titanyl phosphate (KTP). These materials each have unique properties, such as high nonlinear coefficients, thermal stability, refractive indices, and transparency windows, making them advantageous in various nonlinear optical applications.

When selecting nonlinear optical materials for 3D NPCs, various factors need to be considered, such as the material's nonlinear coefficients, phase-matching conditions, loss, and transparency window. Additionally, because the fabrication of 3D NPCs relies on the unique femtosecond laser writing technique, the materials must also meet the requirements of this technology. Specifically, a nonlinear crystal suitable for laser writing should have a relatively low coercive field intensity and Curie temperature; the reasons for this will be discussed in the subsequent poling techniques section. Moreover, the laser writing process should not have a significant impact on the crystal's refractive index, as this could cause unpredictable effects on subsequent optical processes.

Due to these constraints, many common nonlinear optical materials are not suitable for the fabrication of 3D NPCs. For example, lithium niobate, which is widely used and well-known, has a very high Curie temperature and a large coercive field intensity. As a result, it is difficult to achieve high-quality domain inversion using femtosecond laser writing techniques within this material. Therefore, it is necessary to explore alternative nonlinear optical materials that are better suited for femtosecond laser writing techniques when creating 3D NPCs.

Strontium barium niobate (SBN) and calcium barium niobate (CBN) crystals are well-suited for use as 3D NPC materials. They exhibit excellent transparency in the visible light spectrum, have quite low Curie temperatures and coercive field intensity, and possess significant second-order nonlinear coefficients. As a result, they not only meet the conditions for laser writing but also support efficient nonlinear optical processes. SBN and CBN crystals have very similar properties, and most fabrication methods and research models can be applied to both. While compared to SBN, CBN has better thermal stability, making it more advantageous for high-power applications. This thesis focuses on the study of highly efficient 3D NPCs and will involve the interaction of high-power lasers and 3D NPCs. Therefore, CBN is a more excellent choice for this purpose.

Calcium barium niobate (CBN, $\mathrm{Ca_xBa_{1-\mathit{x}}Nb_2O_6}$) is a ferroelectric material with a tetragonal tungsten bronze (TTB) structure. A wide variety of bronze phases exist due to the occupation of different types of sites (A1, A2, and C) in the TTB structure, which can accommodate several cations of suitable size and charge, as shown in figure 2.6.1[83]. Ferroelectric niobates with the bronze type structure, such as strontium barium niobate (SBN, $\mathrm{Sr_xBa_{1-x}Nb_2O_6}$), have been widely investigated due to their excellent electro-optic, photorefractive, pyroelectric, and piezoelectric properties [84]. CBN exhibits similar properties to SBN, with an existence region of calcium between 20 and 40 mol percent. CBN-28 (x = 0.28), demonstrates typical relaxor behavior at the ferroelectric phase transition temperature of about 265 °C [85]. After high-temperature annealing, random needle-like domain structures appear within CBN, with positive and negative domains alternating along the crystal axis at 180° angles [86]. CBN single crystals can be grown by the Czochralski method, later cut into defined thickness and orientation for optical examinations [87]. The principal refractive indices can be determined using a high precision goniometer. However, in practice the measurement results can be approximated using a conventional four parameter Sellmeier equation:

$$n^2(\lambda) = A + \frac{B}{\lambda^2 - C} - D\lambda^2$$

where coefficients A, B, and C are listed in Table 2.6.1.

The light absorption spectra can be collected using an absorption spectroscope, and the nonlinear components can be measured by comparing the nonlinear signals with other known nonlinear material [79], [83]. The linear absorption spectrum and nonlinear coefficients for as-grown CBN-28 crystal are shown in the figure 2.6.2 and Table 2.6.2.

In summary, CBN shares many similarities with the well-studied SBN and has been successfully grown as single crystals for various characterizations. Its unique combination of material properties, such as high nonlinear optical coefficients, broad transparency window, and compatibility with femtosecond laser writing techniques, make it an ideal candidate for 3D nonlinear photonic crystal applications.

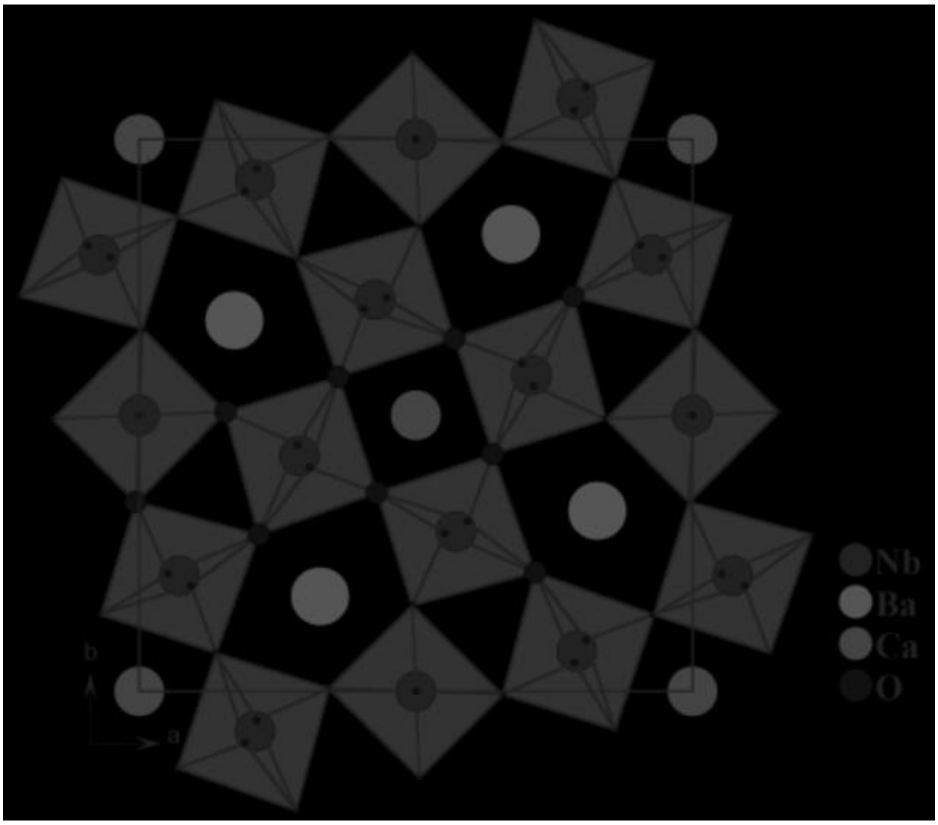

Fig. 2.6.1 Projection parallel to the c-axis with unit cell of CBN-25 [83]

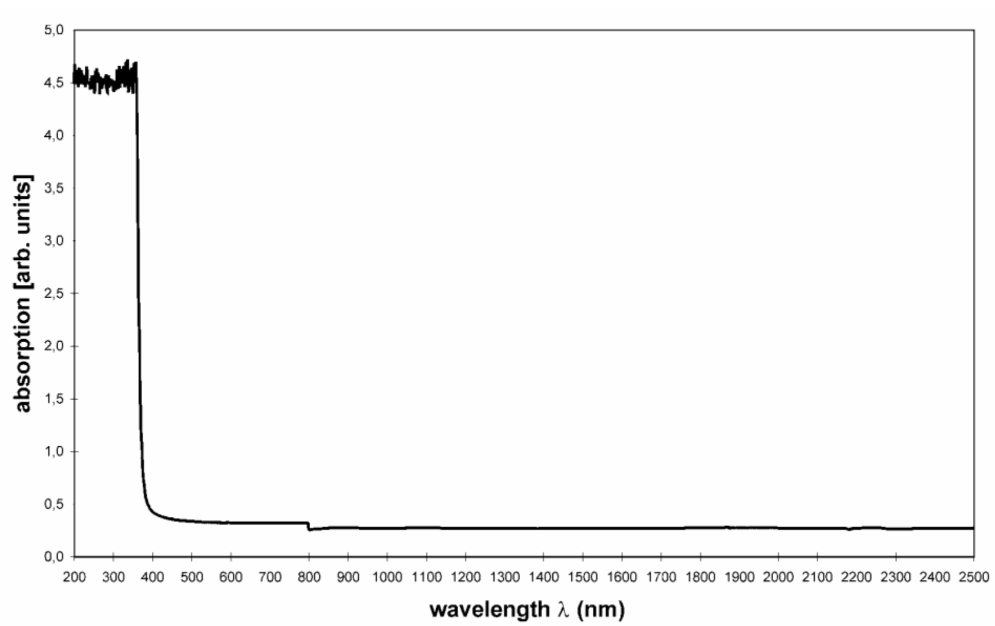

Figure 2.6.2 Light absorption spectrum of a (001)-plate of CBN-28 (thickness: 2.52 mm). The kink at 800 nm is caused by a lamp change. [83]

Table 2.6.1 Sellmeier parameters for the indices of refraction of unpoled CBN-28 [83].

	A	B	C	D	χ^2
n_e	4.74803	0.11165	0.05062	0.02164	$1.0699*10^{-7}$
n_o	4.99401	0.13513	0.05446	0.02675	$4.4569*10^{-8}$

Table 2.6.2 Nonlinear susceptibility components of CBN thin film [79].

	d_{15}	d_{32}	d_{33}
d (pm/V)	5.0 ± 2	3.1 ± 0.4	9 ± 2

2.7 Summary

Chapter 2 introduces the fundamental concepts in nonlinear photonic crystals (NPCs). It begins with a broad overview in section 2.1, providing context and explaining the importance of NPCs in various fields of study.

Section 2.2 delves into harmonic generation, a key process in nonlinear optics, discussing the formation of new frequencies as light passes through nonlinear materials. This sets the groundwork for understanding the behaviors and applications of NPCs.

In section 2.3, the concept of phase mismatching is introduced and various phase matching techniques are explored. The birefringent phase matching technique (2.3.1) and the quasi-phase matching technique (2.3.2) are elaborated upon, giving insight into ways to overcome the phase mismatch problem.

Section 2.4 discusses the reciprocal lattice vectors and Fourier transform, both critical mathematical tools for understanding the behavior of light in NPCs.

The reciprocal lattice vector (2.4.1) provides a way to visualize the periodic structure of a photonic crystal, while the Fourier transform (2.4.2) and the Convolution Theorem (2.4.3) allow for the analysis of light behavior in the frequency domain.

Section 2.5 discusses the design and simulation of nonlinear wavefront shaping in 3D NPCs. Section 2.5.1 elaborates on the simulation of far-field SHG patterns, providing a practical approach to predict and analyze SHG from a given NPC structure. In section 2.5.2, the concept of nonlinear volume holography is introduced, a technique for designing and manufacturing highly efficient and flexible 3D NPCs.

Section 2.6 delves into the crucial properties of nonlinear optical materials within the scope of 3D NPCs created through infrared laser direct poling. It compares several types of nonlinear optical materials and specifically emphasizes the superior characteristics of CBN (Calcium Barium Niobate). The research conducted in this thesis is based on this particular material.

Chapter 3 Nonlinear wavefront shaping in 3D NPC

3.1 Introduction

3D NPC fabrication based on laser writing is a breakthrough technology. However, in initial research by Xu and Wei, they each only fabricated the simplest 3D square lattice structure to demonstrate the technology without further exploring the potential functions of 3D NPCs. In fact, this technology making many previously theoretical functions a reality and greatly advancing the research of 3D nonlinear structures. These include but are not limited to nonlinear wavefront shaping, multidimensional entanglement photon generation, all-optical controlled chips, volume nonlinear holography, nonlinear multiplexing, and cascaded nonlinear effects[88]. Among these, nonlinear wavefront shaping is the basis for many potential applications. Unlike linear optical wavefront shaping which not change the wavelength of modulated light, nonlinear wavefront shaping can modulate light at new frequencies. This opens up possibilities for exciting new applications, including entangled photon generation, all-optical self-routing, and ultrafast light techniques. [51], [89], [90]. It's also worth emphasizing that initially modulating the wavefront linearly and then converting the frequency often doesn't work, as the phase of the nonlinear waves does not follow the fundamental wave.

Nonlinear wavefront shaping based on NPCs doesn't actually modulate the phase of an existing nonlinear beam. Instead, it assigns different initial phases to the nonlinear beams during the nonlinear conversion process that generates the beams. Since nonlinear wavefront shaping is based on nonlinear frequency conversion, quite naturally, QPM plays a significant role. Depending on the different modes of phase matching, this can be further divided into Bragg diffraction[91], Cherenkov emission[92], and nonlinear Raman-Nath diffraction[93]. Among them, the phase matching condition for Raman-Nath diffraction is the easiest to achieve, the nonlinear wavefront shaping is not critically depends on the pump light wavelengths. There are many existing studies on nonlinear wavefront shaping based on this mode, successfully generating nonlinear Airy beams, vortex beams, and Bessel beams [51], [56], [94]. Figure 3.1.1 (a) is a schematic diagram of second harmonic Raman-Nath diffraction based on a 2D NPC. The fundamental frequency (FF) light with plane wavefront is incident on a 2D NPC, which has a spatial modulation of $\chi^{(2)}$on the plane perpendicular to the incident light. The interaction of the FF with the 2D NPC generates a second harmonic (SH) with a designed initial phase and intensity. After the SH exits the crystal and propagates to the far field position, it exhibits the wavefront of a vortex beam.

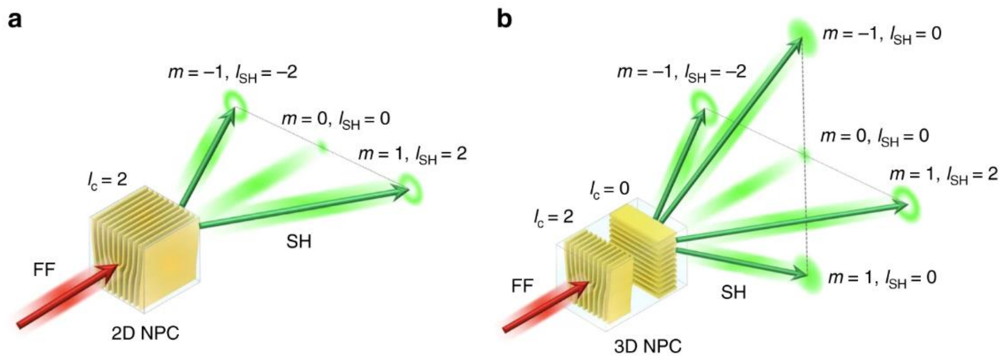

Figure 3.1.1 Schematic of nonlinear wavefront shaping based on NPCs. (a) A 2D NPC can achieve a single function of nonlinear wavefront shaping. (b) In contrast, a 3D NPC can simultaneously achieve the functions of multiple 2D NPCs [75].

It is quite challenging to stack multiple wavefront shaping functions on a 2D NPC, but a 3D NPC can easily solve this problem. As shown in Figure 3.1.1(b), by adding another layer of 2D NPC with different function behind a single layer of 2D NPC, the two layers of 2D NPCs can work simultaneously to complete two different nonlinear wavefront shaping functions. Traditional electric field poling methods cannot fabricate such complex multilayer structures, while it is quite straightforward for 3D laser poling methods. In the next section, the experimental setup and operation parameters of 3D laser poling will be discussed in detail.

3.2 Experimental setup

3D laser poling setup is illustrated in Figure 3.2.1, near infrared ultrafast laser (MIRA, Coherent) operating at $\lambda = 800\ nm$, with a pulse duration of $\tau = 80\ fs$ and a repetition rate of $f = 76\ MHz$. A shutter controls the output of the laser, with the laser's output power managed by a half-wave plate and a polarizer. Both the shutter and the half-wave plate are connected to the computer and controlled by software. After adjusting the power of the laser, the beam passes through a 2/98 beam splitter, with the majority of light continuing on. The beam then enters and focuses within the CBN crystal through the z-surface, facilitated by a 50x/NA0.65 objective lens. The crystal is placed on a motor-driven stage that can move in three dimensions, allowing for controlled, free movement under computer guidance. On the backside of the crystal, a blue LED is used for illumination. The blue light propagates in the opposite direction of the optical path, passing through the objective lens and is reflected by the beam splitter towards a CCD. In front of the CCD, there is a short pass filter that blocks the 800 nm writing beam while allowing the blue light to pass through and focus onto the CCD through a lens. This lens and the objective together form a microscope used for real-time monitoring of the laser writing process.

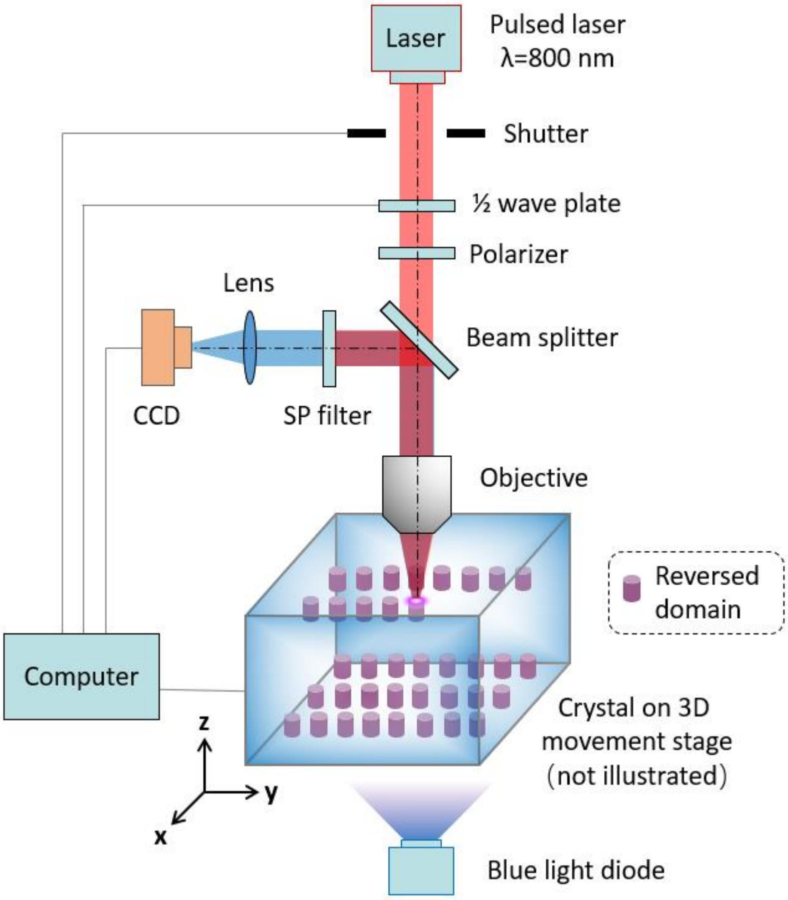

Figure 3.2.1 Laser writing setup sketch.

The poling of the crystal is achieved by scanning the laser focus within the crystal. The laser is directed to enter and focus inside the CBN crystal from the z-surface. Then, the focus is scanned along the z-axis towards the surface of the crystal, i.e., scanning from deep to shallow, at a speed of 2.5μm/s. After scanning for 20μm, the shutter is closed, completing one poling operation.

A columnar reversed domain forms in the area scanned by the laser, with a length of about 20μm and a diameter of approximately 1μm. The cylinder's axis is along the z-axis. By changing the focus position in the x and y directions and repeating the above steps for laser poling, multiple reversed domains can be connected to form the designed pattern, thereby realizing laser writing NPC. The distance between two poling regions is approximately 0.5μm, ensuring that adjacent domains merge together.

During the fabrication of multi-layer NPCs through laser poling, the sequence of fabrication is crucial. The deeper layer of NPC must be fabricated first, followed by the fabrication of the shallower layer. If not done in this order, the shallow layer's laser-engineered structure could interfere with subsequent laser poling. Additionally, the power of the laser also needs to be adjusted according to the different scanning depths as poling at greater depths requires higher power. The cause of this change in poling power threshold is not due to the crystal's absorption of light but rather due to the birefringence of the crystal leading to a degradation of the focus [95]. This point will be discussed in detail in Chapter 5.

3.3 Versatile control of nonlinear interactions with 3D NPCs

To demonstrate a single 3D Nonlinear Photonic Crystal (NPC) performing the functions of multiple 2D NPCs, we have fabricated two 3D NPCs each with a 3-layer structure. The structure of the first 3D NPC is shown in Figure 3.3.1(a), which consists of three layers of independent fork-shaped 2D NPCs, each layer being rotated by 60° compared to its adjacent layer. Figure 3.3.1(b) shows a 3D imaging picture of this structure taken by a nonlinear microscope, where the three-layer domain structures all present finely detailed fork structures. It is important to note that there are substantial gaps between the three layers in the image, which were intentionally adjusted to clearly illustrate each layer's structure. In reality, the multilayer structure is closely stacked together. This also reflects the fine control of the laser poling technique over the length of the poling domains, with the gap between the layers being less than 5 μm, and not overlapping with each other. Such complex 3D NPCs cannot be fabricated using traditional electrical poling methods. The far-field SHG pattern of this structure is displayed in Figure 3.3.1(c), where six independent donut beams are arranged in a hexagonal pattern, with every two diagonally opposite donuts originating from the SHG of the same layer of domain structure. The laser source for exciting the SHG comes from the Coherent Chameleon + Chameleon OPO system, with a pulse width of 200 fs, a repetition rate of 80 MHz, and a tunable wavelength range of 680-1600 nm. Each layer of domain structure produces a nonlinear shaped beam with similar intensity and quality. This is because the laser poling technique only modulates the $\chi^{(2)}$property of the material while having almost no impact on the linear properties of the material. Consequently, the fundamental light can pass through the multiple $\chi^{(2)}$ structures unhindered and engage in similar nonlinear optical processes with each layer.

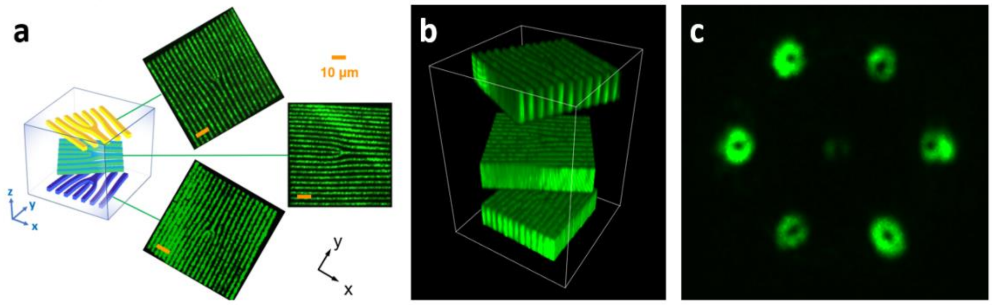

Figure 3.3.1 3D NPC with 3-layer fork structure. (a) Schematic of the multilayer fork structure, with the crystal orientation identified by the coordinate system on the left. The three images on the right are z-direction imaging pictures taken by a nonlinear optical microscope, with the scale bar corresponding to a length of 10 μm. (b) 3D image composed after the structure was scanned in layers by a nonlinear optical microscope. The interlayer spacing was artificially enlarged during the image processing stage, for the purpose of clearly illustrating the structure of each domain layer. (c) Far-field diffraction pattern of the SHG generated by this structure, with six donut beams independently produced by the three-layer fork structure.

Similarly, we have also fabricated another three-layer 3D NPC, where each layer of this 3D NPC is composed of completely different structures, unlike the previous one which consisted of identical structures, each layer merely rotated by 60°. The structure of this 3D NPC is shown in Figure 3.3.2 (a), where the top layer has a fork shape, the second layer is a one-dimensional periodic grating, and the bottom layer is a concentric rings structure. Despite the completely different styles of the three layers, they all have some kind of periodicity, and the size of the periods is the same, 3 um. Specifically, each ring of the concentric rings is 3um apart from the inner ring, each line in the grating is 3um apart from the adjacent line, and while the fork structure is not entirely periodic, it resembles a grating pattern, with the distance between each line approximately 3 um. This identical periodicity ensures that they will have the same emission angle when generating SHG, as we see in Figure 3.3.2 (c). The far-field SHG pattern of this structure consists of three patterns: two donut beams originate from the fork structure of the first layer, the two Gaussian beams come from the one-dimensional grating, and the large ring comes from the concentric rings structure. Here, it can be observed that the brightness of the large ring is noticeably lower than that of the donut beams and Gaussian beams, because the larger covered area of the large ring results in a spread of light intensity, making it appear dimmer.

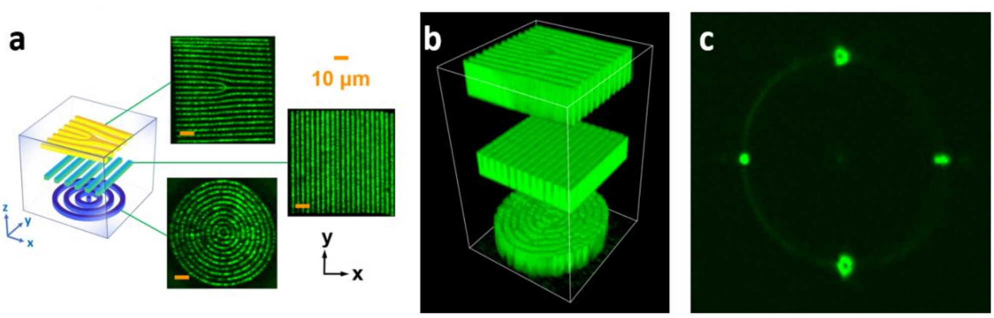

Figure 3.3.2 Multilayer 3D NPC with three different layer structures. (a) Schematic of the multilayer structure, with the crystal orientation identified by the coordinate system on the left. The three images on the right are z-direction imaging pictures taken by a nonlinear optical microscope, with the scale bar corresponding to a length of 10 um. (b) 3D image composed after the structure was scanned in layers by a nonlinear optical microscope. The interlayer spacing was artificially enlarged during the image processing stage, for the purpose of clearly illustrating the structure of each domain layer. (c) Far-field diffraction pattern of the SHG generated by this structure.

Although in this work we have only fabricated 3D NPCs with a three-layer structure, theoretically we could significantly increase the number of layers, allowing a single 3D NPC to simultaneously perform a multitude of functions. This high level of integration is something that 2D NPCs cannot achieve.

3.4 Dynamic control of nonlinear optical waves with 3D NPCs

In addition to integrating multiple 2D NPCs within a single 3D NPC to achieve multiple functions, we have also realized dynamic control of nonlinear optical waves by moving the laser focus longitudinally. Because the focus of the laser is of finite length along the longitudinal direction, this property can be exploited to let the focus only act on one layer of the multilayer 2D NPCs, without interacting with other layers. As shown in Figure 3.4.1(a), we have fabricated a two-layer 3D NPC, with the first layer being a fork structure and the second a one-dimensional grating. There is a substantial distance between the two layers, approximately 322 μm. Such a large gap allows the focused fundamental light to act on one layer without interacting with the other. Figure 3.4.1(c) and (d) show the far-field SHG patterns generated when the fundamental light is focused at different depths. In (c), the laser focus is concentrated on the grating layer, and the SHG pattern can be observed as two Gaussian beams, with almost no visible donut beam generated by the fork layer. Conversely, in (d), the far-field SHG pattern when the laser focus is concentrated on the fork layer clearly shows two donut beams generated by the fork layer, with hardly any Gaussian light generated by the grating layer visible.

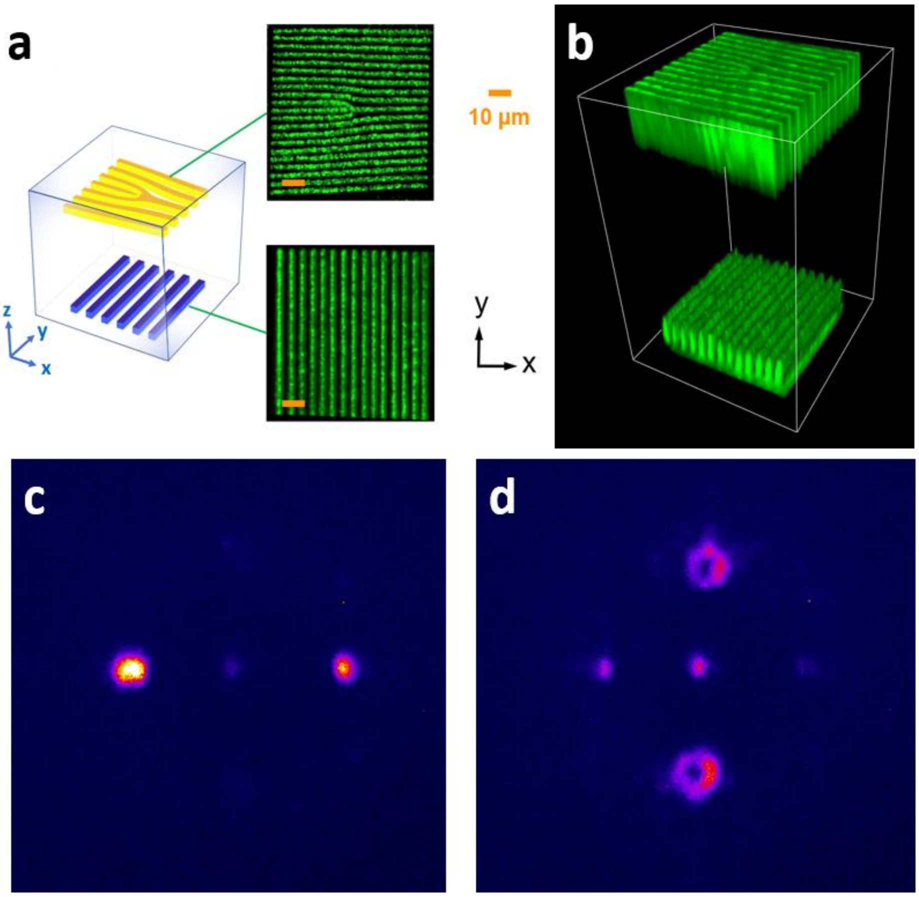

Figure 3.4.1 Dynamic control of nonlinear optical waves with 3D NPCs. (a) Dual-layer 3D NPC, with the first layer being a fork structure and the second a one-dimensional grating. The gap between the two layers is 322 μm. The scale bar corresponds to 10 μm. (b) 3D imaging of the structure taken by a nonlinear optical microscope. (c) and (d) are the far-field SHG patterns when the focus of the fundamental light is on the grating layer and fork layer, respectively.

This characteristic of adjusting the focus position to stimulate different functionalities of a 3D NPC provides enormous flexibility for its applications. A single 3D NPC can not only contain multiple different nonlinear functionalities but also selectively activate some of these functionalities rather than all at once.

3.5 Nonlinear bottle beam

Nonlinear photonic crystals can not only realize 2D nonlinear wave shaping in the far field but also achieve 3D nonlinear wave shaping within the near-field range [96]. The light intensity distribution in the far field is very stable and does not change with the light propagation. In contrast, the light intensity distribution in the near field significantly changes with the propagation distance. This change is controllable. With a reasonably designed nonlinear photonic crystal structure, we can produce the desired 3D nonlinear light intensity distribution. Below, we use the nonlinear bottle beam as an example to illustrate this technique.

Figure 3.5.1 (a) shows an ideal amplitude hologram capable of producing a bottle beam in the near field. As can be seen, the hologram has a structure with two concentric rings, inner and outer. When we illuminate this hologram with Gaussian light, the structures of the inner and outer rings will respectively diffract the Gaussian light into Laguerre–Gaussian modes LG_0^0 and LG_2^0, focusing them at different locations in space. These two diffracted beams interfere with each other, resulting in a continuously changing light intensity distribution along the propagation direction. By thoughtfully designing the parameters of the two-ring structures, we can create a light intensity distribution with a dark core in 3D space, commonly referred to as the bottle beam.

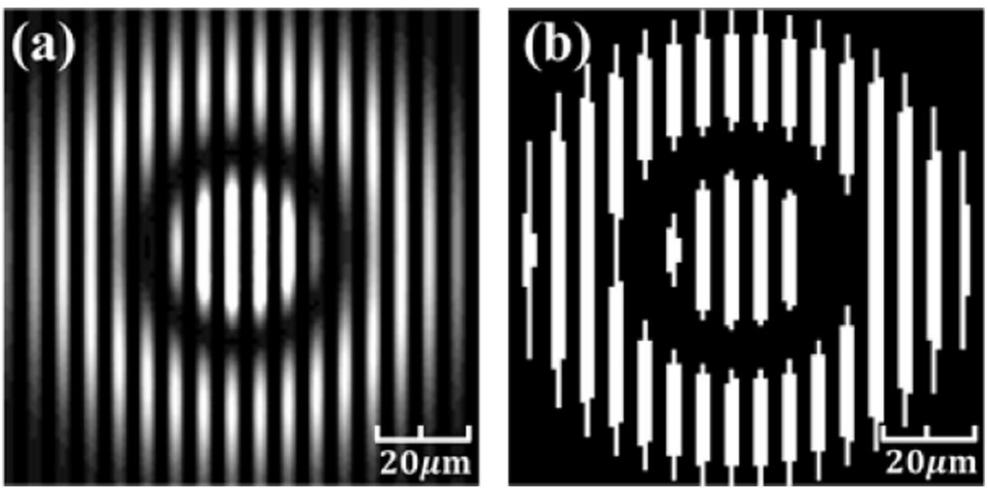

Figure 3.5.1

Due to the constraints of nonlinear crystal materials（$Sr_{0.61}Ba_{0.39}Nb_2O_6$）, we cannot fabricate a nonlinear photonic crystal structure with continuous intensity variations as shown in Figure 3.5.1 (a). However, through simulation, we found that even a binary nonlinear hologram can successfully produce a nonlinear bottle beam. After considering practical experimental conditions such as crystal properties and laser poling fabrication processes, we designed the nonlinear photonic crystal structure as shown in Figure 3.5.1 (b). This structure only has two values, 1 and 0, corresponding to the application of laser poling and maintaining the original state, respectively.

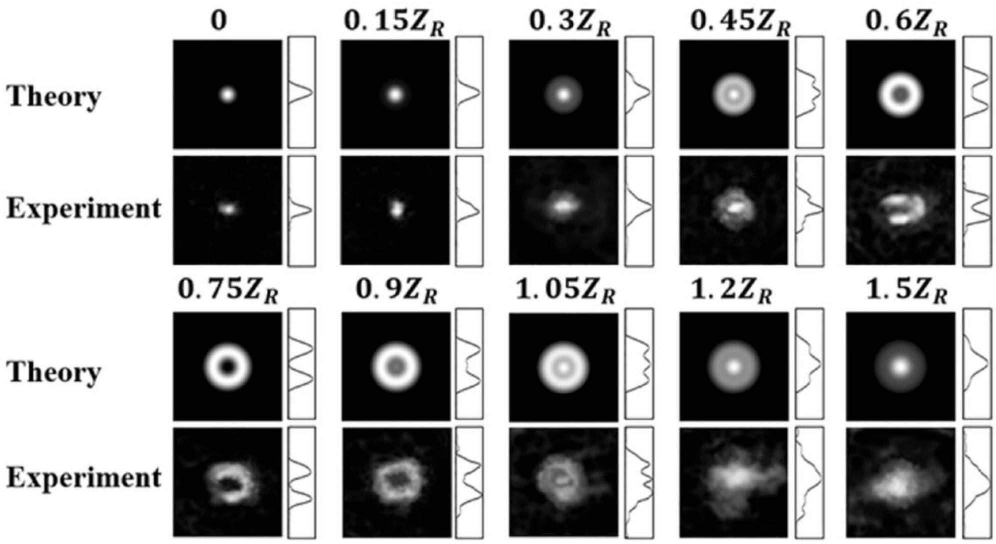

Figure 3.5.2

We used the experimental method described in section 3.3 to conduct the SHG test on this nonlinear photonic crystal. The experimental results, along with the corresponding theoretical simulations, are displayed in Figure 3.5.2. It can be seen, that the SHG is initiated at the nonlinear photonic crystal site and propagates forward. Its light intensity distribution continuously changes with the variation of the propagation distance. Furthermore, a bottle beam is formed within the range of z=0 to 1.5 Z_R, with its dark core located at z=0.9 Z_R. The experimental results are mainly in agreement with the theoretical simulations. However, the binary structure and fabrication errors resulted in some noise.

3.6 Summary

We fabricated three-dimensional nonlinear photonic crystals (3D NPC) in $Ca_{0.28}Ba_{0.72}Nb_2O_6$ ferroelectrics using a laser direct poling technique, which demonstrated an unprecedented capacity for nonlinear wavefront shaping. By integrating a three-layer nonlinear photonic structure consisting of a fork grating, a standard one-dimensional grating, and a circular grating within a single 3D NPC, we simultaneously converted a fundamental Gaussian beam into second harmonic vortex, Gaussian, and conical beams. Additionally, by leveraging the spatial separation of domain structure layers, we demonstrated dynamic control over nonlinear interactions within a 3D NPC. In addition, we also used a 2D NPC to generate a nonlinear bottle beam, demonstrating that we can achieve 3D light field shaping through NPC. These experiments underscore the immense potential of 3D NPCs for nonlinear wavefront shaping, as they allow for the integration of multiple nonlinear functionalities within a single 3D NPC and the selective activation of specific functionalities. The findings presented here pave the way for the development of novel coherent light sources, which can generate shaped beams at new wavelengths—an essential element for many fundamental research studies and industrial applications in optics. In future work, we plan to incorporate QPM into 3D NPCs to enable phase-matched interaction in any designated direction. Such 3D NPCs, which often have highly complex structures, are beyond the capabilities of traditional fabrication methods and can only be realized using our laser poling technique.

Chapter 4 Nonlinear volume hologram

4.1 Introduction

In Chapter 3, we introduced a type of 3D NPC fabricated using laser poling technology, composed of multiple non-interfering 2D NPCs stacked together to simultaneously realize multiple different NWS functionalities. However, its implementation of NWS is based on the low-efficiency Raman-Nath diffraction, resulting in extremely low nonlinear conversion efficiency ($\sim 5 \times 10^{-8}$). Raman-Nath type diffraction is a type of nonlinear diffraction that does not satisfy phase matching, such intrinsic property prevents it from providing high nonlinear conversion efficiency. To improve the nonlinear conversion efficiency, perfect phase matching must be introduced, i.e., nonlinear Bragg diffraction. To realize NWS while satisfying phase matching, using nonlinear volume holography is an excellent solution.

In 2014, Hong and colleagues introduced concepts of hologram known from linear optics into nonlinear optics, and proposed the nonlinear volume holography[59]. According to this technique, a $\chi^{(2)}$ structure capable of performing arbitrary wavefront shaping can be designed. Furthermore, this $\chi^{(2)}$ structure design theory inherently includes the phase-matching relationship between light waves, thereby always enabling highly efficient generation of nonlinear waves. Taking the simplest second harmonic generation (SHG) nonlinear process as an example, the fundamental wave (FW) propagates in the nonlinear medium and excites the nonlinear polarization wave, which has the same propagation velocity as the FW and twice its frequency. Such a nonlinear polarization wave serves as the reference beam, while the objective beam is the SH wave. As shown in Figure 4.1.1 (a), the reference beam and the objective beam interfere with each other in the nonlinear medium to produce interference fringes, which store the intensity, phase, and wavelength information of the objective beam.

In standard holography the information storing is done by directly recording interference fringes in a medium using photosensitive materials. In case of nonlinear holography the storing process requires recording of interference fringes in the medium in the form of $\chi^{(2)}$ variation, which obviously cannot be achieved by a simple light exposure. To realize nonlinear volume holography, one must first simulate the nonlinear interference process on a computer to calculate the pattern of the interference fringes. Then, $\chi^{(2)}$ modulation technique is used to imprint the calculated interference fringes onto the nonlinear medium. The fringe pattern is given by:

$$T(x,y,z) = \left|E_p + E_o\right|^2 = \left|E_p\right|^2 + \ |E_o|^2 + 2E_pE_o cos(\varphi)$$

Where E_p is the polarization wave trigged by reference beam E_r, $E_p \propto E_r^2$; E_o is the object beam electric amplitude; φ is the phase difference between polarization wave and object beam. The background terms $\left|E_p\right|^2$ and $|E_o|^2$ do not contribute to the fringe pattern, thus the normalized fringe function is $T'(x,y,z) = cos\varphi$. Consider the modulation of $\chi^{(2)}$ in NPC is binary, we end up with:

$$T'(x,y,z) = sign(cos\varphi)$$

For 2D nonlinear holography, it can be implemented by polarizing the nonlinear optical crystal with an electric field, whereas for 3D nonlinear volume holography, the laser poling technique is required.

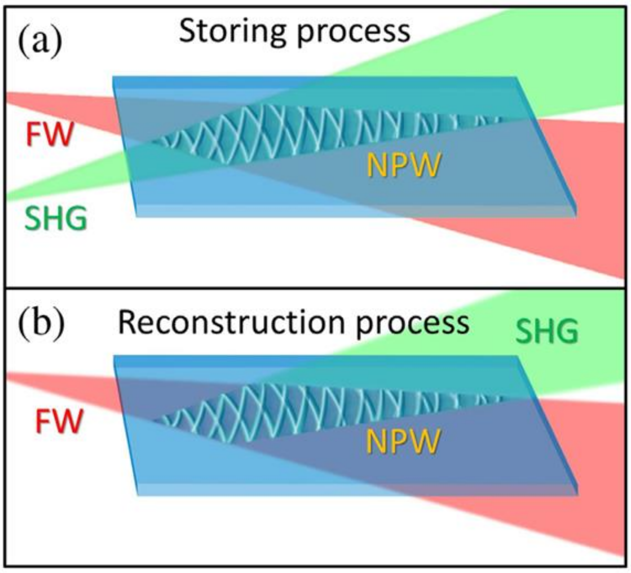

Figure 4.1.1 The concept of nonlinear holography. (a) Information storing process (b) Reconstruction process[59].

The reconstruction process is illustrated in Figure 4.1.1 (b), where the illumination of the FW onto the nonlinear hologram can reconstruct the nonlinear object beam previously stored in the NPC. If a Gaussian beam is chosen as the reference beam and the object beam has a special wavefront, this essentially realizes NWS through the technique of nonlinear volume holography.

4.2 Structure Design and Simulation

Our goal is to design a nonlinear volume hologram for converting a fundamental Gaussian beam into a second harmonic vortex beam. According to the aforementioned nonlinear holography theory, we are to set the reference beam as a plane wave and the object beam as a vortex beam, that is:

$$\mathrm{E_r} = e^{i(\vec{k}_1\vec{r}_1-\omega t)}$$

$$\mathrm{E_o} = e^{i\varphi(x,y)}e^{i(\vec{k}_2\vec{r}_2-2\omega t)}$$

Where $\vec{k}_1$ and $\vec{k}_2$ are the wave vectors of reference and objective beam; $\varphi(x, y) = \tan^{-1}\left(\frac{y}{x}\right)$ is the vortex phase. The computer-generated nonlinear volume hologram has a form of interference fringe between nonlinear polarization wave ($E_p \propto E_r^2$) and second harmonic wave:

$$T(x, y, z) = sign(cos(2k_1(x, y, z) - k_2(x, y, z))$$

Figure 4.2.1 (a) shows the interference fringe simulated by the computer as described above. In this simulation, we set that the medium material is CBN crystal, the FW Gaussian beam propagates along the z-axis, the SH vortex beam has a 5° angle with the propagation direction of the FW, and the topological charge number of the vortex beam is 1. It can be seen that the interference fringes show a fork-like shape in the x-y section, but the shape of the fork changes with the z coordinate. Inside the pattern, there is a twisted spiral structure in the direction at a 5° angle to the z-axis. To show this internal structure more clearly, it is separately enlarged and shown on the right. It can be seen, that this interference pattern has a complex spatial structure. The many curved surfaces make it difficult to process perfectly even with the most advanced laser poling technology. Therefore, we still need to simplify it to some extent, making this structure easy to process without affecting its function.

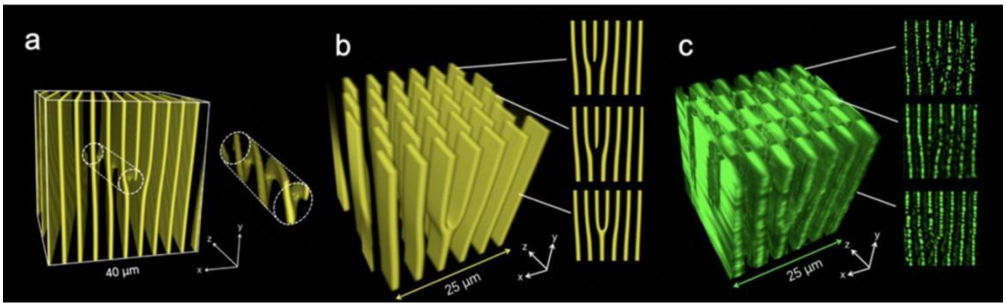

Figure 4.2.1 A nonlinear volume hologram capable of generating SH vortex beam. (a) The perfect hologram structure generated by the computer based on nonlinear volume holography theory. (b) The nonlinear hologram structure after discretization for ease of fabrication. (c) The nonlinear volume hologram fabricated using laser poling technology, as shown in a nonlinear microscopy image [76].

We used a stair-step discrete method to simplify the structure, as shown in Figure 4.2.1 (b). The specific simplification process is as follows: First, slice the xy plane every 6.85 μm along the z-axis direction, delete the structure outside the sliced plane, and then extend the sliced 2D pattern along the z-axis direction to fill the deleted space. After simplification, the original continuous and smooth structure becomes a stair-step discrete structure. This structure is very suitable for fabricating with laser poling technology, and theoretically it can ensure that the original structural function is not lost.

4.3 3D Nonlinear Volume Holograms Recording

We employed the laser poling technology to fabricate the structure described above into a CBN crystal in the form of domain inversion. The laser was focused by a 50x/NA0.65 lens and incident from the z-surface of the crystal, scanning within the crystal at a speed of 2.5mm/s to outline the pre-set pattern. The laser power was automatically adjusted under computer control based on different depths to achieve optimal fabrication results. The fabricated nonlinear volume hologram is depicted in Figure 4.2.1 (c), it is nearly identical to the designed structure in (b). This structure exhibits a fork-like shape in the xy-plane, with a transversal period of ~3.6um, a duty cycle of ~0.2, and an interlayer distance of 6.85um. The total volume of the nonlinear volume hologram is $80 \times 80 \times 80\ \mu\mathrm{m}^3$.

4.4 Reconstruction of the Second Harmonic Vortex Beam

We utilized a femtosecond laser directly from the laser source as the reference beam to reconstruct the object beam, i.e., the SH vortex beam. As depicted in Figure 4.4.1 (a), the reference beam with linear polarization (x-polarized) illuminated on the nonlinear volume hologram along the z-axis of the crystal, successfully generating an SH vortex beam with an approximate 5° emission angle. This result aligns perfectly with our design objective. Notably, unlike the multilayer fork structure states in Chapter 3, which generates the SH vortex via Raman-Nath diffraction, the SH vortex here is produced by Bragg diffraction which satisfying the QPM condition. Figure 4.4.1 (b) provides a schematic of phase matching, illustrating that the nonlinear volume hologram provides a RLV only on the left side, resulting in the generation of the SH vortex exclusively on the left. The fulfillment of QPM condition also realize a high conversion efficiency as high as 6×10^{-6}, which is ~100 times larger than previous work [75]. The QPM condition relies strictly on the wavelength. We tuned the input FW wavelength from 1000 nm to 1600 nm. As shown in Figure 4.4.1 (c), a strong SH signal is only observed near the designed wavelength of 1550nm.

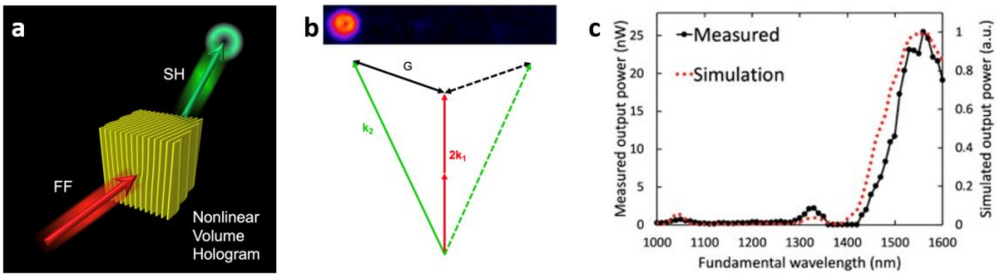

Figure 4.4.1 Reconstruction process of nonlinear volume holography. (a) scheme of reconstruction SH vortex beam via nonlinear volume hologram. (b) Far-field SH pattern and phase matching diagram. (c) Dependence between fundamental wavelength and measured SH power.

4.5 Summary

In this study, we have effectively demonstrated the application of the 3D optical poling technique for fabricating intricate 3D nonlinear structures. Leveraging the approach of nonlinear volume holography, we were successful in designing nonlinear volume hologram for reconstructing arbitrary special beams. For demonstration, an SH vortex beam was reconstructed from a nonlinear volume hologram after illuminated by a fundamental Gaussian beam. This strategic methodology allowed us to significantly enhance conversion efficiency compared to non-phase-matching conditions. However, the current conversion efficiency still has a significant gap from practical application, and there are numerous aspects that can be further optimized. This includes considerations such as the duty cycle of the domain structure, the type of nonlinear material used, and the method of laser poling. These factors all present opportunities for the enhancement of the system's overall efficiency, which will be vital for future research and potential real-world applications.

Chapter 5 Optimization of laser poling

5.1 Introduction

In Chapter 4, we introduced a method of achieving NWS through nonlinear volume holograms. We demonstrated this method by using the laser poling technique to fabricate a 3D NPC of size $80 \times 80 \times 80$ μm^3 for generating SH vortex beams. However, the conversion efficiency of this NPC was still relatively low due to several factors. Firstly, the effective volume of the NPC was too small. The conversion efficiency of an NPC is proportional to the square of its length. Hence, an increase in the size (and subsequently interaction length) of the NPC can significantly enhance the conversion efficiency. Secondly, we didn't optimally utilize the maximum effective nonlinearity of the crystal. The limitations of the laser poling technique restricted us to fabricating complex patterns from the z-surface of the CBN crystal, with a limited depth of fabrication. Consequently, we could only utilize a small effective nonlinearity. This limitation greatly hampered the nonlinear conversion efficiency of the 3D NPC because the conversion efficiency is proportional to the square of the effective nonlinearity. Lastly, the laser writing process inevitably introduced changes in the refractive index of the material. These changes led to linear light scattering, which caused a loss of energy in both the fundamental wave and the second harmonic. More importantly, the change in refractive index could introduce random phase shifts that affect QPM [81]. As phase shifts accumulate during propagation, they can significantly impair the performance of large-volume 3D NPCs. It is clear from these observations that the previous inefficiencies are largely due to the limitations of the laser poling technique. As such, to significantly improve the efficiency of 3D NPCs, we must focus on refining and enhancing this technique.

To tackle the aforementioned issues, we approached the problem from two aspects: focusing objective and laser polarization. We may start with the focusing objective. The theory of laser poling states that poling can only be achieved when the writing laser has a high optical intensity. Therefore, we previously used a high magnification and high numerical aperture objective lens for laser focusing. This inevitably led to a steep change in the optical intensity experienced between the laser-affected area and adjacent areas, resulting in significant differences in refractive index changes caused by the laser. Intuitively, if a lens with relatively weak focusing power is used to focus the laser, the sudden change would become more gradual and would not induce such dramatic changes in refractive index. On the other hand, due to the inherent spherical aberration in the imaging system, a high magnification lens can only focus the beam perfectly within a very small depth range [92]. The quality of focusing deteriorates significantly when the depth is far from that range. This greatly restricts laser writing in the deeper areas of the crystal. Therefore, we opted for using an objective lens with both lower magnification and numerical aperture for laser writing to circumvent these issues.

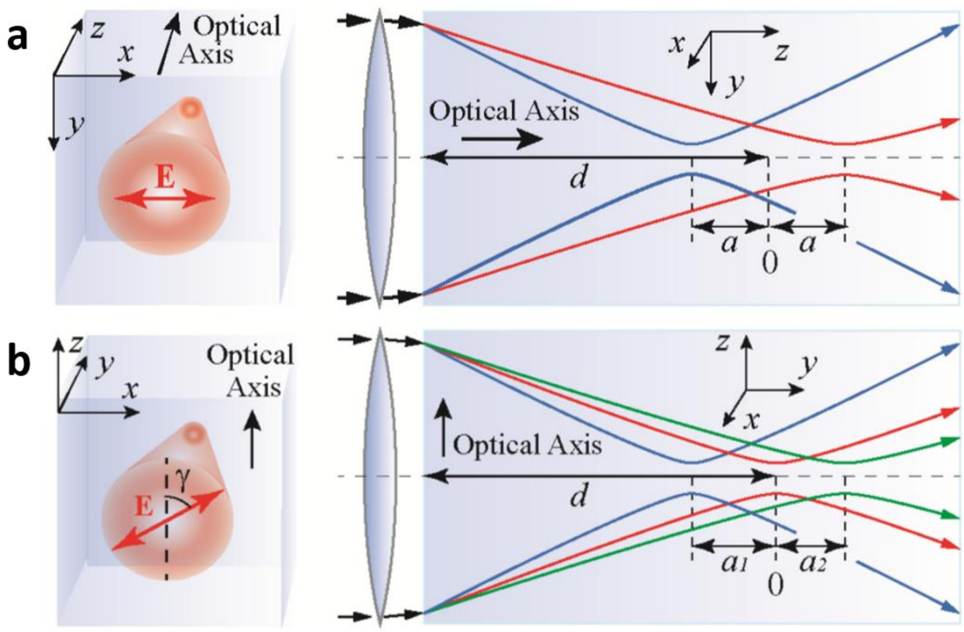

Figure 5.1.1 illustrates the splitting of laser focus in a uniaxial crystal. In panel (a), the laser, after being focused by a lens, is incident along the optical axis of the crystal. This causes the laser to split into two focus within the crystal. In panel (b), the laser, after being focused by a lens, is incident

perpendicular to the optical axis. In this case, depending on its polarization state, the laser can split into one to three different focus. This graphic illustrates the potential challenges presented by focus splitting in a uniaxial crystal during laser writing and imaging [95].

The polarization of the laser in the laser poling technique is a parameter that has been significantly overlooked in the past. Traditional laser poling involves the laser being incident along the c-axis of a uniaxial crystal. Regardless of how the polarization of the laser is changed, the laser appears as ordinary light (o-light or o-polarization) to the crystal. This is based on the assumption that the laser is incident on the crystal as a plane wave, which is not the case in reality, as the laser is focused by an objective lens before it enters the crystal. After focusing, the laser form angles with the c-axis, and thus the same laser beam will exhibit different polarization states after being focused by the objective lens. Specifically, it will become a mixture of ordinary (o-light) and extraordinary (e-light) polarization. Since o-light and e-light correspond to different refractive indices in a birefringent crystal, this will cause dispersion and result in a splitting of the laser focus as shown in Figure 5.1.1 (a) [95]. The extent of splitting is proportional to the focusing depth, which greatly limits the application of the laser poling technique for large volume 3D NPC fabrication. The effect of polarization on laser poling becomes even more pronounced if the laser does not enter the crystal from the c-surface. In this case, even if the incident light is not deflected by the objective lens, it will split into o-light and e-light with different refractive indices within the crystal. The issue of focus splitting mentioned above might be even more severe under these conditions. There could be up to three split foci in the crystal as shown in Figure 5.1.1 (b) [95].

The crystals we are processing are nonlinear crystal, and its nonlinear optical properties play a significant role during the process of laser poling. Here, we propose a hypothesis about nonlinear absorption within the nonlinear crystal. Specifically, the incident light first generates a second harmonic through a nonlinear process, which is then absorbed by the crystal through linear absorption (This hypothesis was subsequently validated by further research [97]). Based on this assumption, the polarization of the laser greatly affects nonlinear absorption, because the second harmonic generation of the fundamental light by the crystal is determined by the effective nonlinear coefficient, which highly depends on the polarization of the laser. Taking CBN crystal as an example, when the laser is incident along the z-axis of the crystal, the nonlinear tensor matrix element d_{11} of the crystal is zero, so the effective nonlinearity is extremely small, making it difficult to generate second harmonics. Conversely, if the laser is incident in a direction perpendicular to the z-axis and the polarization parallel to z-axis, due to the large nonlinear tensor matrix element d_{33}, a strong second harmonic will be generated.

If we optimize the laser poling technique based solely on this nonlinear absorption theory, the writing beam should be incident from the x-surface of the crystal with e-polarization. However, this contradicts the focus splitting problem described in the previous paragraphs. In other words, it is impossible to ensure both a non-split focus and use of the maximum effective nonlinear coefficient of the crystal simultaneously. In order to quantitatively resolve this issue and optimize the parameters of the laser poling technique, we conducted a series of experiments and simulations.

5.2 Femtosecond laser poling with different objective lens

We performed laser poling on CBN crystals using objective lenses with 20x/NA 0.4 and 50x/NA 0.65, respectively, with the incident crystal surfaces being the x-surface and z-surface, respectively. We tested the minimum optical power threshold needed to achieve domain reversal at different depths. The test results are shown in Figure 5.2.1. As seen, under the focus of high magnification lens, the laser can achieve domain reversal in relatively shallow areas of the crystal at very low power. However, as the depth increases, the power threshold curve corresponding to the high-magnification lens rises quickly, soon exceeding the power needed for domain reversal under the low-magnification lens. This is because a tightly focused beam is more sensitive to spherical aberration and focus splitting as talked earlier. It can also be observed that poling with laser incidence from the z-surface is more difficult than from the x-surface, which demonstrates the role of the effective nonlinear coefficient in poling, as the effective nonlinear coefficient when incident from the z-surface is nearly zero, making poling extremely challenging.

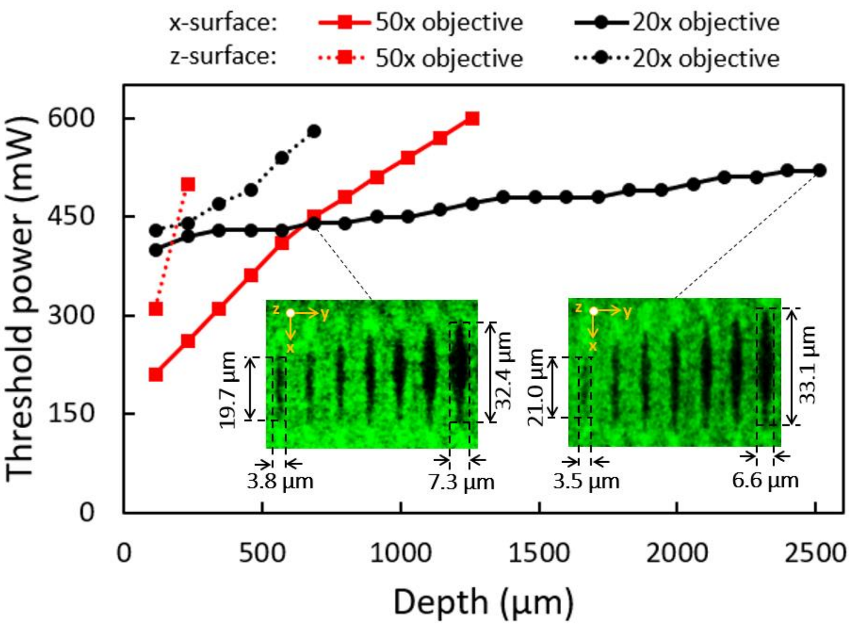

Figure 5.2.1 Laser poling power threshold vs focusing depth. 50x and 20x objective lenses are used to test the threshold of laser poling from both z- and x-surface incidence. Inserts are nonlinear confocal image for laser poling domains at 686 μm and 2628 μm depth respectively, domains are fabricated by 20x/NA0.4 objective lens incident from x-surface of the crystal.

In addition to the power threshold for laser poling, we are also very concerned about the quality of poled domains. In the insets of Figure 5.2.1, we can see images of laser poled domains at depths of ~700 μm and ~2500 μm. There is no significant difference in their quality. Therefore, as long as we choose the appropriate lens and laser polarization, we can achieve high-quality domain reversal at different depths.

Another benefit of focusing the writing laser with a low magnification lens is that it causes relatively small linear index changes. As shown in Figure 5.2.2, (a) is a CBN crystal after laser writing with a 50x/NA0.65 lens, where clear writing traces can be seen. These linear index changes cause diffraction of light, greatly affecting the quality of the 3D NPC. In contrast, (b) is a CBN crystal after laser writing with a 20x/NA0.4 lens, in which no significant refractive index change can be seen in this linear microscope image. To quantitatively study the effect of laser processing on the refractive index of the material, we conducted experiments by comparing the intensities of the diffraction peaks [98]. In Figure 5.2.2 (c), 1st, 2nd, and 3rd order diffractions can be seen, whereas in (d), no diffraction can be seen at all. According to theoretical calculations, the crystal processed with the 50x/NA0.65 lens has a refractive index change of $\sim 3.5 \times 10^{-5}$. This number is slightly larger than the refractive index changes of the domain structure prepared by electric field polarization ($\sim 1.5 \times 10^{-5}$), while the NPC processed with the 20x/NA0.65 lens cannot detect any refractive index change by the method of diffraction.

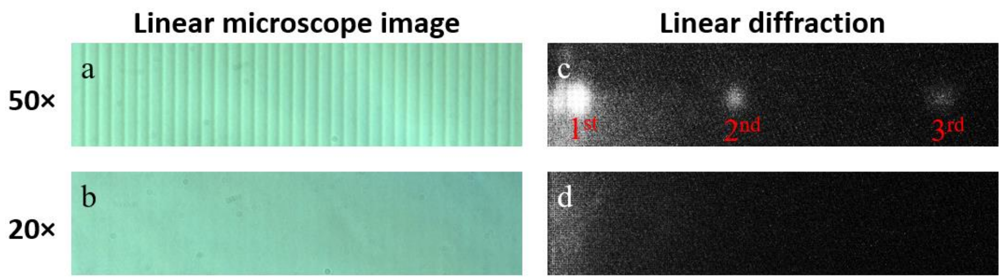

Figure 5.2.2 Laser induced refractive index change. (a) and (b) represent linear microscope images of laser-engineered regions in CBN crystal, with the laser focused by 50x and 20x objective lenses respectively. (c) and (d) depict far-field linear diffraction patterns generated when regions (a) and (b) are illuminated respectively by a 780 nm CW laser.

In summary, focusing the laser for laser poling with a low-magnification lens can achieve high-quality domain reversal over a considerable depth range, which pave the way for large volume 3D NPC fabrication. Additionally, the linear index change induced by laser is much smaller than that of a high-magnification lens, such feature is also crucial for large volume 3D NPC. Although the use of a low-magnification lens inevitably reduces the resolution of laser writing, it still has a transversal resolution of ~3 μm and an axial resolution of ~20 μm, which is sufficient to meet most of the processing requirements for 3D NPCs.

5.3 Femtosecond laser poling with different laser polarizations

Many laser writing technologies do not pay attention to the polarization of the writing beam, such as 3D direct laser written polymer , laser direct written waveguide [99], [100]. However, our laser poling technology is very sensitive to writing beam polarization. As can be seen from Figure 5.3.1, with the change of the polarization of the writing beam, the power threshold for domain poling has changed significantly. When the polarization direction of the laser is parallel to the crystal axis (0°, e-light), the laser can easily achieve domain reversal at a shallow depth with a very low power. However, the power threshold for domain reversal under this polarization will rise rapidly with the increase in depth. When the depth reaches 2285μm, its threshold has exceeded 600mW. Conversely, when the polarization direction of the laser is perpendicular to the crystal axis (90°, o-light), although the poling laser needs a higher power to achieve domain reversal at a shallow depth, the threshold does not rise rapidly with the increase in depth. Even at a depth of 2285μm, a power of only 480mW is needed to achieve laser domain reversal. The situation at 45° polarization is the worst. Not only does it require a relatively high power to achieve poling at a shallow depth, but the energy threshold rises very quickly with the increase in depth, even faster than at 0°. The threshold exceeds the maximum power of the laser, 600mW, when the depth is only 1143μm. The different performances of different polarized writing beams need to be explained from two aspects: the role of SH in laser poling and the split of the laser focus in the uniaxial crystal.

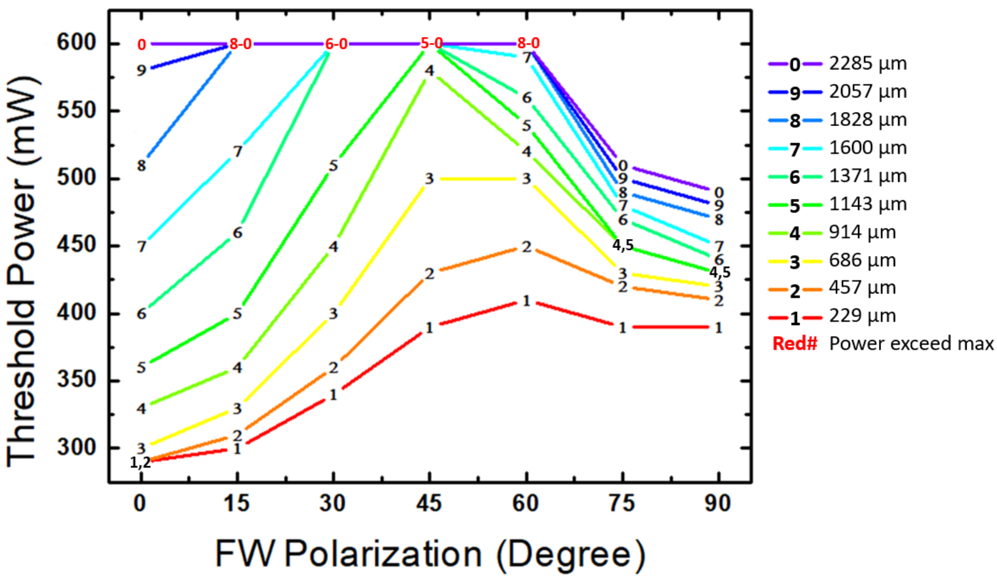

Figure 5.3.1 Effect of writing beam polarization on the laser power threshold for domain reversal

The process of laser poling often comes with observable SH signals. Researchers use the SH signals observed during the laser writing process as one of the bases for real-time monitoring of laser poling [70]. In fact, the SH signal generated during the laser poling process is not just a by-product, it deeply participates in the poling process. The fundamental frequency writing beam can transmit to the interior of the crystal to generate SH, and the crystal is non-transmitted to the wavelength of SH, thereby absorbing a large amount of SH, triggering a thermoelectric field, and then realizing ferroelectric domain poling. Figure 5.3.2 (a) depicts two laser poling processes with all conditions the same except for the polarization state of the writing beam. On the left, o-polarized laser is used for poling, at which time almost no SH signal is generated and poling cannot be carried out. On the right, the e-polarized laser produces strong SH and successfully achieves laser poling. An intuitive explanation is that the d_{31} tensor element of the CBN crystal's nonlinear coefficient is much smaller than d_{33}, so poling with o-light cannot generate strong enough SH to support poling. To further verify our thoughts, we studied the SH light intensity excited by the FW light of different polarization states, the results of which are shown in Figure 5.3.2(b). It can be clearly seen that this curve is inversely proportional to the 229μm depth curve in Figure 5.3.1, which indirectly verifies our hypothesis. However, this correspondence is mainly consistent when the laser is focused at relatively shallow positions under the crystal surface. When the laser is focused deeper into the crystal, the splitting of the laser focus becomes the dominant factor that affects laser poling.

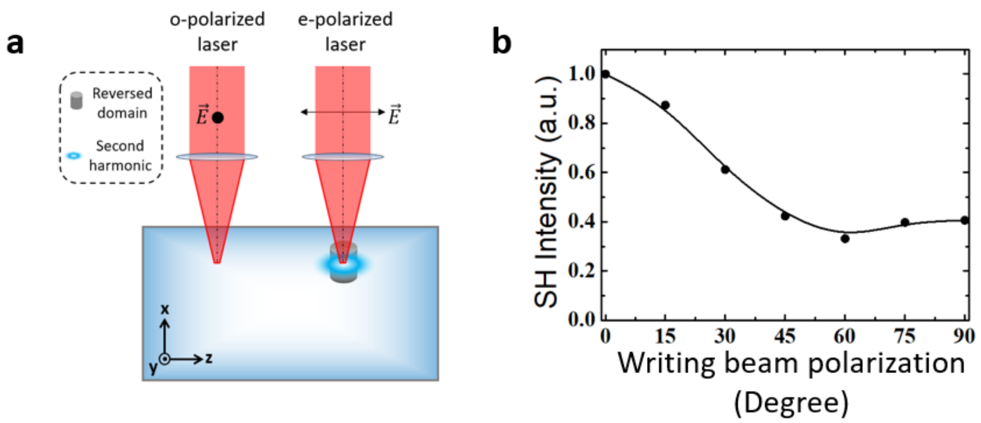

Figure 5.3.2 The impact of different laser polarization states on laser poling. (a) Schematic diagram of laser poling under different polarization states, using e-polarized light for poling in CBN crystal can easily excite strong SH. (b) The relationship between FW (forward writing) polarization and SH intensity in CBN crystal.

When a focused laser is incident on a uniaxial crystal, the splitting of the focus may take place, thereby affecting the quality of poling. In the study by Karpinski et al., they pointed out that this focus split can only be avoided when the laser is incident from the direction perpendicular to the crystal axis and the laser is o-polarized[95]. However, this is in conflict with the nonlinear absorption mentioned above. According to Figure 5.3.2 (b), when the polarization of the laser is e-polarized, it is most conducive to the generation of harmonics and poling. In order to study the impact of focus splitting and nonlinear absorption on laser poling more quantitatively, we first simulated the writing beam intensity in the crystal under different polarization states (see Eqs. 4(a)(b) in [95]). As previously mentioned, CBN crystals are strongly absorptive for SH wavelength. We assume that most of the SH is rapidly absorbed by the crystal soon after generation, and does not continue to propagate forward. Therefore, the local SH intensity only depends on the local FW intensity and the crystal's nonlinear coefficient, while factors like the length of the crystal and phase mismatching can be ignored. We calculated the locally generated second-harmonic intensity by $I \propto d_{33}^2 E_z^4 + d_{31}^2 E_x^4 + 4d_{15}^2 E_z^2 E_x^2$, where $d_{33} \approx 9$, $d_{31} \approx 3.1$ and $d_{15} \approx 5$ are the non-zero nonlinear coefficients of the CBN crystal [79]. Figure 5.3.3 shows the distribution of writing beam and its SH intensity inside the crystal when lasers of different polarizations are incident from the x-surface of the CBN crystal. The simulation focus depth is 1600μm, and the refractive index and nonlinear matrix of the crystal are from CBN crystal[83], [87]. It can be seen that when the laser has e-polarization, the focus split is the most serious, and the light intensity is weakest at the focus. There is no focus split when the laser is o-polarized, and the light intensity at the focus is strongest. After taking the second-order nonlinear coefficient into account, we simulated the spatial intensity distribution of the second harmonic inside the crystal. It can be seen that at a depth of 1600μm, although e-light can excite the ee-e process to use the largest nonlinear coefficient d_{33}, due to the deterioration of focusing quality, the SH intensity at this time is not as good as the o-polarized light using the smaller nonlinear coefficient d_{31}.

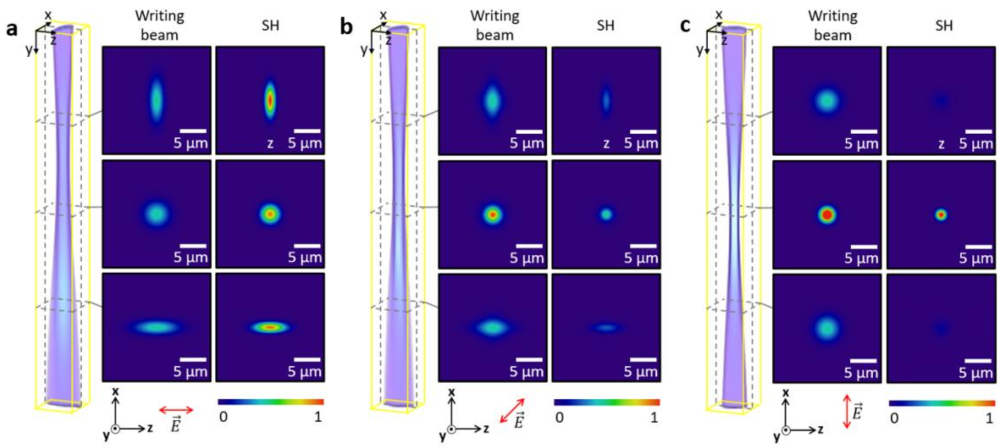

Figure 5.3.3 Writing beam and its SH intensity distribution in CBN crystal. Laser incident from x-surface and focused by a 20x/NA0.4 objective lens, focus is 1600μm under the surface and laser polarization against z-axis are 0° (a), 45° (b) and 90° (c) respectively.

5.4 Summary

In summary, the polarization of the laser plays an important role in the process of optical poling. On the one hand, because the focused laser will exhibit focus splitting inside a birefringent crystal, and the degree of focus splitting is related to the polarization of the laser. On the other hand, because the nonlinear absorption of the laser inside the crystal is related to the nonlinear coefficient of the crystal, and the effective nonlinear coefficient is related to the polarization of the laser. These two factors influence the laser power required for laser poling, and each plays a dominant role at different focal depths. We performed an experiment in CBN crystal and conducted numerical simulations, which led to the following conclusions. When the laser is focused shallowly, the focus splitting is not significant and the nonlinear absorption rate plays a dominant role, so e-light should be used for poling at shallow depth. When the laser is focused deep inside the crystal, focus splitting becomes the dominant factor, so o-light should be used for poling to avoid it.

Chapter 6 Highly efficient large volume 3D NPC

6.1 Introduction

In Chapter 4, we discussed some of the current limitations of nonlinear volume holography (NVH). Due to the limitations of the laser poling process, it is very difficult to fabricate a highly efficient large volume nonlinear volume hologram based on 3D NPC. In Chapter 45, we purposefully studied and improved the laser poling process to enable it to fabricate large volume 3D NPCs. In this chapter, we will use the latest laser poling technique to fabricate large volume 3D NPC structures, which were previously difficult to achieve, for highly efficient nonlinear wavefront shaping.

The pursuit of high efficiency and high-quality nonlinear wavefront shaping is a fundamental issue in this research field, and it is the cornerstone of many practical applications. However, previous NWS either had extremely low efficiency or could only achieve shaping in one dimension. Specifically, Wei et al. achieved 2D NWS in lithium niobate using a multi-layer fork structure fabricated by laser $\chi^{(2)}$ erasing technique, but its normalized conversion efficiency was only $1.4 \times 10^{-10} W^{-1}$[82]. Chen et al. designed a multiplexing nonlinear hologram by means of inverse Fourier transform method and fabricated using the same $\chi^{(2)}$ erasing technique, a normalized coversion efficiency of $4.25 \times 10^{-11} W^{-1}$ was achieved. Ellenbogen et al. used the traditional electric poling method to prepare 2D NPC in lithium niobate, achieving an NWS efficiency as high as $\sim 10^{-5} W^{-1}$, but could only achieve 1D shaping. Various factors limit the performance of NWS in 3D NPC. First, the size of 3D NPC is limited by the laser processing technology of the time. When the laser is tightly and deeply focused into the crystal, the focusing quality will be severely deteriorated due to spherical aberration and focus splitting [95]. Therefore, the laser can only process at a depth of a few hundred micrometers below the crystal surface, and the processing quality varies with the depth. This is the reason that previously reported 3D NPCs often only has a size of 100~200 μm, which seriously affected the nonlinear conversion efficiency. Secondly, laser processing technology often brings strong refractive index changes to nonlinear media, especially when it is necessary to use very high-power lasers for processing deep inside the media. The dramatic disturbance of the linear index to the beam propagating in the media not only causes scattering loss, but also severely interferes with QPM, causing the nonlinear process to not proceed as designed[101]. This problem can be alleviated by reducing the duty cycle of the NPC, but reducing the duty cycle will also lead to a decrease in NPC efficiency. Additionally, 3D NPCs inherently have more complex spatial structures, which make processing errors difficult to avoid. In extreme cases, these errors may cause the 3D NPC to completely fail to achieve its intended functions[73].

This thesis is dedicated to the study and resolve the aforementioned problems, with the ultimate goal of achieving highly efficient NWS. In Chapter 4, we examined the design theory of nonlinear volume holography in 3D NPCs and put this into practice. This research not only allows us to theoretically design the most efficient 3D NPC structures for NWS but also provides us with the know-how of fabrication processes. In Chapter 5, we further optimized laser poling technology based on the nonlinear medium we use, which is the calcium barium niobate (CBN) crystal. This research enables us to fabricate large volume and low loss 3D NPCs in CBN crystals. Based on these preliminary studies, we were finally able to achieve highly efficient NWS in 3D NPCs.

6.2 Design and simulation of highly efficient 3D NPC

In the research of Chapter 4, we have actually mastered the design and manufacturing methods of 3D NPCs that can be used to achieve arbitrary NWS. However, the nonlinear conversion efficiency in that research was very low.

We will summarize the reasons for its low efficiency and carry out targeted optimization based on this, ultimately achieving high-efficiency NWS.

First of all, the effective volume is too small. According to the nonlinear analysis, conversion efficiency for pulsed laser pump reads[102]:

$$\eta = \frac{16\pi^2 d_{eff}^2 P_\omega l_t t_{rep}}{n_\omega n_{2\omega} c \varepsilon_0 \lambda_1^3 \tau} \frac{L}{b'}$$

For long pulsed laser and CW laser pump ($t_{rep}/\tau = 1$):

$$\eta = \frac{4\omega^2 d_{eff}^2 P_\omega t_{rep}}{n_\omega n_{2\omega} c^3 \varepsilon_0 \lambda_1 \tau} \frac{L^2}{b'}$$

Where d_{eff} is the effective nonlinear coefficient, t_{rep} is the repetition period, L is the length of the NPC, c is the speed of light, ε_0 is the vacuum permittivity, τ is the pulse width, b' is the confocal parameter of the input beam, l_t is the walk-off length, and n_ω and $n_{2\omega}$ are refractive indices of the FW and SH, respectively.

When a short-pulsed laser is used as a pump, the nonlinear conversion efficiency is directly proportional to the length of the NPC. When a CW laser is used as a pump, the nonlinear conversion efficiency is proportional to the square of the length of the NPC. Therefore, increasing the length of the NPC can effectively improve the efficiency of the nonlinear process. However, in previous research, the 3D NPCs we prepared only have a volume of $80 \times 80 \times 80 \mu m^3$, so there is a lot of room for improvement in improving efficiency by increasing the volume of NPC. An important concept here is the effective volume. That is, only the NPC structure that interacts with light is meaningful. This makes the previous NPC design fundamentally difficult to achieve a high-efficiency nonlinear process, because the NWS achieved by that structure is non-collinear, that is, the propagation direction of the FW light and the SH light are not in the same direction. According to the recording design theory of NVH, the maximum volume of the NPC is the volume where the FW and SH intersect in space, and the non-collinear nonlinear process limits the maximum volume of the NPC. Therefore, to achieve high-efficiency NWS, the NPC should have a collinear configuration, based on which it is possible to achieve a large volume, and possibly high efficiency.

On the other hand, the effective nonlinear coefficient d_{eff} of the NPCs prepared in previous work is too small, and the nonlinear efficiency is proportional to the square of the d_{eff}. Therefore, the conversion efficiency can be improved by increasing the effective nonlinear coefficient. The d_{eff} is related to the nonlinear properties of the material and the propagation direction of the FW and the SH. For example, in our previous work, the FW was incident along the z-axis, and the SH has an angle of 5° with the z-axis. Its effective nonlinear coefficient is:

$$d_{eff} = d_{31}\, sin(5°) = 0.27pm/V$$

This is a very small number, which greatly limits the nonlinear conversion efficiency. If it is chosen that both FW and SH propagate along the y-axis of the crystal and have z-polarization, then its effective nonlinear coefficient is:

$$d_{eff} = d_{33} = 9pm/V$$

This optimization can theoretically increase the NPC efficiency in CBN by $\frac{9^2}{0.27^2} \approx 1000$ times.

In summary, in order to achieve highly efficient NWS, we need to design a 3D NPC where both the FW and the SH propagate along the y-axis of the CBN crystal, both FW and SH have z-polarization, and the length of this NPC in the y-axis direction should be enlengthen as much as possible. According to the theory of NVH we only need to make the two beams co-linear during the recording process. We still choose a vortex beam as the SH for recording process of NVH, and we obtain a 3D structure as shown in Figure 6.2.1 (a). This structure is not novel, similar structures have been introduced in several existing studies[55], [73]. However, due to the limitations of the manufacturing technology at the time, no one has actually made this structure. In fact, even with the most advanced laser poling technology, this structure is still difficult to fabricate perfectly, which is mainly attributed to the low longitudinal resolution of the laser poling technology. Therefore, this structure needs to be simplified for fabrication. The simplified structure is shown in Figure 6.2.1 (d), which was proposed by Karnieli and Arie [103]. Compared with the ideal structure shown in (a), the structure in (b) uses 4 grating structures instead, without complex curve surfaces, making it easy to fabricate. Figures 6.2.1 (c) and (f) show the NWS simulation results for the ideal structure and the simplified structure, respectively. It can be seen that the simplified structure can still produce a vortex beam with a dark center.

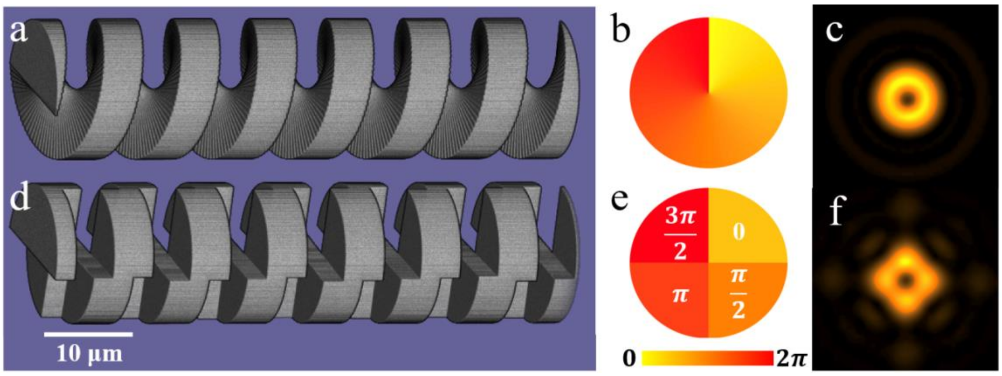

Figure 6.2.1 3D NPC for SH vortex generation. a) The ideal structure and the calculated b) transverse phase and c) intensity distribution of the far-field SH. d) The discretization of four gratings structure and the calculated e) phase and f) intensity of the far-field SH.

The simplification of a continuous spiral structure into four discrete gratings is actually a special case of a more general simplification method. Here, with the aid of Figure 6.2.2, we explain this optimization approach. Figure 6.2.2 (a) is a 3D NPC structure used to generate a SH vortex beam with a topological charge of 5. This structure contains many curved surfaces, and its period is too small to be fabricated. The first step of simplification is to sample periodically along the y-axis direction. The black plane in the figure (a) represents the sampling plane, and the sampling results are shown in (b). The sampled cross-sections appear as 5 sectors at different angles. As each sector has an acute angle, it is still difficult to fabricate, requiring further simplification. Figure 6.2.2 (c) presents the simplified cross-section. The simplification method involves finding the centroid of each sector and constructing a square centered at the centroid to replace the sector. By stretching the processed cross-section (c) in the y-direction, the 2D square becomes a cube in space, resulting in the final simplified structure in (d). We simulated the far-field SH patterns for structures (a) and (b), with results shown in the top and bottom images of (f), respectively. The simplified structure still generates a ring-shaped vortex beam. This simplification method can be applied to almost any co-linear 3D NPC structure, simplifying any complex 3D NPC structure to a fabricable structure while maintaining its original functionality.

It's worth emphasizing that the period of the original structure (a) is much smaller than that of the simplified structure (d), meaning the sampling period is much larger than the original structure period. Therefore, one must be careful when choosing the sampling period; if the sampling period is an integer multiple of the original structure period, each sampling result will be identical, rendering the method ineffective. Naturally, this simplification method can also be used for structures with larger original periods and the sampling period will be smaller than the original periods. For example, the structure in Figure 6.2.1 is one such case where the sampling period in the simplification process is one-quarter of the original period, resulting in a simplified structure of four gratings.

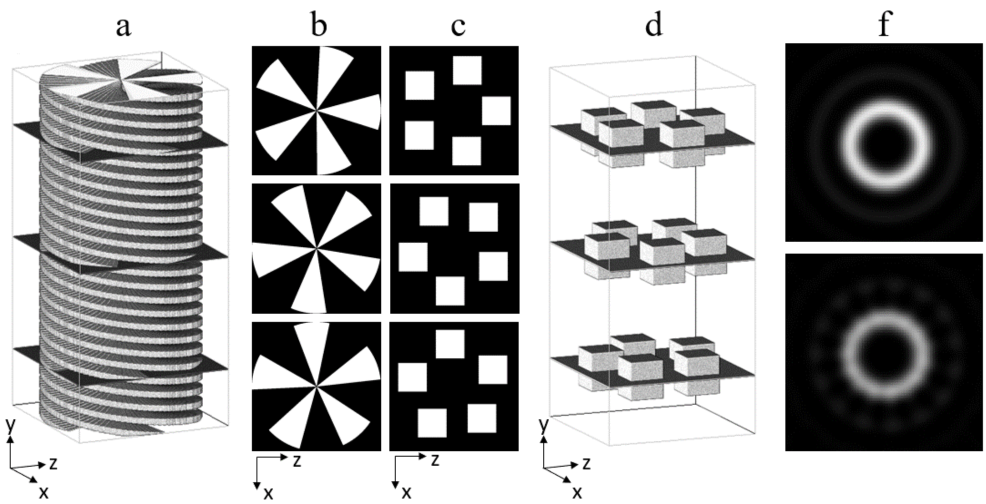

Figure 6.2.2 The general simplification method of complex 3D NPCs. a) The ideal structure for collinear generation of the SH vortex beam with topological charge of 5. b) The cross-sections obtained by sampling at three discrete planes. c,d) The simplified 2D and 3D structures by replacing the five segments containing complex and continuing varied spatial details with rectangular and cuboids, respectively. e,f) The simulated far-field SH intensity distributions from the ideal structure and the simplified structure, respectively.

6.3 Fabrication of large volume 3D NPC

In Chapter 5, we conducted a systematic study of laser poling in CBN. In summary, we should use an o-polarized writing beam incident from the x-surface of the CBN crystal for poling, which allows for poling deep inside the crystal without causing a significant change in the refractive index. Figure 6.3.1 is a schematic diagram of laser poling. The writing beam is generated by a femtosecond oscillator (MIRA, Coherent), with a wavelength of 780nm, pulse width of 180fs, and repetition rate of 76MHz. The laser is focused into the CBN crystal from its x-surface by a 20x/NA0.4 objective lens. The power and polarization of the incident laser are adjusted by a combination of a polarizer and a half-wave plate so that the laser is o-polarized and the laser power matches the writing depth. The laser power is chosen to be 10mW higher than the poling threshold, with specific values referring to Figure 5.2.1. The laser focus scans along the z-axis direction inside the crystal, with a scanning speed of 20μm/s and a scanning distance of 50μm. One scan can polarize a region of $20 \times 2 \times 50\ \mu m^3$ $(x \times y \times z)$. After the scan is completed, the laser shutter is closed, the focus is moved to the next position, and the above scanning process is repeated.

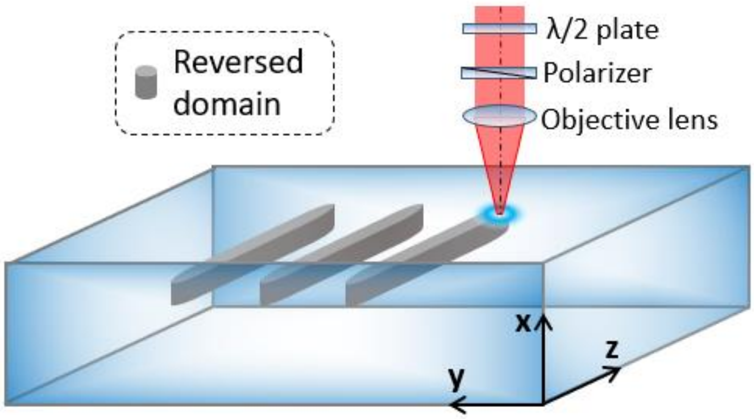

Figure 6.3.1 The schematic diagram of the laser poling setup. The polarization and intensity of the poling laser are controlled by a half-wave plate and a polarizer. After being focused by the objective, the laser enters the crystal from the x-surface of the crystal. The crystal is moved at a uniform speed along the z-axis by the moving stage to realize the scanning of the laser focus inside the crystal. The scanned area will form a uniform strip-shaped ferroelectric single domain.

To achieve bulky poling, we chose to set the x-direction interval between two scans at 10μm and the y-direction interval at 1μm, ensuring that the poled domains produced by two adjacent scans can merge to form a larger domain. We successfully fabricated the domain structure shown in Figure 6.2.1(b), and its nonlinear confocal microscopy images are displayed in Figures 6.3.2 (a) and (b). The 3D model on left side is a schematic of the domain structure, and the nonlinear imaging diagrams of the two blue cross-sectional positions are respectively (a) and (b). It can be seen from the figures that the quality and precision of the 3D NPC we fabricated are both high, which can meet the needs of highly efficient NWS. The figure shows only a part of the entire structure, and the total volume of this 3D NPC is $100 \times 1000 \times 100\mu m^3$ $(x \times y \times z)$. It's worth mentioning that the 3D NPC sample we prepared has a square cross-sectional shape on the x-z plane, which is inconsistent with the circular cross-sectional design in Figure 6.2.1. However, because the FW beam we use is a Gaussian beam with a diameter less than 100μm, the effective volume of 3D NPC structure still has a circular cross-section, consistent with the original design.

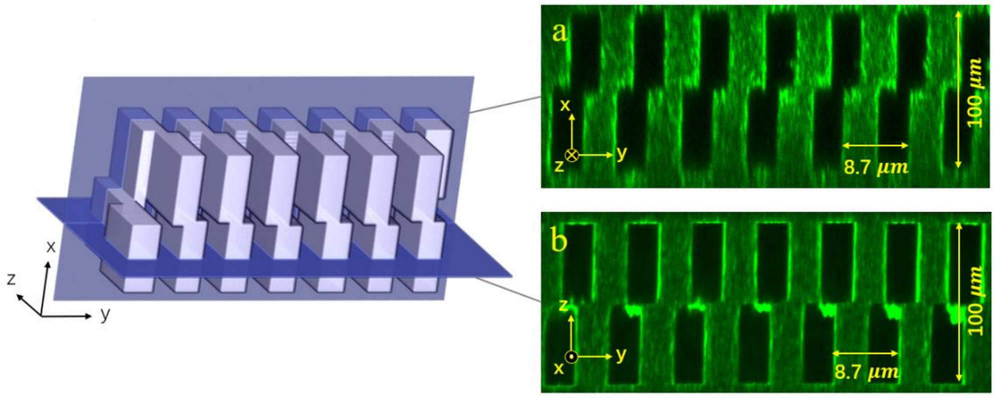

Figure 6.3.2 Left: The 3D model of the experimentally fabricated domain structure. There are two blue sections in the figure, and the cross-sectional views they cut are shown in (a) and (b) respectively. Right: (a) and (b) are images from the nonlinear confocal microscope. The black part is the poled single domain, and the green part is the unpoled random background domain. The picture has been elongated by 5 times along the y-axis in order to clearly show more details.

6.4 Efficient nonlinear generation of vortex beam

We used both femtosecond laser and CW laser as the pump to excite the sample and successfully produced the designed vortex beam. Their intensity distribution maps are shown in Figure 6.4.1 (a) and (b), respectively. You can see that the intensity distribution is in the shape of a donut with a dark center, which is completely in line with our expectations. Moreover, they exhibited extremely high nonlinear conversion efficiency, with a normalized nonlinear conversion efficiency of $2.9 \times 10^{-6} W^{-1}$ when pumped with a femtosecond laser and $1.2 \times 10^{-5} W^{-1}$ when pumped with a CW laser.

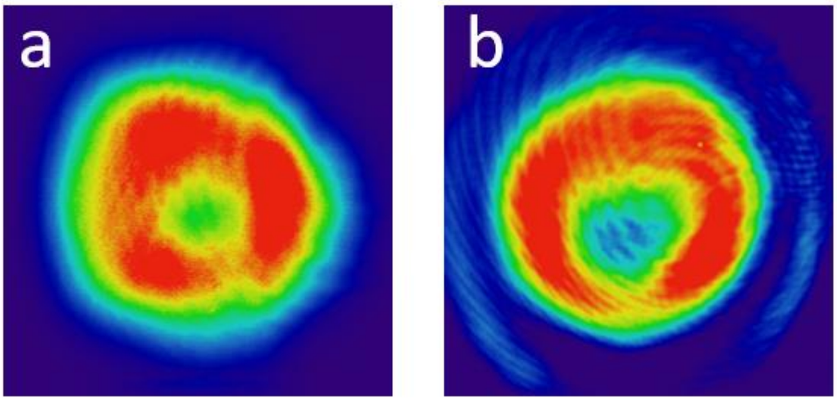

Figure 6.4.1 The second harmonic vortex beam generation with a (a) pulsed and (b) CW fundamental Gaussian beam. The SH beams were directly recorded by CCDs after remove the FW.

When using the femtosecond laser as the pump, we used the Coherent Chameleon OPO system to generate the pump beam, with a wavelength of 1200nm, a pulse width of about 200fs, and a repetition frequency of 80MHz. We set the laser to z-polarization to maximize the effective nonlinear coefficient of the crystal (d_{33}) and use a lens with a focal length of 40mm to focus the laser on the sample. After focusing, the laser had a beam diameter of ~90μm and a Rayleigh length of ~10mm, allowing us to approximate it as a plane wave. At the output end of the crystal, we used a low-pass filter to filter out the FW, and then used a CCD and power meter to measure the intensity distribution and actual power of the SH.

For CW experiments we used a combination of a TSL-570 laser and a doped fiber amplifier to generate the pump beam. The focal length of the lens for focusing the laser was 35mm. At the output end of the crystal, we used a dichroic mirror to separate the FW and SH, and then used a CCD and power meter to measure the SH.

6.5 Summary

We successfully fabricated large-scale 3D NPCs using femtosecond laser direct poling technology and achieved high-efficiency nonlinear wave shaping, which improved the normalized nonlinear conversion efficiency by four orders of magnitude. This breakthrough was dependent on our solution to the difficulties in the fabrication of large-scale 3D NPCs. On the one hand, we adopted the appropriate writing beam polarization to avoid the splitting of the laser focus within the birefringent crystal. This allowed the laser to be effectively focused deep within the crystal, a prerequisite for fabricating large-size samples. On the other hand, we chose a relatively weak focusing objective lens, which greatly reduced the side effect of refractive index change caused by laser writing, thereby reducing the overall loss of the sample and ensuring that the QPM condition was not disturbed. For the design process of the NPC structure, we considered the parameters of the improved laser direct poling technology. By optimizing the complex structure, we designed a structure that is easy to fabricate. In the end, we successfully fabricated 3D NPC samples that are 1mm long. By a CW laser pumping, the sample produced the designed nonlinear vortex beam, with a normalized conversion efficiency as high as $1.2 \times 10^{-5} W^{-1}$. This breakthrough has great potential in the field of quantum optics, such as the generation of multi-dimensional quantum entanglement.

Chapter 7 Conclusions and outlook

7.1 Outcomes

Nonlinear photonic crystals can efficiently realize designed nonlinear optical processes. Research and applications of nonlinear photonic crystals have spanned several decades, and products like periodically poled lithium niobate and potassium titanyl phosphate have become very mature and commercialized. However, traditional electric field poling techniques can only fabricate one-dimensional or two-dimensional nonlinear photonic crystals, and it is challenging to achieve sub-micron precision. It was not until 2018 that Xu and Wei independently adopted femtosecond laser direct writing technology to fabricate three-dimensional nonlinear photonic crystals [32], [33]. This technique relies on focusing ultra-short pulse femtosecond lasers inside nonlinear crystals, heating the crystal at the laser focus through multi-photon absorption, thereby inducing a thermal electric field to complete the local polarization reversal in the crystal. This technology not only enables the fabrication of three-dimensional nonlinear photonic crystals, but its precision also far exceeds traditional processes, achieving sub-micron level precision. This groundbreaking technology is so novel that both its mechanisms and applications warrant further research.

In Chapter 3 we focused on the application of this brand-new technology, namely the fabrication of 3D nonlinear photonic crystals. We have designed and successfully fabricated 3D nonlinear photonic crystals with multiple functionalities to simultaneously achieve three different types of nonlinear wave front shaping, as well as dynamically regulate the morphology of the second harmonic by altering the focus of the pump light. These innovative functionalities are unattainable through traditional 2D nonlinear photonic crystals. Furthermore, this research also demonstrates the feasibility of using femtosecond laser direct writing technology to fabricate complex 3D structures, paving the way for our subsequent studies.

However, this initial attempt at utilizing the new technology also has its evident limitations, the most apparent being the extremely low nonlinear conversion efficiency. This is due to our attempt to implement multiple NWS on a single nonlinear photonic crystal without adequately considering the phase matching of the nonlinear optical processes. On the other hand, our understanding of the capabilities of femtosecond laser poling technology is still limited, and we have not fully exploited the potential of this technique.

In Chapter 4, to address the issue of low efficiency in achieving NWS with three-dimensional nonlinear photonic crystals, we made structural improvements to the 3D nonlinear photonic crystals. Nonlinear holography technology served as a theoretical guide, enabling us to design theoretically the most efficient three-dimensional nonlinear photonic crystals. However, the theoretically designed 3D nonlinear photonic crystals have extremely fine structures, and require the material's polarization to continuously vary from -1 to +1. These conditions are unattainable with existing laser direct writing technology and the characteristics of nonlinear materials. Consequently, we optimized the designed structure to maintain its nonlinear optical functionality while making it manufacturable with our existing laser fabrication technology. The 3D nonlinear photonic crystals designed and fabricated using nonlinear holography, also known as nonlinear volume holograms, significantly improved the efficiency of SHG by fulfilling the QPM conditions for nonlinear optical processes. Our fabricated nonlinear hologram not only achieves nonlinear wave mixing but also meets the requirements for efficient nonlinear optical processes.

In this work, we have achieved more efficient NWS by improving the structure of the 3D NPC. To further enhance the nonlinear conversion efficiency, one of the most direct methods is to increase the overall volume of the entire 3D NPC structure. However, some limitations inherent in current laser direct writing technology make this goal challenging to achieve. To pursue high-efficiency NWS further, it is essential to improve the existing laser poling techniques.

In Chapter 5, based on the experimental results from the previous two chapters, we analyzed the issues with the existing laser poling technology, which can be primarily summarized into two points. Firstly, the depth of laser poling is too shallow, reaching only a few hundred microns below the surface of a crystal. This depth is sufficient for small-volume NPC structures but severely limits the fabrication of larger volume NPC structures. On the other hand, the existing laser fabrication technology strongly affects the crystal's refractive index while achieving poling, leading to significant scattering losses. To address these two issues, we conducted a systematic study of the interaction between focused laser's and nonlinear crystals. Through simulations of the propagation of focused lasers with different polarization states inside the crystal and corresponding nonlinear absorption simulations, we optimized the parameters of laser poling. The final experimental results aligned well with the theoretical simulations, successfully resolving the aforementioned issues. This achievement enables us to fabricate ultra-large volume 3D NPCs, laying the foundation for ultra-high-efficiency nonlinear optical beam processing.

In Chapter 6, we integrated the outcomes of previous studies. Applied the nonlinear volume holography theory from Chapter 4 to design a collinear, high-efficiency 3D NPC for generating nonlinear vortex light. This was then fabricated using the optimized laser poling technique from Chapter 5, with a sample length of 1mm. Using a femtosecond laser as the pump source, we achieved a nonlinear conversion efficiency of 4.6%, with a corresponding normalized nonlinear conversion efficiency of $2.9 \times 10^{-6} W^{-1}$. We also accomplished NWS with CW laser pumping, achieving a normalized nonlinear conversion efficiency of $1.2 \times 10^{-5} W^{-1}$. To our best knowledge, there has been no prior research on using CW laser pumping for SHG in 3D NPCs.

7.2 Outlook and future work

The initial stunning manifestation of the femtosecond laser poling technique lies in its ability to make the fabrication of 3D NPCs possible, allowing experimental concepts that were once purely theoretical to be realized. As this technology has matured, the research field has become increasingly active. At the time of completing this thesis, many researchers have proposed a variety of experimental concepts based on 3D NPCs. For example, using 3D NPCs to study the topological Hall effect and to generate high-order entangled photon pairs[104], [105]. These experimental ideas place high demands on the conversion efficiency of 3D NPCs, which aligns with the primary focus of this thesis. Fabricating the 3D NPCs conceptualized in theory is a solid research direction for the future.

Additionally, in subsequent research on femtosecond laser direct writing technology, this technique has demonstrated many unique and superior characteristics. For example, the laser can re-pole a nonlinear crystal that has already been poled, making the concept of programmable nonlinear photonic crystals feasible[106]. Moreover, the precision of this technology far exceeds initial expectations. As of the completion of this thesis, related studies have achieved crystal polarization with ultra-narrow linewidths of 30 nm [107]. Combined with the high-efficiency 3D NPCs studied in this thesis, the fabrication of programmable, large-scale integrated 3D NPCs also presents as an exciting research direction.

References

[1] A. Einstein, “Zur quantentheorie der strahlung,” *First Publ. In*, pp. 121–128, 1916.

[2] A. L. Schawlow and C. H. Townes, “Infrared and Optical Masers,” *Phys. Rev.*, vol. 112, no. 6, pp. 1940–1949, Dec. 1958, doi: 10.1103/PhysRev.112.1940.

[3] T. H. Maiman, R. H. Hoskins, I. J. D’Haenens, C. K. Asawa, and V. Evtuhov, “Stimulated Optical Emission in Fluorescent Solids. II. Spectroscopy and Stimulated Emission in Ruby,” *Phys. Rev.*, vol. 123, no. 4, pp. 1151–1157, Aug. 1961, doi: 10.1103/PhysRev.123.1151.

[4] F. J. Duarte, *Tunable laser optics*. CRC Press, 2017.

[5] P. A. Franken, A. E. Hill, C. W. Peters, and G. Weinreich, “Generation of Optical Harmonics,” *Phys. Rev. Lett.*, vol. 7, no. 4, pp. 118–119, Aug. 1961, doi: 10.1103/PhysRevLett.7.118.

[6] M. Bass, P. A. Franken, A. E. Hill, C. W. Peters, and G. Weinreich, “Optical Mixing,” *Phys. Rev. Lett.*, vol. 8, no. 1, pp. 18–18, Jan. 1962, doi: 10.1103/PhysRevLett.8.18.

[7] R. C. Miller, “OPTICAL SECOND HARMONIC GENERATION IN PIEZOELECTRIC CRYSTALS,” *Appl. Phys. Lett.*, vol. 5, no. 1, pp. 17–19, Jul. 1964, doi: 10.1063/1.1754022.

[8] A. W. Smith and N. Braslau, “Observation of an Optical Difference Frequency,” *J. Appl. Phys.*, vol. 34, no. 7, pp. 2105–2106, Jul. 1963, doi: 10.1063/1.1729748.

[9] C. C. Wang and G. W. Racette, “Measurement of Parametric Gain Accompanying Optical Difference Frequency Generation,” *Appl. Phys. Lett.*, vol. 6, no. 10, pp. 213–213, May 1965, doi: 10.1063/1.1754138.

[10] J. A. Giordmaine and R. C. Miller, “Tunable Coherent Parametric Oscillation in LiNb O 3 at Optical Frequencies,” *Phys. Rev. Lett.*, vol. 14, no. 24, pp. 973–976, Jun. 1965, doi: 10.1103/PhysRevLett.14.973.

[11] Y. Pao and P. M. Rentzepis, “Multiphoton Absorption and Optical-Harmonic Generation in Highly Absorbing Molecular Crystals,” *J. Chem. Phys.*, vol. 43, no. 4, pp. 1281–1286, Aug. 1965, doi: 10.1063/1.1696915.

[12] C. R. Giuliano, “LASER-INDUCED DAMAGE TO TRANSPARENT DIELECTRIC MATERIALS,” *Appl. Phys. Lett.*, vol. 5, no. 7, pp. 137–139, Oct. 1964, doi: 10.1063/1.1754087.

[13] R. W. Hellwarth, “Theory of Stimulated Raman Scattering,” *Phys. Rev.*, vol. 130, no. 5, pp. 1850–1852, Jun. 1963, doi: 10.1103/PhysRev.130.1850.

[14] J. A. Armstrong, N. Bloembergen, J. Ducuing, and P. S. Pershan, “Interactions between Light Waves in a Nonlinear Dielectric,” *Phys. Rev.*, vol. 127, no. 6, pp. 1918–1939, Sep. 1962, doi: 10.1103/PhysRev.127.1918.

[15] D. A. Kleinman, “Nonlinear Dielectric Polarization in Optical Media,” *Phys. Rev.*, vol. 126, no. 6, pp. 1977–1979, Jun. 1962, doi: 10.1103/PhysRev.126.1977.

[16] J. E. Midwinter and J. Warner, “The effects of phase matching method and of uniaxial crystal symmetry on the polar distribution of second-order non-linear optical polarization,” *Br. J. Appl. Phys.*, vol. 16, no. 8, pp. 1135–1142, Aug. 1965, doi: 10.1088/0508-3443/16/8/312.

[17] Y. Sheng, A. Best, A. Arie, and K. Koynov, “Three-dimensional ferroelectric domain visualization by Cˇ erenkov-type second harmonic generation,” 2010.

[18] W. M. Steen and J. Mazumder, *Laser material processing*. springer science & business media, 2010.

[19] C. Schlickriede, S. S. Kruk, L. Wang, B. Sain, Y. Kivshar, and T. Zentgraf, “Nonlinear Imaging with All-Dielectric Metasurfaces,” *Nano Lett.*, vol. 20, no. 6, pp. 4370–4376, Jun. 2020, doi: 10.1021/acs.nanolett.0c01105.

[20] D. E. Chang, V. Vuletić, and M. D. Lukin, “Quantum nonlinear optics — photon by photon,” *Nat. Photonics*, vol. 8, no. 9, pp. 685–694, Sep. 2014, doi: 10.1038/nphoton.2014.192.

[21] Y. Sheng, X. Chen, T. Lukasiewicz, M. Swirkowicz, K. Koynov, and W. Krolikowski, “Calcium barium niobate as a functional material for broadband optical frequency conversion,” *Opt. Lett.*, vol. 39, no. 6, p. 1330, Mar. 2014, doi: 10.1364/OL.39.001330.

[22] A. R. Khan *et al.*, “Optical Harmonic Generation in 2D Materials,” *Adv. Funct. Mater.*, vol. 32, no. 3, p. 2105259, 2022, doi: https://doi.org/10.1002/adfm.202105259.

[23] P. S. Kuo, J. Bravo-Abad, and G. S. Solomon, “Second-harmonic generation using -quasi-phasematching in a GaAs whispering-gallery-mode microcavity,” *Nat. Commun.*, vol. 5, no. 1, p. 3109, Jan. 2014, doi: 10.1038/ncomms4109.

[24] P. Karpinski *et al.*, “Nonlinear diffraction in orientation-patterned semiconductors,” *Opt Express*, vol. 23, no. 11, pp. 14903–14912, Jun. 2015, doi: 10.1364/OE.23.014903.

[25] H. Nasu *et al.*, “Second-harmonic generation from electrically poled SiO2 glasses: effects of OH concentration, defects, and poling conditions,” *J Opt Soc Am B*, vol. 12, no. 4, pp. 644–649, Apr. 1995, doi: 10.1364/JOSAB.12.000644.

[26] V. Berger, “Nonlinear Photonic Crystals,” *Phys Rev Lett*, vol. 81, no. 19, pp. 4136–4139, Nov. 1998, doi: 10.1103/PhysRevLett.81.4136.

[27] D. J. Armstrong, W. J. Alford, T. D. Raymond, A. V. Smith, and M. S. Bowers, “Parametric amplification and oscillation with walkoff-compensating crystals,” *J Opt Soc Am B*, vol. 14, no. 2, pp. 460–474, Feb. 1997, doi: 10.1364/JOSAB.14.000460.

[28] M. Yamada, N. Nada, M. Saitoh, and K. Watanabe, “First-order quasi-phase matched LiNbO3 waveguide periodically poled by applying an external field for efficient blue second-harmonic generation,” *Appl. Phys. Lett.*, vol. 62, no. 5, pp. 435–436, 1993, doi: 10.1063/1.108925.

[29] L. E. Myers, R. C. Eckardt, M. M. Fejer, R. L. Byer, W. R. Bosenberg, and J. W. Pierce, “Quasi-phase-matched optical parametric oscillators in bulk periodically poled LiNbO3,” *J Opt Soc Am B*, vol. 12, no. 11, pp. 2102–2116, Nov. 1995, doi: 10.1364/JOSAB.12.002102.

[30] S. Zhu, Y. Zhu, Y. Qin, H. Wang, C. Ge, and N. Ming, “Experimental Realization of Second Harmonic Generation in a Fibonacci Optical Superlattice of LiTa\mathrmO_3,” *Phys Rev Lett*, vol. 78, no. 14, pp. 2752–2755, Apr. 1997, doi: 10.1103/PhysRevLett.78.2752.

[31] N. G. R. Broderick, G. W. Ross, D. J. Richardson, and D. C. Hanna, “HeXLN: A 2-Dimensional nonlinear photonic crystal,” in *Nonlinear Guided Waves and Their Applications*, Optica Publishing Group, 1999, p. PD1. doi: 10.1364/NLGW.1999.PD1.

[32] D. Wei *et al.*, “Experimental demonstration of a three-dimensional lithium niobate nonlinear photonic crystal,” *Nat. Photonics*, vol. 12, no. 10, pp. 596–600, Oct. 2018, doi: 10.1038/s41566-018-0240-2.

[33] T. Xu *et al.*, “Three-dimensional nonlinear photonic crystal in ferroelectric barium calcium titanate,” *Nat. Photonics*, vol. 12, no. 10, pp. 591–595, Oct. 2018, doi: 10.1038/s41566-018-0225-1.

[34] S. Matsumoto, E. J. Lim, H. M. Hertz, and M. M. Fejer, “Quasiphase-matched second harmonic generation of blue light in electrically periodically-poled lithium tantalate waveguides,” *Electron. Lett.*, vol. 27, no. 22, pp. 2040-2042(2), Oct. 1991, [Online]. Available: https://digital-library.theiet.org/content/journals/10.1049/el_19911263

[35] A. Arie and N. Voloch, “Periodic, quasi-periodic, and random quadratic nonlinear photonic crystals,” *Laser Photonics Rev.*, vol. 4, no. 3, pp. 355–373, 2010, doi: https://doi.org/10.1002/lpor.200910006.

[36] L. E. Myers, R. C. Eckardt, M. M. Fejer, R. L. Byer, and W. R. Bosenberg, "Multigrating quasi-phase-matched optical parametric oscillator in periodically poled LiNbO3," *Opt Lett*, vol. 21, no. 8, pp. 591–593, Apr. 1996, doi: 10.1364/OL.21.000591.

[37] P. E. Powers, T. J. Kulp, and S. E. Bisson, "Continuous tuning of a continuous-wave periodically poled lithium niobate optical parametric oscillator by use of a fan-out grating design," *Opt Lett*, vol. 23, no. 3, pp. 159–161, Feb. 1998, doi: 10.1364/OL.23.000159.

[38] K. Kintaka, M. Fujimura, T. Suhara, and H. Nishihara, "Third harmonic generation of Nd:YAG laser light in periodically poled $LiNbO_3$ waveguide," *Electron. Lett.*, vol. 33, no. 17, pp. 1459-1461(2), Aug. 1997, [Online]. Available: https://digital-library.theiet.org/content/journals/10.1049/el_19970990

[39] M. A. Arbore, A. Galvanauskas, D. Harter, M. H. Chou, and M. M. Fejer, "Engineerable compression of ultrashort pulses by use of second-harmonic generation in chirped-period-poled lithium niobate," *Opt Lett*, vol. 22, no. 17, pp. 1341–1343, Sep. 1997, doi: 10.1364/OL.22.001341.

[40] A. H. Norton and C. M. de Sterke, "Aperiodic 1-dimensional structures for quasi-phase matching," *Opt Express*, vol. 12, no. 5, pp. 841–846, Mar. 2004, doi: 10.1364/OPEX.12.000841.

[41] S. M. Saltiel and Y. S. Kivshar, "All-optical deflection and splitting by second-order cascading," *Opt Lett*, vol. 27, no. 11, pp. 921–923, Jun. 2002, doi: 10.1364/OL.27.000921.

[42] S. Saltiel and Y. S. Kivshar, "Phase matching in nonlinear $\chi(2)$ photonic crystals," *Opt Lett*, vol. 25, no. 16, pp. 1204–1206, Aug. 2000, doi: 10.1364/OL.25.001204.

[43] N. G. R. Broderick, R. T. Bratfalean, T. M. Monro, D. J. Richardson, and C. M. de Sterke, "Temperature and wavelength tuning of second-, third-, and fourth-harmonic generation in a two-dimensional hexagonally poled nonlinear crystal," *J Opt Soc Am B*, vol. 19, no. 9, pp. 2263–2272, Sep. 2002, doi: 10.1364/JOSAB.19.002263.

[44] A. Chowdhury, C. Staus, B. F. Boland, T. F. Kuech, and L. McCaughan, “Experimental demonstration of 1535–1555-nm simultaneous optical wavelength interchange with a nonlinear photonic crystal,” *Opt Lett*, vol. 26, no. 17, pp. 1353–1355, Sep. 2001, doi: 10.1364/OL.26.001353.

[45] I. Dolev, T. Ellenbogen, and A. Arie, “Switching the acceleration direction of Airy beams by a nonlinear optical process,” *Opt Lett*, vol. 35, no. 10, pp. 1581–1583, May 2010, doi: 10.1364/OL.35.001581.

[46] A. Chong, W. H. Renninger, D. N. Christodoulides, and F. W. Wise, “Airy–Bessel wave packets as versatile linear light bullets,” *Nat. Photonics*, vol. 4, no. 2, pp. 103–106, Feb. 2010, doi: 10.1038/nphoton.2009.264.

[47] R. Shiloh and A. Arie, “Spectral and temporal holograms with nonlinear optics,” *Opt Lett*, vol. 37, no. 17, pp. 3591–3593, Sep. 2012, doi: 10.1364/OL.37.003591.

[48] G. Imeshev, M. Proctor, and M. M. Fejer, “Lateral patterning of nonlinear frequency conversion with transversely varying quasi-phase-matching gratings,” *Opt Lett*, vol. 23, no. 9, pp. 673–675, May 1998, doi: 10.1364/OL.23.000673.

[49] T. Ellenbogen, A. Ganany-Padowicz, and A. Arie, “Nonlinear photonic structures for all-optical deflection,” *Opt Express*, vol. 16, no. 5, pp. 3077–3082, Mar. 2008, doi: 10.1364/OE.16.003077.

[50] J. R. Kurz, A. M. Schober, D. S. Hum, A. J. Saltzman, and M. M. Fejer, “Nonlinear physical optics with transversely patterned quasi-phase-matching gratings,” in *Summaries of Papers Presented at the Lasers and Electro-Optics. CLEO ’02. Technical Diges*, 2002, pp. 377–378 vol.1. doi: 10.1109/CLEO.2002.1034105.

[51] T. Ellenbogen, N. Voloch-Bloch, A. Ganany-Padowicz, and A. Arie, “Nonlinear generation and manipulation of Airy beams,” *Nat. Photonics*, vol. 3, no. 7, pp. 395–398, Jul. 2009, doi: 10.1038/nphoton.2009.95.

[52] A. Shapira, I. Juwiler, and A. Arie, “Nonlinear computer-generated holograms,” *Opt Lett*, vol. 36, no. 15, pp. 3015–3017, Aug. 2011, doi: 10.1364/OL.36.003015.

[53] A. Shapira, R. Shiloh, I. Juwiler, and A. Arie, “Two-dimensional nonlinear beam shaping,” *Opt Lett*, vol. 37, no. 11, pp. 2136–2138, Jun. 2012, doi: 10.1364/OL.37.002136.

[54] A. Shapira, I. Juwiler, and A. Arie, “Tunable nonlinear beam shaping by non-collinear interactions,” *Laser Photonics Rev.*, vol. 7, no. 4, pp. L25–L29, 2013, doi: https://doi.org/10.1002/lpor.201300026.

[55] A. Bahabad and A. Arie, “Generation of Optical Vortex Beams by NonlinearWave Mixing,” *Opt Express*, vol. 15, no. 26, pp. 17619–17624, Dec. 2007, doi: 10.1364/OE.15.017619.

[56] N. V. Bloch, K. Shemer, A. Shapira, R. Shiloh, I. Juwiler, and A. Arie, “Twisting Light by Nonlinear Photonic Crystals,” *Phys Rev Lett*, vol. 108, no. 23, p. 233902, Jun. 2012, doi: 10.1103/PhysRevLett.108.233902.

[57] J. Chen and X. Chen, “Phase matching in three-dimensional nonlinear photonic crystals,” *Phys Rev A*, vol. 80, no. 1, p. 013801, Jul. 2009, doi: 10.1103/PhysRevA.80.013801.

[58] J. Chen and X. Chen, “Generation of conical and spherical second harmonics in three-dimensional nonlinear photonic crystals with radial symmetry,” *J Opt Soc Am B*, vol. 28, no. 2, pp. 241–246, Feb. 2011, doi: 10.1364/JOSAB.28.000241.

[59] X.-H. Hong, B. Yang, C. Zhang, Y.-Q. Qin, and Y.-Y. Zhu, “Nonlinear Volume Holography for Wave-Front Engineering,” *Phys Rev Lett*, vol. 113, no. 16, p. 163902, Oct. 2014, doi: 10.1103/PhysRevLett.113.163902.

[60] Y. Zhang, Y. Sheng, S. Zhu, M. Xiao, and W. Krolikowski, “Nonlinear photonic crystals: from 2D to 3D,” 2021.

[61] V. Ya. Shur, A. R. Akhmatkhanov, and I. S. Baturin, “Micro- and nano-domain engineering in lithium niobate,” *Appl. Phys. Rev.*, vol. 2, no. 4, Oct. 2015, doi: 10.1063/1.4928591.

[62] Y. Sheng, T. Wang, B. Ma, E. Qu, B. Cheng, and D. Zhang, “Anisotropy of domain broadening in periodically poled lithium niobate crystals,” *Appl. Phys. Lett.*, vol. 88, no. 4, Jan. 2006, doi: 10.1063/1.2168727.

[63] G. Rosenman, Kh. Garb, A. Skliar, M. Oron, D. Eger, and M. Katz, “Domain broadening in quasi-phase-matched nonlinear optical devices,” *Appl. Phys. Lett.*, vol. 73, no. 7, pp. 865–867, Aug. 1998, doi: 10.1063/1.121969.

[64] P. Mackwitz, M. Rüsing, G. Berth, A. Widhalm, K. Müller, and A. Zrenner, “Periodic domain inversion in x-cut single-crystal lithium niobate thin film,” *Appl. Phys. Lett.*, vol. 108, no. 15, p. 152902, Apr. 2016, doi: 10.1063/1.4946010.

[65] H. Steigerwald *et al.*, “Origin of UV-induced poling inhibition in lithium niobate crystals,” *Phys Rev B*, vol. 82, no. 21, p. 214105, Dec. 2010, doi: 10.1103/PhysRevB.82.214105.

[66] C. L. Sones *et al.*, “Precision nanoscale domain engineering of lithium niobate via UV laser induced inhibition of poling,” *Appl. Phys. Lett.*, vol. 92, no. 7, Feb. 2008, doi: 10.1063/1.2884185.

[67] A. C. Muir *et al.*, “Direct-writing of inverted domains in lithium niobate using a continuous wave ultra violet laser,” *Opt Express*, vol. 16, no. 4, pp. 2336–2350, Feb. 2008, doi: 10.1364/OE.16.002336.

[68] H. Steigerwald, Y. J. Ying, R. W. Eason, K. Buse, S. Mailis, and E. Soergel, “Direct writing of ferroelectric domains on the x- and y-faces of lithium niobate using a continuous wave ultraviolet laser,” *Appl. Phys. Lett.*, vol. 98, no. 6, Feb. 2011, doi: 10.1063/1.3553194.

[69] A. Boes *et al.*, “Tailor-made domain structures on the x- and y-face of lithium niobate crystals,” *Appl. Phys. B*, vol. 115, no. 4, pp. 577–581, Jun. 2014, doi: 10.1007/s00340-013-5639-3.

[70] X. Chen *et al.*, “Ferroelectric domain engineering by focused infrared femtosecond pulses,” *Appl. Phys. Lett.*, vol. 107, no. 14, Oct. 2015, doi: 10.1063/1.4932199.

[71] X. Chen *et al.*, “Quasi-phase matching via femtosecond laser-induced domain inversion in lithium niobate waveguides,” *Opt Lett*, vol. 41, no. 11, pp. 2410–2413, Jun. 2016, doi: 10.1364/OL.41.002410.

[72] J. Thomas, V. Hilbert, R. Geiss, T. Pertsch, A. Tünnermann, and S. Nolte, “Quasi phase matching in femtosecond pulse volume structured x-cut lithium niobate,” *Laser Photonics Rev.*, vol. 7, no. 3, pp. L17–L20, 2013, doi: https://doi.org/10.1002/lpor.201200116.

[73] J. Imbrock, L. Wesemann, S. Kroesen, M. Ayoub, and C. Denz, “Waveguide-integrated three-dimensional quasi-phase-matching structures,” *Optica*, vol. 7, no. 1, p. 28, Jan. 2020, doi: 10.1364/OPTICA.7.000028.

[74] P. Chen *et al.*, “Quasi-phase-matching-division multiplexing holography in a three-dimensional nonlinear photonic crystal,” *Light Sci. Appl.*, vol. 10, no. 1, p. 146, Jul. 2021, doi: 10.1038/s41377-021-00588-5.

[75] S. Liu *et al.*, “Nonlinear wavefront shaping with optically induced three-dimensional nonlinear photonic crystals,” *Nat. Commun.*, vol. 10, no. 1, p. 3208, Jul. 2019, doi: 10.1038/s41467-019-11114-y.

[76] S. Liu, L. M. Mazur, W. Krolikowski, and Y. Sheng, “Nonlinear Volume Holography in 3D Nonlinear Photonic Crystals,” *Laser Photonics Rev.*, vol. 14, no. 11, p. 2000224, Nov. 2020, doi: 10.1002/lpor.202000224.

[77] S. Liu, Y. Sheng, and W. Krolikowski, “Polarization-dependent optical engineering of ferroelectric domains,” *ChemPhysMater*, 2023, doi: https://doi.org/10.1016/j.chphma.2023.02.006.

[78] S. Liu *et al.*, “Highly Efficient 3D Nonlinear Photonic Crystals in Ferroelectrics,” *Adv. Opt. Mater.*, vol. 11, no. 14, p. 2300021, 2023, doi: https://doi.org/10.1002/adom.202300021.

[79] S. Bancelin, S. Vigne, N. Hossain, M. Chaker, and F. Légaré, “Nonlinear optical properties of calcium barium niobate epitaxial thin films,” *Opt. Express*, vol. 24, no. 15, p. 17497, Jul. 2016, doi: 10.1364/OE.24.017497.

[80] P. D. Maker, R. W. Terhune, M. Nisenoff, and C. M. Savage, "Effects of Dispersion and Focusing on the Production of Optical Harmonics," *Phys. Rev. Lett.*, vol. 8, no. 1, pp. 21–22, Jan. 1962, doi: 10.1103/PhysRevLett.8.21.

[81] Chung Tang and P. Bey, "Phase matching in second-harmonic generation using artificial periodic structures," *IEEE J. Quantum Electron.*, vol. 9, no. 1, pp. 9–17, Jan. 1973, doi: 10.1109/JQE.1973.1077381.

[82] D. Wei *et al.*, "Efficient nonlinear beam shaping in three-dimensional lithium niobate nonlinear photonic crystals," *Nat. Commun.*, vol. 10, no. 1, p. 4193, Sep. 2019, doi: 10.1038/s41467-019-12251-0.

[83] M. Eßer *et al.*, "Optical characterization and crystal structure of the novel bronzetype CaxBa1-xNb2O6 (x = 0.28; CBN-28)," *Cryst. Res. Technol.*, vol. 38, no. 6, pp. 457–464, Jun. 2003, doi: 10.1002/crat.200310057.

[84] R. R. Neurgaonkar, J. R. Oliver, and L. E. Cross, "Ferroelectric properties of tetragonal tungsten bronze single crystals," *Ferroelectrics*, vol. 56, no. 1, pp. 31–36, Apr. 1984, doi: 10.1080/00150198408012713.

[85] L. E. Cross, "Relaxor ferroelectrics," *Ferroelectrics*, vol. 76, no. 1, pp. 241–267, Dec. 1987, doi: 10.1080/00150198708016945.

[86] B. Wang *et al.*, "Comparative analysis of ferroelectric domain statistics via nonlinear diffraction in random nonlinear materials," *Opt. Express*, vol. 26, no. 2, p. 1083, Jan. 2018, doi: 10.1364/OE.26.001083.

[87] M. Eßer, M. Burianek, D. Klimm, and M. Mühlberg, "Single crystal growth of the tetragonal tungsten bronze CaxBa1−xNb2O6 (x=0.28; CBN-28)," *J. Cryst. Growth*, vol. 240, no. 1–2, pp. 1–5, Apr. 2002, doi: 10.1016/S0022-0248(02)00868-0.

[88] S. Keren-Zur and T. Ellenbogen, "A new dimension for nonlinear photonic crystals," *Nat. Photonics*, vol. 12, no. 10, pp. 575–577, Oct. 2018, doi: 10.1038/s41566-018-0262-9.

[89] H. Y. Leng *et al.*, "On-chip steering of entangled photons in nonlinear photonic crystals," *Nat. Commun.*, vol. 2, no. 1, p. 429, Aug. 2011, doi: 10.1038/ncomms1439.

[90] M. Ayoub, H. Futterlieb, J. Imbrock, and C. Denz, "3D Imaging of Ferroelectric Kinetics during Electrically Driven Switching," *Adv. Mater.*, vol. 29, no. 5, p. 1603325, 2017, doi: https://doi.org/10.1002/adma.201603325.

[91] I. Freund, "Nonlinear Diffraction," *Phys Rev Lett*, vol. 21, no. 19, pp. 1404–1406, Nov. 1968, doi: 10.1103/PhysRevLett.21.1404.

[92] S. M. Saltiel *et al.*, "Cerenkov-Type Second-Harmonic Generation in Two-Dimensional Nonlinear Photonic Structures," *IEEE J. Quantum Electron.*, vol. 45, no. 11, pp. 1465–1472, 2009, doi: 10.1109/JQE.2009.2030147.

[93] S. M. Saltiel, D. N. Neshev, R. Fischer, W. Krolikowski, A. Arie, and Y. S. Kivshar, "Generation of Second-Harmonic Conical Waves via Nonlinear Bragg Diffraction," *Phys Rev Lett*, vol. 100, no. 10, p. 103902, Mar. 2008, doi: 10.1103/PhysRevLett.100.103902.

[94] S. Saltiel, W. Krolikowski, D. Neshev, and Y. S. Kivshar, "Generation of Bessel beams by parametric frequency doubling in annular nonlinear periodic structures," *Opt Express*, vol. 15, no. 7, pp. 4132–4138, Apr. 2007, doi: 10.1364/OE.15.004132.

[95] P. Karpinski, V. Shvedov, W. Krolikowski, and C. Hnatovsky, "Laser-writing inside uniaxially birefringent crystals: fine morphology of ultrashort pulse-induced changes in lithium niobate," *Opt Express*, vol. 24, no. 7, pp. 7456–7476, Apr. 2016, doi: 10.1364/OE.24.007456.

[96] X. Hu, S. Liu, T. Xu, Y. Sheng, R. Zhao, and W. Krolikowski, "Nonlinear generation of an optical bottle beam in domain-engineered ferroelectric crystals," *Opt Lett*, vol. 48, no. 21, pp. 5527–5530, Nov. 2023, doi: 10.1364/OL.501932.

[97] S. Wang *et al.*, “Ferroelectric domain engineering with femtosecond pulses of different wavelengths,” *Opt Express*, vol. 31, no. 4, pp. 5843–5852, Feb. 2023, doi: 10.1364/OE.483162.

[98] J.-G. Hua, F. Yu, Z.-N. Tian, Y.-H. Yu, and Y.-S. Yu, “Characterization of Refractive Index Change Induced by Femtosecond Laser in Lithium Niobate,” *J. LASER MICRO Nanoeng.*, vol. 12, no. 3, pp. 207–211, Dec. 2017, doi: 10.2961/jlmn.2017.03.0006.

[99] E. Sedghamiz, M. Liu, and W. Wenzel, “Challenges and limits of mechanical stability in 3D direct laser writing,” *Nat. Commun.*, vol. 13, no. 1, p. 2115, Apr. 2022, doi: 10.1038/s41467-022-29749-9.

[100] X. Dong, B. Zhang, X. Sun, Y. Jia, and F. Chen, “1.8-µm laser operation based on femtosecond-laser direct written Tm:YVO4 cladding waveguides,” *Opt Express*, vol. 31, no. 10, pp. 16560–16569, May 2023, doi: 10.1364/OE.487296.

[101] T. Wang *et al.*, “Fabrication of lithium niobate fork grating by laser-writing-induced selective chemical etching,” *Nanophotonics*, vol. 11, no. 4, pp. 829–834, 2022, doi: doi:10.1515/nanoph-2021-0446.

[102] A. M. Weiner, *Ultrafast optics*. in Wiley series in pure and applied optics. Hoboken, N.J: Wiley, 2009.

[103] A. Karnieli and A. Arie, “Fully controllable adiabatic geometric phase in nonlinear optics,” *Opt Express*, vol. 26, no. 4, pp. 4920–4932, Feb. 2018, doi: 10.1364/OE.26.004920.

[104] A. Karnieli, S. Tsesses, G. Bartal, and A. Arie, “Emulating spin transport with nonlinear optics, from high-order skyrmions to the topological Hall effect,” *Nat. Commun.*, vol. 12, Feb. 2021, doi: 10.1038/s41467-021-21250-z.

[105] O. Yesharim, S. Pearl, J. Foley-Comer, I. Juwiler, and A. Arie, “Direct generation of spatially entangled qudits using quantum nonlinear optical holography,” *Sci. Adv.*, vol. 9, no. 8, p. eade7968, 2023, doi: 10.1126/sciadv.ade7968.

[106] X. Chen *et al.*, “Optical Induction and Erasure of Ferroelectric Domains in Tetragonal PMN-38PT Crystals,” *Adv. Opt. Mater.*, vol. 10, no. 4, p. 2102115, 2022, doi: https://doi.org/10.1002/adom.202102115.

[107] X. Xu *et al.*, “Femtosecond laser writing of lithium niobate ferroelectric nanodomains,” *Nature*, vol. 609, no. 7927, pp. 496–501, Sep. 2022, doi: 10.1038/s41586-022-05042-z.